NEUTRON FLUX PARAMETERS AND RESONANCE INTEGRALS

A THESIS SUBMITTED FOR THE AWARD OF
THE DEGREE OF DOCTOR OF PHILOSOPHY
OF THE UNIVERSITY OF LONDON

BY

ABDUL HAKIM NABOULSI

APRIL 1989

IMPERIAL COLLEGE REACTOR CENTRE
DEPARTMENT OF MECHANICAL ENGINEERING
IMPERIAL COLLEGE OF SCIENCE AND TECHNOLOGY

DEDICATED

TO

MY Mother and Father

ABSTRACT

The purpose of the work is to measure and evaluate thermal and epithermal neutron activation data for irradiation facilities at the Imperial College Reactor Centre, including resonance integrals, thermal cross-sections and decay data for neutron capture products. These are data required for routine activation analysis and calculation of activation in reactor materials.

The work includes:

(1) A detailed look at high precision gamma-ray spectroscopy with special emphasis on peak area evaluation, manual and analytical, pulse pile-up, coincidence summing effects and the generation of precise efficiency curves.

(2) The proposal and testing of an empirical efficiency formula as a function of distance and energy. This method removes the necessity to carry out measurements at only pre-calibrated source-detector distances.

(3) A description of a neutron flux convention used to characterize the thermal and epithermal neutron fluxes in an irradiation facility and the use of a generalized least-squares technique, which, from measured reaction rates, determines the best values of the flux parameters and the nuclear data of the measured isotopes.

(4) A method for flux normalization is proposed and used to ensure irradiation under the same conditions required by neutron activation analysis.

(5) The use of the flux convention in the calibration of the irradiation positions at Imperial College Reactor Centre and the measurement of nuclear data for the following

isotopes:

^{71}Ga, ^{75}As, ^{81}Br, ^{86}Sr, ^{115}In, ^{121}Sb, ^{133}Cs, ^{152}Sm, ^{158}Gd, ^{159}Tb, ^{165}Ho, ^{169}Tm, ^{175}Lu, ^{179}Hf, ^{181}Ta, ^{186}W, ^{197}Au, and ^{238}U.

(7) A comparison of the nuclear data values obtained in this work with reported literature values.

ACKNOWLEDGEMENTS

I would like to thank my supervisor Dr. Desmond MacMahon not only for the invaluable advise but also for his patience and understanding throughout the course of my work.

Also special thanks to Dr. Peter Gray for his help, useful suggestions and contributions toward the statistical side of the work.

Also I would like to thank the staff and students of the Reactor Centre for making my stay a pleasant and enjoyable one.

CONTENTS

CHAPTER ONE

INTRODUCTION

Resonance integrals, as defined in chapter four, are important nuclear data which are required in fields such as experimental reactor physics, reactor shielding, epithermal neutron activation analysis, neutron flux standarization, in the measurement of slowing down spectra and in checking nuclear resonance parameters. In the measurement of resonance integrals, one of the major requirements is an accurate and consistent flux convention where the reaction rate for a radiative capture reaction, in which the fast neutron contribution is negligible, is formulated in terms of the effective thermal cross-section and the resonance integral.

Flux conventions are also required in the fields of neutron fluence measurements, the purpose of the flux convention being to simplify the calculation of reaction rates and hence enabling the experimenter to unfold as much information as possible from the experimental results.

In the characterization of thermal and epithermal neutron fields, use has often been made [1,2,3] of the assumption that the neutron flux distribution can be represented by a Maxwellian thermal component and an epithermal slowing down spectrum proportional to 1/E. Unfortunately, because there is an overlap of the two components it is not possible to choose an energy cut-off which will excatly divide all Maxwellian neutrons from those in the 1/E distribution. WESTCOTT [1] suggested that it be assumed that the epithermal flux goes to zero at five times

the energy corresponding to the Maxwellian temperature T, i.e. 5 kT, where k is the Boltzmann's constant. Also a 1/E slowing down spectrum is only valid in systems where the slowing down density is constant and this can only be expected in the absence of leakage and absorption. WILLIAMS [4] has shown that in the case of energy independent buckling and absorption cross-section the flux per unit energy is approximately proportional to $1/E^{1+\alpha}$. Functions containing this type of deviation from the 1/E spectrum have also been proposed on empirical grounds by many authors [5,6,7,8,9].

It has been shown [5,6,8] that failure to account for deviation from a 1/E epithermal spectrum can result in severe changes in the apparent resonance integral, and this is believed [10,11] to be one of the reasons for the large scatter in the compilation of resonance integrals by GRYNTAKIS and KIM [12].

In the flux conventions cited in literature [8,9,11,13,14] the reaction rate is given in terms of certain flux and nuclear parameters. AHMAD [11] has proposed a neutron flux convention in which the neutron flux destribution is described in terms of three parameters, and any deviations from a 1/E spectrum are assumed to be of the form $1/E^{1+\alpha}$. The validity of this flux convention has been tested [10,15] and proved to be reliable. This flux convention is the one used in this work.

The standard method is to calibrate an irradiation site by measuring the reaction rates of two or three isotopes in the same position, depending on the number of flux parameters, then substituting in the equation relating reaction rate to flux parameters to obtain values for these

parameters. Then these flux parameters can be used to determine nuclear parameters for other isotopes from measured reaction rates. However, when determining these flux parameters the nuclear parameters (resonance integral, thermal cross-section, etc), are considered constants. This leads to bias in the measured flux parameters, and ignoring the uncertainties of the nuclear parameters (particularly the resonance integral cross-sections) would significantly affect the estimated uncertainties in the flux parameters. This approach in turn leads to bias in the measured nuclear parameters using these flux parameters.

A logical solution to this problem is to determine the flux parameters of the irradiation position, the nuclear parameters of the isotopes of interest and their uncertainties simultaneously from the measured reaction rates and their uncertainties. The best method to estimate these parameters is the one which requires more measured quantities than the minimum in order to produce an over determined set of simultaneous equations. The best values for these parameters can then be obtained by applying a generalized least square approach.

A description of the flux convention used in this work, the methods for measuring the flux and nuclear parameters simultaneously from measured activation data and their uncertainties alone, is given in chapter four.

The purpose of the experiment described in chapter six was to carry out the method described in chapter four, for the calibration of the three irradiation positions used in the Imperial College Reactor Centre and shows the new independent set of nuclear parameters obtained from that experiment for

the isotopes used in this work.

Throughout this work, use is made of the (n,γ) reaction in the experimental measurement of saturated activities. The detecting method employed is high resolution Ge(Li) gamma-ray spectroscopy. Chapter two gives a detailed description of the experimental procedure followed in this work to obtain results with high precision when using gamma-ray spectroscopy.

One of the important factors in gamma-ray spectroscopy is the detector efficiency calibration. The best method (see chapter two) is by employing a set of standard gamma-ray sources of known emission rate and energies. However, this provides an efficiency calibration for that particular source-to-detector distance and the measuring procedure is to be repeated for every source-to-detector distance to be used. So it is easier, and less time consuming, if the efficiency can be calculated for any energy and distance. Chapter three describes the experimental procedure used to develop an empirical efficiency function, in terms of energy and distance, for the Ge(<Li) detector used in this work.

In neutron activation analysis (NAA) use is made of the assumption that all samples are irradiated in the same flux. However, since the irradiation of the standards and samples are usually done at different times, unless the flux is constant a method for flux normalization is required to obtain any meaningful results. In chapter five a method for flux normalization is proposed and tested in the Imperial College Reactor Centre using the coolant outlet temperature as a normalization indicator.

Chapter seven summarizes the results obtained in this work and draws the final conclusions.

CHAPTER TWO

GAMMA-RAY SPECTROSCOPY

Recently precision measurements of gamma-ray intensities have been required for non-destructive nuclear fuel investigation. Precision measurements are also required for the investigation of nuclear fuel burn-up rates, nuclear fission cross-sections, activation analysis and nuclear spectroscopy.

The accuracy of gamma-ray intensities obtained depend on the following factors:

1) A good knowledge of the capabilities and limitations of the system in use,
2) the peak area determination,
3) applying the appropriate corrections (coincidence summing, pulse pile-up, dead-time etc)
4) and the determination of the detector peak efficiency at that energy.

The literature was reviewed for each of the above factors and various methods were selected for this work. A set of single line gamma-ray standard sources was used for peak and total efficiency measurements.

2.1 System Limitation

For precision measurements it is important to determine the limitation of the experimental system. In this case it is the counting system which consists of a Ge(Li) detector, pre-amplifier, amplifier, analog to digital converter and a multichannel analyser. In this work the

concern is with the capability of the counting system in determining the disintegration rate of a radio-nuclide within the statistical errors.

To carry out the test a radioactive isotope of known disintegration rate, and a long half-life compared to the test period is to be used. Also the source is to be measured at the same position and for the same counting period.

^{137}Cs is chosen for this test and the measurements are taken over a period of five weeks and the photopeak from the 661-keV line was used and the peak area evaluated using the method outlined in section 2.2.1b.

For n measurements the reduced chi-square is given by:

$$\chi^2_{n-i} = \frac{1}{n-1} \sum_{i=1}^{n} \frac{(N_i - \bar{N})^2}{\sigma^2_{N_i}}$$

where i refers to the i^{th} measurement, $\bar{N} = \sum_{i=1}^{n} \frac{N_i}{n}$ and σ_{N_i} is the uncertainty in the i^{th} measurement.

The obtained value of χ^2 is 5.32 which fails the chi-square test at the 95% probability level. This indicates an extra error which is purely systematical, and is given by:

$$\sigma^2_s = 5.32\sigma^2_{N_i} - \sigma^2_{N_i}$$

the relative error in N_i is 0.2%, hence an additive systematic error of 0.4% is found.

2.2 Peak Area Determination

The purpose of any peak area analysis, manual or analytical, should be to provide a representation of the area and position of the peak independent of the spectral background. If the same method is used to represent the areas for the efficiency calibration spectra and the unknown spectra, it is not necessary to determine or even define a "true" area. Two methods are examined 1) manual, and 2) analytical.

2.2.1 Manual Method

The basis of this method is to determine the boundaries of the peak between which the summation is to take place, and the shape of the background function under the peak. Two methods are used and compared for consistency at different count rates and energies.

a) By summing all recorded counts in the interval $(C-4\sigma,\ C+4\sigma)$, where C is the peak centroid and σ is F.W.H.M/2.35; and subtracting the counts recorded in the intervals $(C-9\sigma,\ C-5\sigma)$ and $(C+5\sigma,\ C+9\sigma)$ for background. This method is known as the modified DEBERTIN method [16,10].

b) By summing all recorded counts between two points, the first point is on the lower energy tail of the photopeak and is taken where the actual spectrum deviates significantly from a straight line fitted to the background which is arising from multiple Compton events. The second point is where the upper tail of the photopeak reaches a point where it is no longer significantly above the background [17].

When measuring high intensity gamma-ray sources at short source-detector distances, distortion in the peak shape

due to pulse pile-up results in loss of shape symmetry and a long tailing on the high energy side of the peak. Method (a) fails to account for the extra tailing, while method (b) showed an independence of the peak shape and symmetry.

After determining the peak boundaries the construction of the background in the peak region should be done in such a way that the resulting peak area is independent of the background. In practice if the background contribution is small compared with the peak area in the photopeak region, then errors in the background construction under the peak do not affect the accuracy or the precision of the measurement. However if the background contribution is not small (e.g if weak gamma-rays are measured in the presence of a strong higher energy gamma-ray) then small errors in the background construction may cause large errors in the peak area [18].

For this work the background is constructed as follows: Once the peak boundaries are defined (l , u), where l and u are the lower and upper boundaries respectively (see fig.2.1), suitable regions adjacent to these are chosen for background determinations. Each region is fitted to a straight line and then the two lines are extrapolated to the peak centroid C, and the background regions (B_1,B_2) are then fitted as shown in fig.2.1. The net peak area is then defined as:

$$N = T - B$$

where $$T = \sum_{i=l}^{u} c_i$$ total area

$B = B_1+B_2$ where B_1 and B_2 are function of the counts in the regions indicated

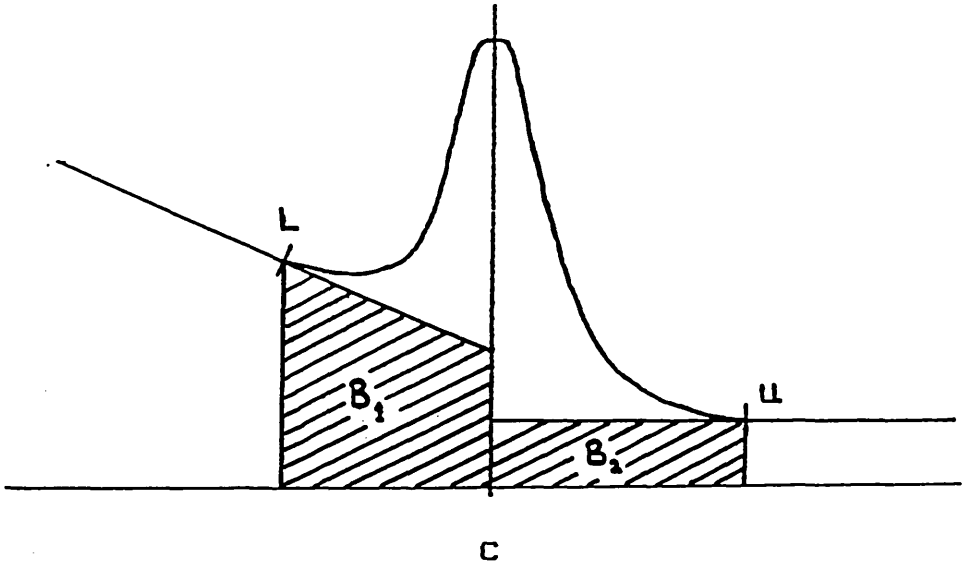

Fig. (2.1) Background construction under photopeak area.

c_i = number of counts in channel number i

and the error in the net peak area N is

$$\sigma_N = (T + \sigma_B^2)^{1/2}$$

where σ_B is determined from the error in the parameters constructing the background.

2.2.2 Analytical Method

In complicated spectra, where peaks are close together or overlapping, the manual method is very difficult or impossible to apply. So the use of some sort of an analytical function is necessary. Also for well isolated peaks, the analytical fitting of the photopeak could add more information by reducing the variance in the net peak area.

In this work, all gamma-ray peaks under study are of known energies, so the priority in the analytical fitting is for the best fitting functional form to a gamma-ray photopeak.

A wide variety of analytical fitting functions have been proposed in literature to represent the shape of a gamma-ray photopeak from a Ge semiconductor detector. Some of these functions (especially those of SAMPO [19] and GAMANAL [20]) are widely used. In some comparisons of the quality of fits [21,22] to specific peaks, the advantage of the more complex (i.e, those with more free parameters) functions have been indicated.

The primary contribution to the photopeak in a semiconductor detector is a gaussian distribution arising from the statistical fluctuation in the division of absorbed energy between ionization and heating of the crystal lattice (Fano factor). The degree to which the experimental data deviate

from this fundamental description is dependent on the detector, associated electronics and other experimental considerations.

The impurities of the semiconductor crystal of the detector in use affect the charge collection processes and the electronic noise associated with the leakage current. Low-energy tailing and worsened resolution result from loss of free charges in the device due to recombination, uncompensated impurities which act as traps and the escape of photoelectrons from the sensitive region.

Instrumental effects, such as instability in the amplifier or the analyser can affect line width at higher energies, especially if the data acquisition is over a long duration. Finally, random summing of pulses at high count rate can broaden the photopeak and give rise to tailing on the high energy side of the peak.

From these considerations of experimental effects and detector properties, it is apparent that the mathematical representation of the full energy peak should include a basic gaussian shape. For the low and high energy tailing, the main deviation from the simple gaussian form, should be included in the functional description. Most of the analytical functions in use [19,20,22-27] have a gaussian or a skew gaussian as the functional main portion, and an exponential as the additive tailings.

After taking several spectra and studying the shape of the photopeaks produced by the detector in use, the functional form chosen to represent the photopeak in this work is a main gaussian plus an exponential tailing on both sides of the peak.

The spectral background in the region of the peak consists of three components:

1) pulses related to radiation from other sources (i.e., the background radiation),
2) pulses from higher energy gamma-rays from the source being measured, and
3) pulses from the desired gamma-ray energy but for which enough energy is lost from the sensitive volume of the detector to put the count in the spectral distribution below the peak.

It is assumed that the first two contributions can be represented by a constant or a low order polynomial (often a linear function). The third contribution could be represented by a step like function [25,26,28-31].

The individual contributions to the final analytical shape chosen in this work to unfold an experimental photopeak are given by:

$$F1(i) = p_1 . e^{(-\frac{1}{2}(\frac{i - p_2}{p_3})^2)}$$

where p_1 is the gaussian amplitude at the centroid p_2, p_3 is a parameter of the gaussian width and i is the channel number. An exponential at the lower energy side, accounting for incomplete charge collection is given by:

$$F2(i) = \frac{p_4 . e^{(\frac{i - p_2}{p_3}) . p_5}}{(1 + e^{(\frac{i - p_2}{p_3})})^4}$$

An exponential on the peak's high energy side accounting for pulse pile-ups is given by:

$$F3(i) = \frac{P_6 . e^{(\frac{i - P_2}{P_3}) . P_7}}{(1 + e^{-(\frac{i - P_2}{P_3})})^4}$$

where P_4 and P_6 are the exponential amplitudes, P_5 and P_7 are the exponential ranges. The multiplication of the exponentials by a step like function to the power four is to ensure a rapid decay of the exponential contribution in the vicinity of the peak.

The background at the low energy side of the peak is represented by a step like function, decaying in the peak region. the function is

$$F4(i) = \frac{P_8}{(1 + e^{(\frac{i - P_2}{P_3})})^2}$$

where P_8 is the step amplitude.

The natural background is represented by a first order polynomial,

$$F5(i) = P_9 . i + P_{10}$$

The total functional form to represent a photopeak is then given by:

$$F = F1 + F2 + F3 + F4 + F5$$

$$F = P_1 . e^{(-\frac{1}{2}(\frac{i - P_2}{P_3})^2)} + \frac{P_4 . e^{(\frac{i - P_2}{P_3}) . P_5}}{(1 + e^{(\frac{i - P_2}{P_3})})^4} +$$

$$\frac{P_6 \cdot e^{\left(\frac{i - P_2}{P_3}\right) \cdot P_7}}{\left(1 + e^{-\left(\frac{i - P_2}{P_3}\right)}\right)^4} + \frac{P_8}{\left(1 + e^{\left(\frac{i - P_2}{P_3}\right)}\right)^2} +$$

$$P_9 \cdot i + P_{10}$$

The function is tested on photopeaks with energies ranging from 60 keV to 1115 keV at different count rates.

The general least-square model is used to perform the fitting. Using the CERN library code MINUIT [32], minimization is performed on the function

$$\chi^2 = \sum_{i=1}^{n} \frac{(c_i - F(i, P_1 - P_{10}))^2}{c_i} .$$

where c_i = data at channel i.

The evaluation of the fit is normally by studying the χ^2 value. However, this method of evaluation has been proved to be inadequate [33], so the final goodness of fit test, was done visually with plots and detailed scans of residuals.

Some examples of the photopeak fittings are shown in figs 2.2 to 2.5, where figs 2.2 and 2.3 show the fitting for ^{241}Am and ^{137}Cs photopeaks from a Ge(Li) detector with a long counting time and 8192 channel conversion gain. Figs 2.4 and 2.5 show the fittings for ^{241}Am and ^{137}Cs photopeaks from a Ge detector with a short counting time and 2048 channel conversion gain.

The advantage of such a function is also that, by studying the variation of functions F2 and F3 which account for deviation from a pure gaussian, with respect to the pure gaussian F1, one gains useful information about the detecting

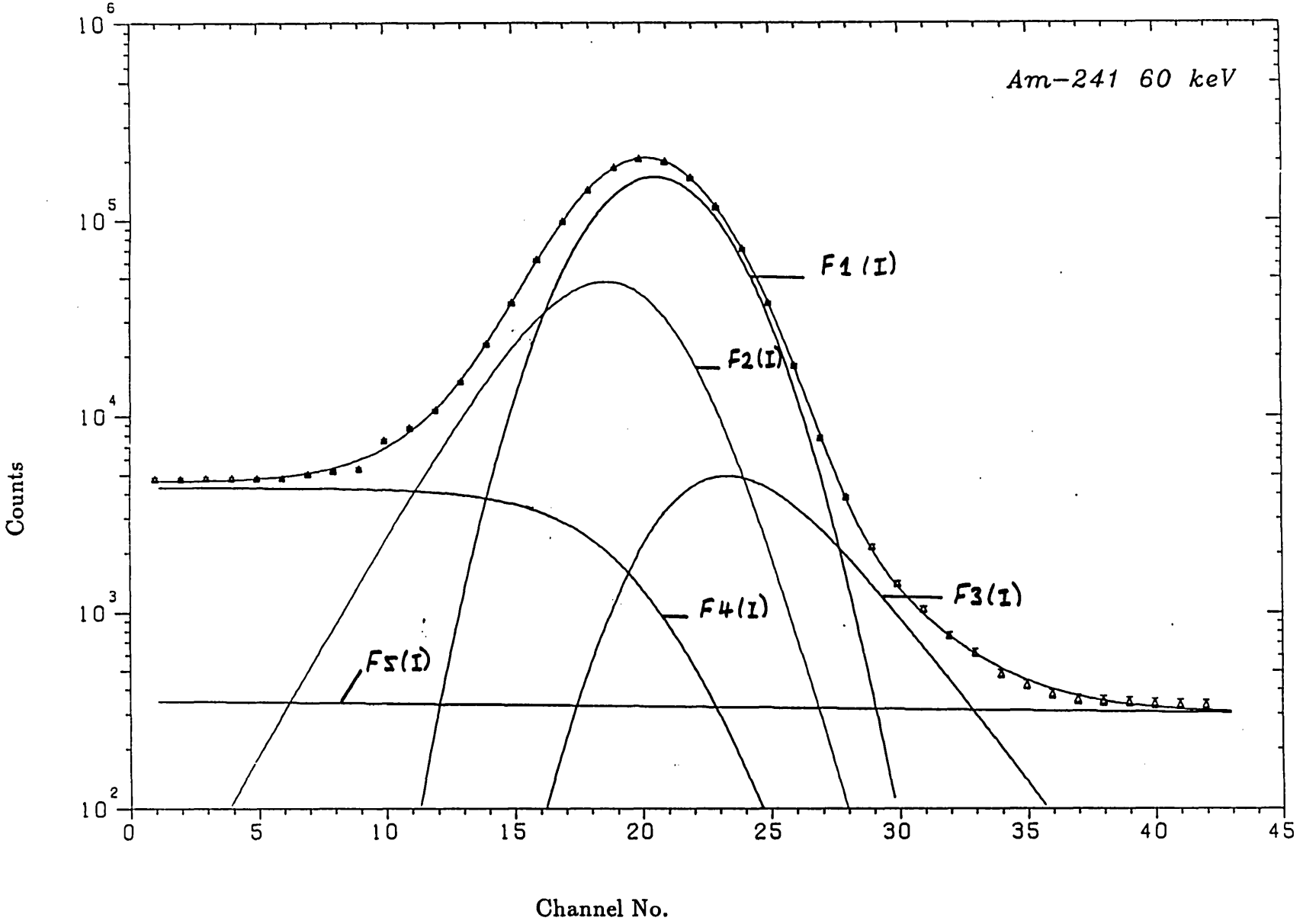

Fig. (2.2) Fitted photopeak of ^{241}Am form a Ge(Li) detector.

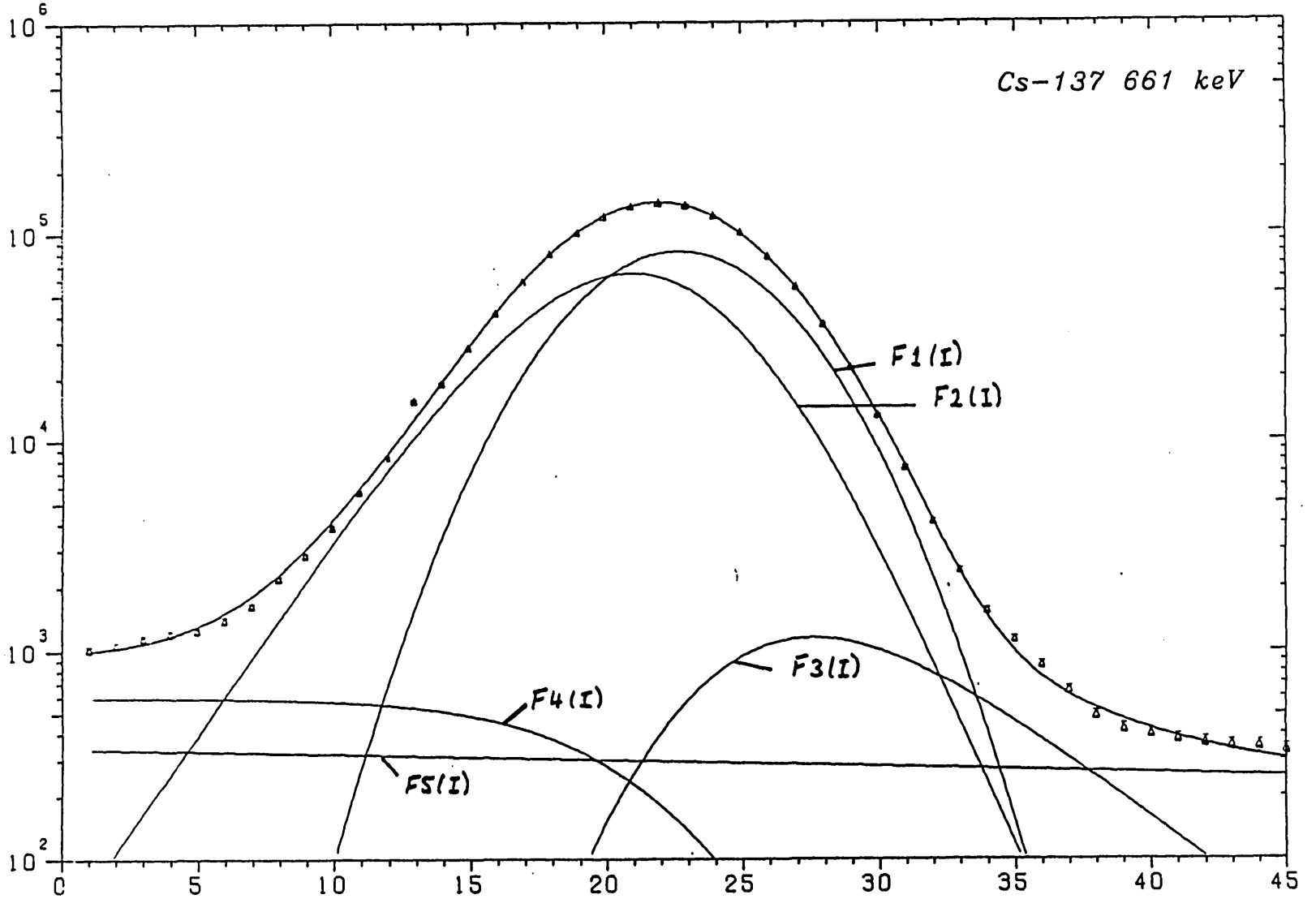

Fig. (2.3) Fitted photopeak of ^{137}Cs form a Ge(Li) detector.

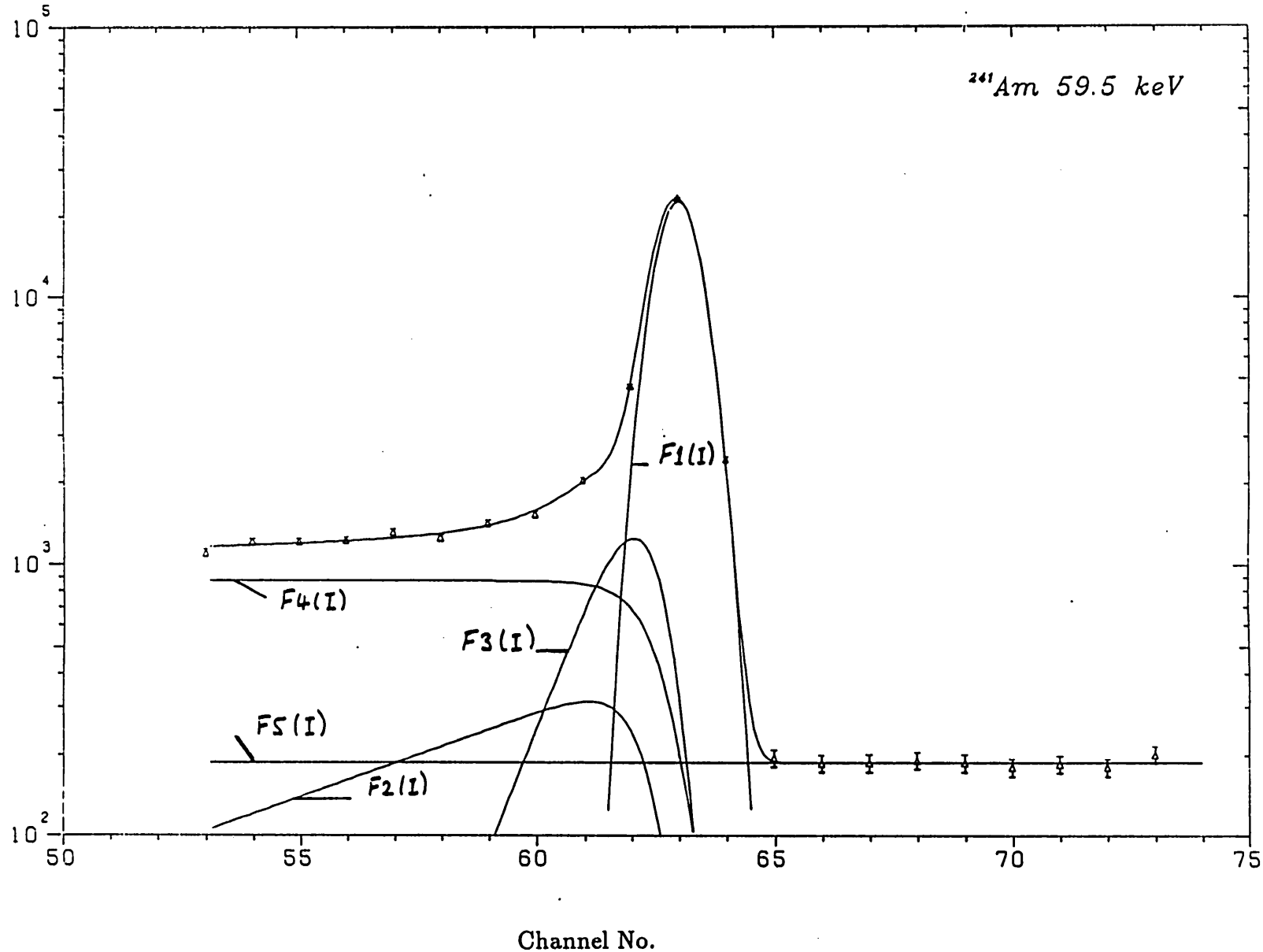

Fig. (2.4) Fitted photopeak of ^{241}Am form a Ge detector.

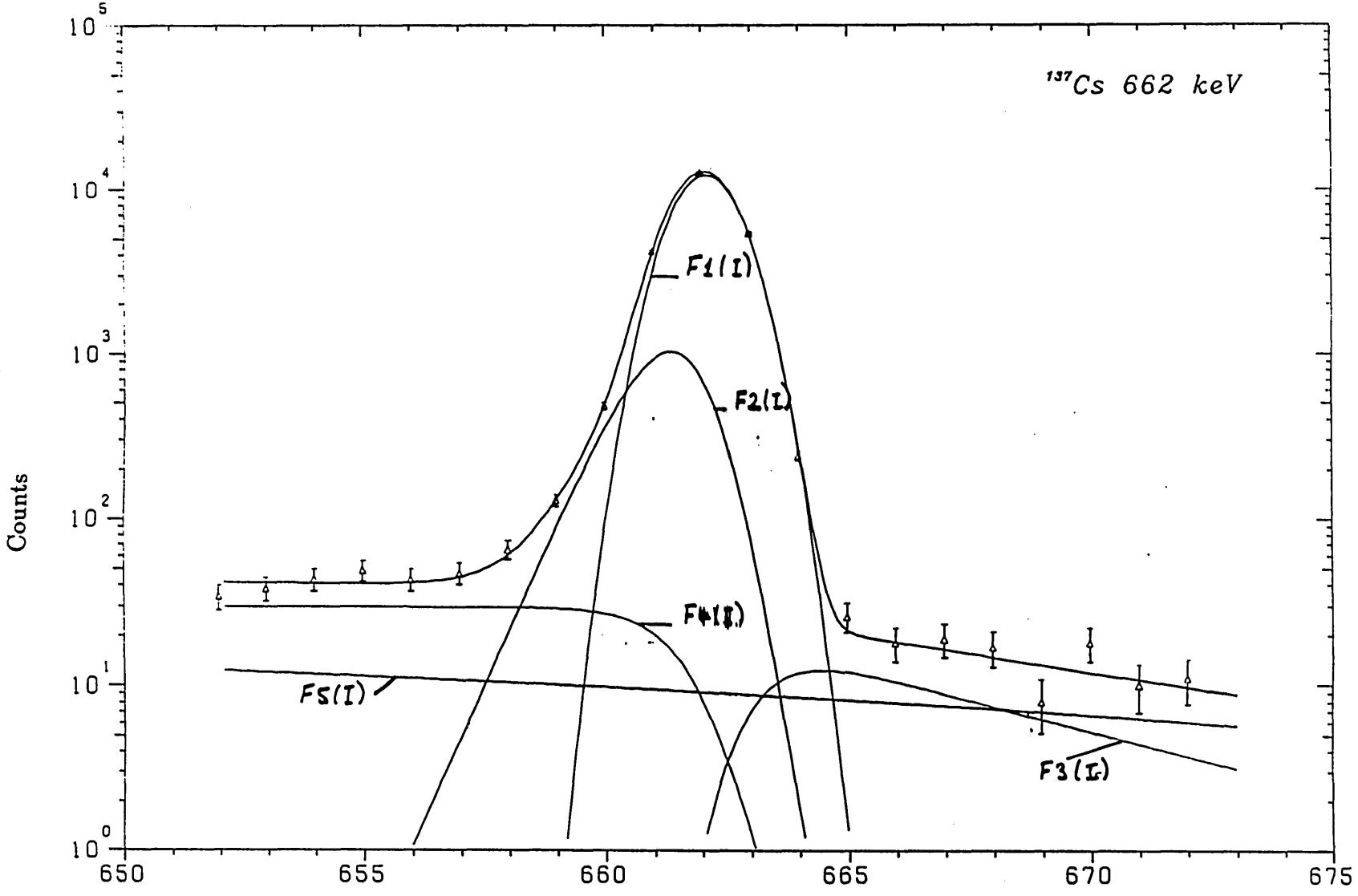

Fig. (2.5) Fitted photopeak of ^{137}Cs form a Ge. detector.

system stability.

The net peak area is calculated from F1, F2 and F3 by integrating each of these functions from $-\infty$ to $+\infty$, hence getting over the problem of deciding on the peak limits. The integrals of F2 and F3 are approximated to a Beta function and then it can easily be shown that the net peak area is given by:

$$N = (2\pi)^{\frac{1}{2}} \cdot p_1 \cdot p_3 + p_3 \cdot p_4 \cdot \left(\frac{\Gamma(p_5) \cdot \Gamma(4-p_5)}{6}\right) + p_3 \cdot p_6 \cdot \left(\frac{\Gamma(p_7) \cdot \Gamma(4-p_7)}{6}\right)$$

In general good fits are obtained using this functional representation. The gaussian peak width parameter p3 obtaind from fitting standard gamma energies photopeaks is plotted against energy in fig.2.6, which shows a linear relation. This expected linear dependence is another indication of a good analytical representation.

This analytical peak evaluation method and the manual method described in section 2.2.1 were used throughout this work.

2.3 Dead-Time and Pulse Pile-up Correction

When a signal is accepted by the multichannel analyser, there is a finite time taken for the signal to be processed, analysed and stored, during that time the analyser does not accept any signal. This leads to count losses and this effect is known as the "dead time" effect.

Count losses from the full energy peak are also

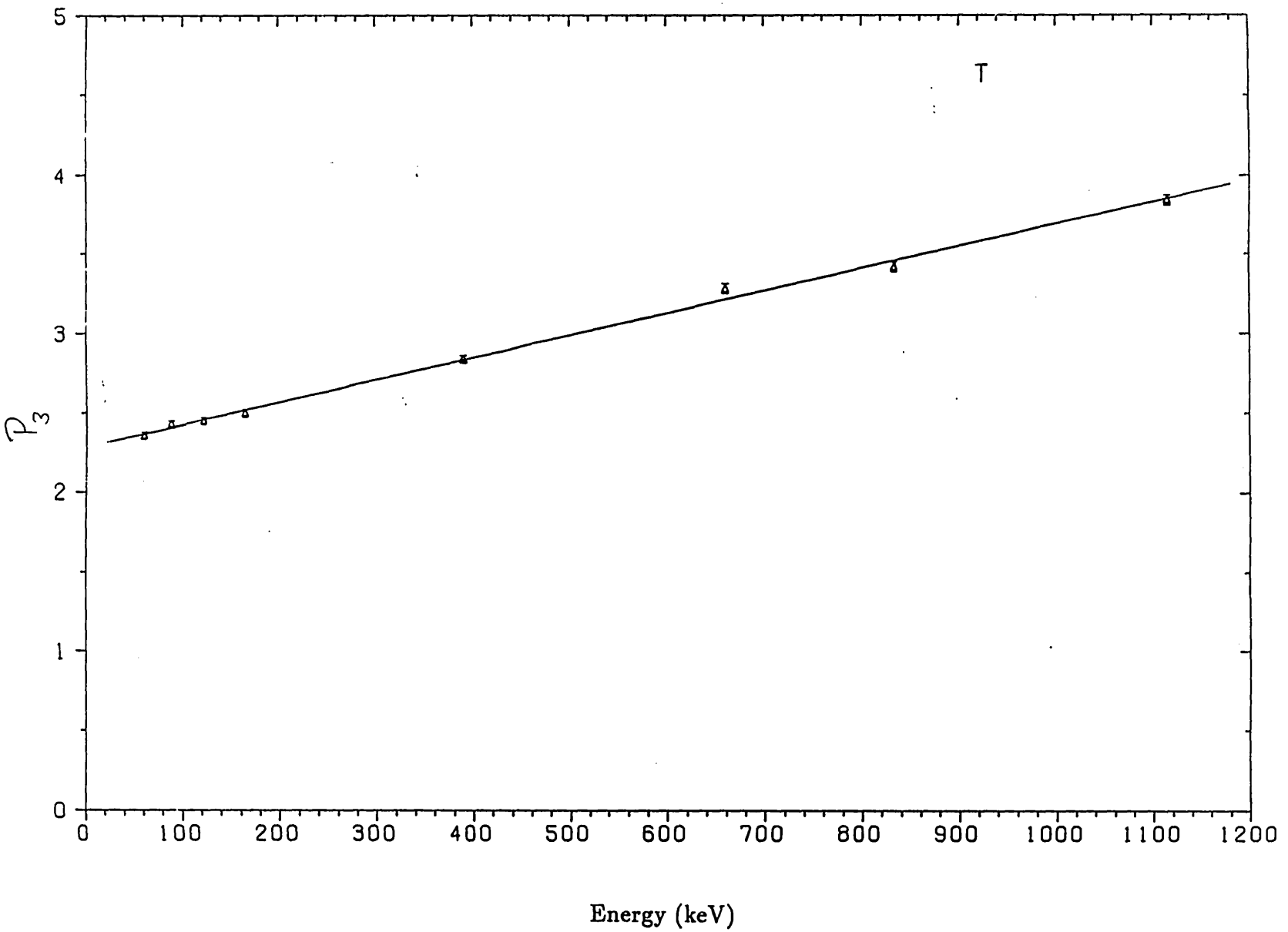

Fig. (2.6) Gaussian peak width Vs Energy.

caused from spectrum distortion due to pulse pile-up. This effect can be divided into two categories: resolution degradation and sum distribution. The first category is caused mainly by the long term time constant in the pulse shaping circuits, and is commonly called the tail pile-up, and the result is a general degradation of resolution and shifting and smearing of the spectrum [35]. The second category arises because the processes of radioactive disintegration are completely random in time, and the resolving time of the electronic system is finite, pulses from two events can overlap in time and the two events will sum in amplitude. This probability of random summing is proportional to the square of the input pulse rate i.e. prob(random summing) $\propto N^2$ where N is the input pulse rate.

The problem of dead-time and pulse pile-up is always encountered in precision gamma-ray intensity measurements. Several methods have been proposed to correct for the above effects [34-42], but most reviews [38,39,43] showed the advantage of the pulser method. This method was originally proposed by ANDERS [38] and BOLOTIN et al [39] which considers that pulses from the pulser if introduced along with the detector events will suffer losses in the same proportion as those coming from the detector.

The pulser method is chosen for this work. In the method, a pulser signal of known repetition rate is introduced along with the detector events. The area of the pulser peak, divided by the number of generated pulses, gives the correction for pile-up and dead-time:

$$\frac{N}{N_r} = \frac{P.T_c}{P_r}$$

where N = number of nuclear events, with zero dead-time and pulse pile-up

N_r = recorded number of nuclear events.

P = generated rate of pulser events.

P_r = recorded number of pulser signals.

T_c = real (clock) counting time.

In order for the above relation to hold, three criteria have to be satisfied to assure that the pulser signals are introduced in the spectral distribution as if they were a true spectral component:

1) The shape of the pulser signals entering the preamplifier must resemble that of the detector signals.
2) The pulser signals have to be introduced in a random sequence with respect to the detector signals.
3) the pulser rate must be always at a constant fraction of that of the detector rate.

The first criterion was satisfied by feeding pulses from the detector and the pulser simultaneously into the preamplifier. The amplifier output of these two sources were then viewed on an oscilloscope and the pulser signals were shaped to resemble the detector pulses by adjusting the rise and fall times of the pulser signals.

When detecting long lived nuclides or when the change in the count rate during counting is negligible, criterion (3) is satisfied by keeping the pulser signal at constant rate during counting (constant pulser method). When the source decay rate is not negligible during counting, criterion (3) can be satisfied by using the proportional feedback method

[26] which works as follows: A fast discriminator continuously monitors the number of pulses arriving from the preamplifier and the output pulses of the discriminator are applied to a fast scaler that resets after a preset number of counts. At the end of the scaling cycle, a trigger output from the scaler is used to initiate a pulse generator signal that is injected into the amplifier input. The scaler is reset and a new cycle is started.

The combination of fast discriminator, pulse shaping circuitry and recycling scaler in the above method will introduce an uncertainty [35] in the counting losses, also the proportional feedback method only gives more accurate results than the constant pulser method when the counting rate of the detector is time dependent [35]. According to JUNOD [37], the detector count rate can be considered time independent as long as the counting period does not exceed 2% of the nuclide's half-life.

The constant pulser method is the one chosen in this part of the work, since all nuclides used are long lived (compared to the counting period).

In using the pulser method, extra care has to be taken [35] to avoid the systematic error arising due to the fact that pulser signals come evenly spaced in time, and thus they are able to interact with the detector signals, which are randomly distributed, but not with themselves. As they are also part of the dead-time causing population, the sampling is not correct, because the losses suffered by the pulser signals will correspond to the dead-time produced by the detector signals only, whereas the detector signals will be lost at a rate determined by the combined dead-time produced by the

pulser and detector. This problem was recognized by BOLOTIN et al [39] and he recommended the use of a pulse rate as low as possible, in order to maintain its dead-time contribution at negligible levels.

On the other hand the interactions between the detector and the pulser signals are random events, and as such are governed by statistical laws, and the precision of the measurements will grow with the number of counted signals. With relatively long-lived nuclides, the low repetition rate of the pulser may be compensated by a sufficiently long counting period, so that the statistical error due to the pulser will be negligible. But when short-lived nuclides are being counted, the initial counting rate must be high and the counting period short if meaningful results are to be obtained [44].

Since the lost pulser pulses are due to random interaction with the detector events, the variance in the dead-time and pulse pile-up correction is then estimated as:

$$\sigma^2_{P_r} = P.T_c - P_r$$

assuming any fluctuations in P are negligible.

The variance in the total count in the net peak area is then given by:

$$\sigma^2_N = N^2 \left[\left(\frac{\sigma_{P_r}}{P_r}\right)^2 + \left(\frac{\sigma_{N_r}}{N_r}\right)^2 \right] .$$

2.4 Coincidence Summing

In high precision gamma-ray intensity measurements,

another summing correction has to be taken into account which is known as coincidence summing.

Since the lifetimes of nuclear levels for gamma-ray decay are much shorter then the charge collection time in a Ge(Li) detector, coincidence summing will occur with radionuclides emitting two or more cascading photons within the resolving time of the detector. If for example, the first photon deposits its total energy in the germanium crystal and if the second photon is also detected, a sum pulse is recorded. The event is lost from the full energy peak of the first photon. The probability and magnitude of such summing occuring depends on the specific features of the decay scheme, and it increases with decreasing source-to-detector distance, but is independent of the count rate.

Several authors [45-48] have pointed to this problem and have given useful correction formulae. Consider the simple decay scheme shown in fig.2.7 which is used in explaining the principle of the coincidence summing correction factors.

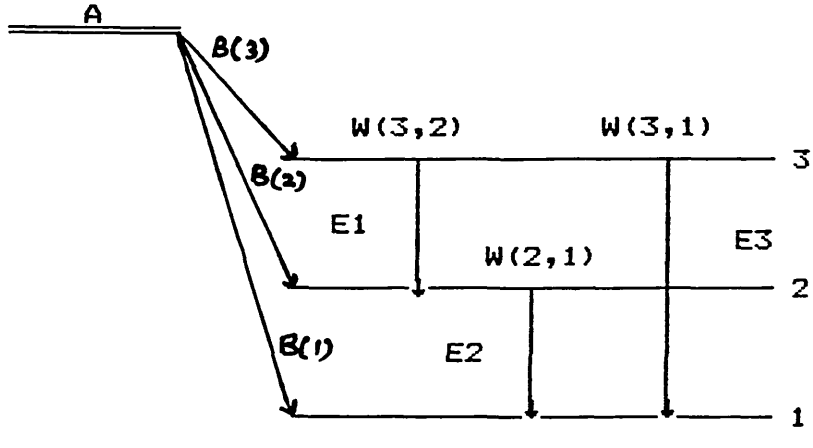

Fig.2.7 Simple cascade decay scheme

where A = Activity in disintigration per sec.

B(I) = probability of direct transitions to level I per sec

W(j,k) = Total branching ratio (i.e gamma-ray plus internal conversion for transitions from level j to level k.

Neglecting coincidence summing, the number of gamma-rays with energy E2 in the photopeak are

$$= A.B(2).W(2,1).\epsilon_p(2,1).\frac{1}{(1+\alpha(2,1))} + A.B(3).W(3,2).W(2,1).\epsilon(2,1).\frac{1}{(1+\alpha(2,1))} \quad (2.1)$$

where $\alpha(2,1)$ = Internal conversion coefficient for transitions from level 2 to level 1 (which is the ratio of the number of internal Conversion electrons to the number of gamma-rays emitted)

ϵ_p = photopeak detection probability.

When including coincidence summing but assuming that angular correlation between gamma-rays can be ignored, the recorded number of gamma-rays with energy E2 in the photopeak is smaller. Since each gamma with energy E1 is followed by a gamma with energy E2 in coincidence, it may happen that both gamma rays are detected at the same time thus leading to a single pulse. So the true number of detected E2 gammas are:

$$= A.B(2).W(2,1).\epsilon_p(2,1).\frac{1}{1+\alpha(2,1)} + A.B(3).W(3,2).W(2,1).\epsilon_p(2,1).\frac{1}{1+\alpha(2,1)} -$$

$$A.B(3).W(3,2).W(2,1).\frac{1}{1+\alpha(3,2)}.\epsilon_T(3,2).\epsilon_p(2,1).\frac{1}{1+\alpha(2,1)} -$$

$$A.B(3).W(3,2).\frac{\alpha_K}{1+\alpha(3,2)}.\Omega_K.\epsilon_T(X).W(2,1).\epsilon_p(2,1).\frac{1}{1+\alpha(2,1)}$$

——— (2.2)

where ϵ_T = Total gamma-ray detection probability.

$\epsilon_T(X)$ = Total X-ray detection probability.

α_K = K-conversion coefficient.

Ω_X = Fluorescence efficiency.

$\frac{\alpha_K}{1+\alpha(I,J)}$ = prob. of internal conversion from K-shell.

In the case of an electron capture (E.C) decay scheme, the B(I)'s represent the percentage of E.C decays to level I per sec. Then each B(I) in equation (2.2) is multiplied by

$$(1 - \epsilon_T(X).PK.\Omega_K)$$

where PK = prob. of E.C from K-shell.

Ω_K = prob. of K X-ray being emitted in preference to an auger electron.

Therefore the net peak area of E2 is to be multiplied by the correction factor

$$C1 = \frac{eqn(2.1)}{eqn(2.2)}$$

Similar correction expressions can be obtained for E1 and E3, except that the observed E3 rate will be greater than the true rate due to gamma-rays E1 and E2 being detected simultaneously.

In order to determine the true detection rate, these correction factors have to be applied. Several programs are available which calculate the correction factors [45-47]. Programm KORSUM [47] is the one chosen for this work because it allows for coincidence summing of gamma-rays with X-rays following internal conversion or electron capture.

The following input data are required by program KORSUM : type of decay (beta, E.C), emission probabilities, mean energy of K X-rays, fluorescence yield. Also at each source-to-detector distance to be used, a set of values of photopeak and total efficiency have to supplied, from which efficiency curves are set up and the photopeak and total efficiency for any energy can be calculated.

The parabolic fit for ℓn(efficiency) vs ln(energy used by KORSUM for efficiency curves is replaced by a better efficiency function (see section 2.5 below).

Coincidence summing can be ignored if [47] the source-to-detector distance is greater than 20 cm.

2.5 Efficiency and Efficiency Curves

Accurate calibration of the detecting system for the full energy gamma-ray peak efficiency as a function of energy is necessary in order to make precise and accurate measurements of gamma-ray emission rates and intensities. The most accurate efficiency calibration is achieved experimentally by using a set of single line gamma-ray standard sources, of known energies and activities which covers the energy range of interest, or a few sources that provide a series of lines of known intensities, as long as the count rates in the peak areas are corrected for coincidence

summing effects.

To calibrate the detector used in this work, a set of single-line gamma-ray standard sources with well known absolute activities and energies ranging from 59-1115 keV were used. The sources are ^{241}Am (59 keV), ^{109}Cd (88 keV), ^{57}Co (122 and 136 keV), ^{139}Ce (165 keV), ^{113}Sn (391 keV), ^{137}Cs (661 keV), ^{54}Mn (834 keV) and ^{65}Zn (1115 keV).

The photopeak efficiency is calculated from the following relation:

$$\epsilon_p = \frac{N_c}{A_0 P_\gamma . D . C} \qquad (2.3)$$

where N_c = the count rate in the net peak area corrected for dead-time, pulse pile-up and coincidence summing.

A_0 = the source absolute activity at some reference time

P_γ = the gamma-ray emission probability.

$D = e^{-\lambda t_d}$

= correction factor for the source decay between its reference time and the time of counting, where λ is the decay constant and t_d is the decay time.

$$C = \frac{(1 - e^{-\lambda t_c})}{\lambda}$$

= correction factor for the source decay during counting, where t_c is the counting time.

and the error in the efficiency is given by:

$$\sigma^2_{\epsilon_p} = \epsilon_p^2 \left[\left(\frac{\sigma_{N_c}}{N_c}\right)^2 + \left(\frac{\sigma_{A_0}}{A_0}\right)^2 + \left(\frac{\sigma_{P_\gamma}}{P_\gamma}\right)^2 + \left(\frac{\sigma_D}{D}\right)^2 + \left(\frac{\sigma_C}{C}\right)^2 \right]$$

where $$\left(\frac{\sigma_D}{D}\right)^2 = t_d^2 \, \sigma^2_\lambda$$

and $$\left(\frac{\sigma_C}{C}\right)^2 = \left[\left(\frac{\sigma_\lambda}{\lambda}\right) + \frac{t_c e^{-\lambda t_c}}{1 - e^{-\lambda t_c}} \right]^2 \sigma^2_\lambda$$

assuming any errors in t_c and t_d are negligible.

In the total efficiency calculation, for each source the pulse height spectrum was recorded on an energy calibrated multichannel analyser. The total efficiency is calculated using eqn (2.3), but N_c in this case is the total count rate between the threshold energy and the maximum energy [47] after subtracting the background. Pulses below the threshold energy w ere taken into account, by fitting the low energy side of the spectrum with a polynomial (first order polynomial was adequate), and integrating between zero and the threshold energy.

For the sources used, small contributions of weak X-rays have to be subtracted (for more detail see DEBERTIN [47]).

The uncertainties in the ϵ_T obtained in this work vary from 2% to 8%, mainly due to the extrapolation to zero energy and the subtraction of the low energy X-ray and gamma-ray contributions.

In practice the gamma-ray emission rates under study are of energies different from the ones used to calibrate the detector. So a construction of an approximate efficiency

curve from the measured efficiences is needed so that the curve can be used to determine efficiencies at different energies.

Many classes of functions have been proposed by different authors to fit the efficiency data with a smooth continuous curve. P.W.GRAY and A.AHMAD [49] carried out a survey of these fitting functions, and they showed that most of these functions are non-linear in the parameters which could lead to bias in the estimate of any interpolated points and their errors.

As a result of their survey they proposed the following linear function:

$$\epsilon_{cal} = (P_1+P_2\ell nE+P_3(\ell nE)^2+P_4(\ell nE)^3+P_5(\ell nE)^5+P_6(\ell nE)^7)/E$$

where P_1— P_6 are parameters to be determined by the experimental data and E is the gamma ray energy in MeV. The last term $(P_6(\ell nE)^7)$ is only needed if the energy range is extanded [49] below 120 keV or above 1836 keV.

The photopeak and total efficiency data were fitted to the above functional form using a least-squares method. The measured and fitted efficiencies are shown in fig.2.8. and fig.2.9.

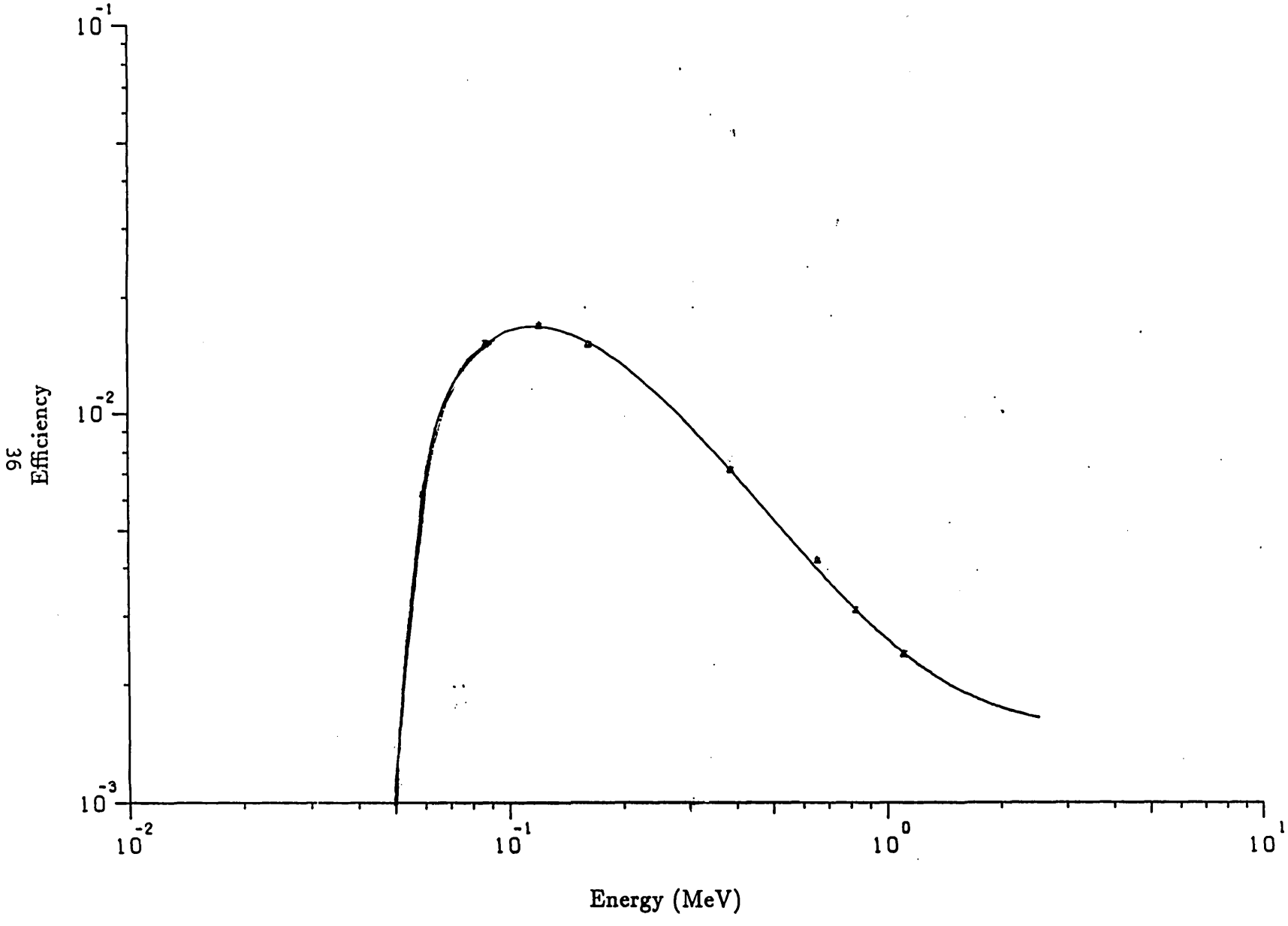

Fig. (2.8) Peak Efficiency versus Energy.

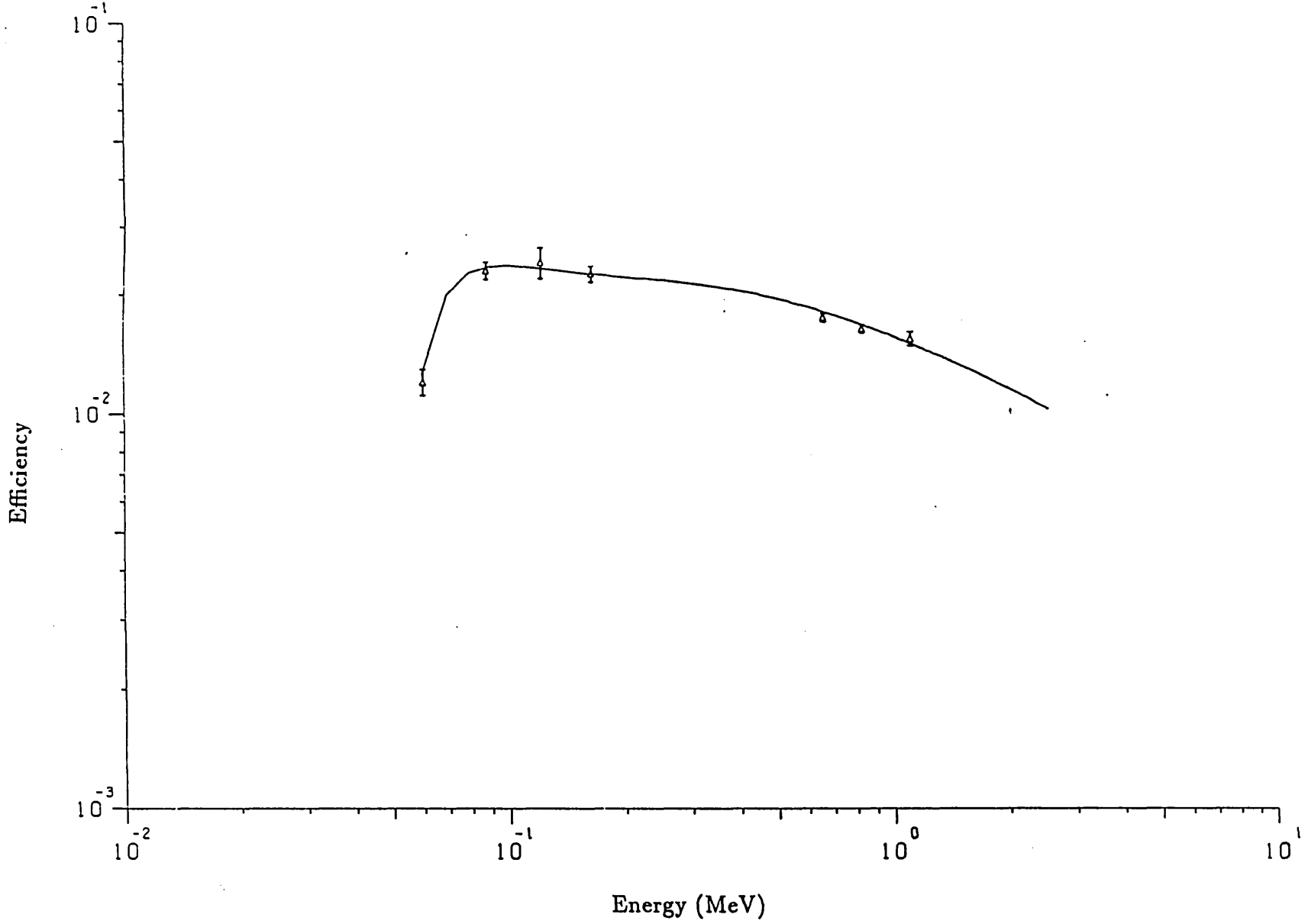

Fig. (2.9) Total Effieciency Vs Energy.

CHAPTER THREE

GERMANIUM DETECTOR RESPONSE FUNCTION

In the last several years Ge and Ge(Li) detectors have been widely used for measuring the intensities and energies of gamma-rays, because of their excellent energy resolution. The accuracy of the gamma-ray intensities obtained depends critically on how precisely the full-energy peak efficiency of the detector in use is known.

Usually the most accurate efficiency determination (as discussed in chapter two) is done by employing a set of standard reference gamma-ray sources of well known emission rates and energies which cover the range of interest.

The points of interest in the precise calibration of Ge and Ge(Li) detectors have been discussed and studied in detail by several authors [16,46,47,50]. They calibrated their detectors with errors of about 1% or less. Normally one determines the efficiency for several source-to-detector distances and then to use these efficiencies we are limited to these particular geometries. The constraint of using the same geometry limits the comparison to source intensities of almost the same order of magnitude of that of the standard source. Comparison between measurements of different geometries introduces the need for solid angle corrections.

There are many papers [51-54] dealing with different methods of efficiency calculation using solid angle geometry corrections. This involves a large number of complex measurements, and the geometrical solid angle alone cannot fully account for the geometrical aspects of the peak

efficiency [51]. Also using the active volume dimensions of the detector to calculate these corrections is not feasible [55], because they are only known to a first order approximation.

Thus it would be convenient, if the detector efficiency could be calculated rather than measured for any source-to-detector distance with the least possible calculations and knowledge of the detector dimensions.

In this work an empirical function for representing the photopeak efficiency as a function of energy and distance (in the X-axis direction) based on the point detector model is proposed and tested.

3.1 Experimental Set-up and Detecting System

The detecting system consists of a closed-end up right Harshaw Ge(Li) detector, model AC066 with a 70 cc crystal and 2.1 keV resolution at 1.33 MeV. The accompanying electronics are an Ortec 472 amplifier, Ortec 459 power supply, a Northen Econ II series A.D.C and multi-channel analyser with a 1024 channel memory and a B.N.C FB.4 pulse generator.

The standard gamma-ray sources used are listed in section 2.4 and were commercially obtained. The sources are in the form of liquid, deposited and encapsuled between two thin polythene sheets. The sources are within 3 mm in diameter. A drawing of the source assembly is show in fig 3.1b.

A plastic source holder is constructed so as to position the sources at various distances from 1 - 16 cm at 1 cm intervals from the top of the detector aluminium can

assembly which encloses the germanium crystal. A drawing of the detector-sample holder assembly is shown in fig.3.1a.

3.2 Experimental Procedure

The experimental procedure to determine the photopeak efficiency is as follows: A source is placed at a selected distance from the detector aluminum cap. A spectrum of that particular source and geometry is accumulated in the MCA memory, then printed out on a teletype printer. This procedure is repeated for each source at each selected distance. Measurements are made at the following distances: 1., 2., 3., 4., 5., 10. and 16. cm.

The efficiency (photopeak efficiency) is calculated using the relation described in section 2.5. But since in this part of the work, the efficiency is measured as a function of distance, and at short source-to-detector distances the standard sources can not be considered as point sources any more, the efficiency measured with a finite source is multiplied by a correction factor to determine the efficiency for a point source. The point source photopeak efficiency is then given by:

$$\epsilon_p = \frac{N_c}{A_0 P_\gamma D.C} (1 + B)$$

where B is the correction factor for deviation from a point source, and it is given by (see appendix A):

$$B = \frac{1}{(x + d_0)^2} . (R^2 - \frac{H^2}{2}).$$

Fig. (3.1a) Detector-Sample Holder Assmbly.

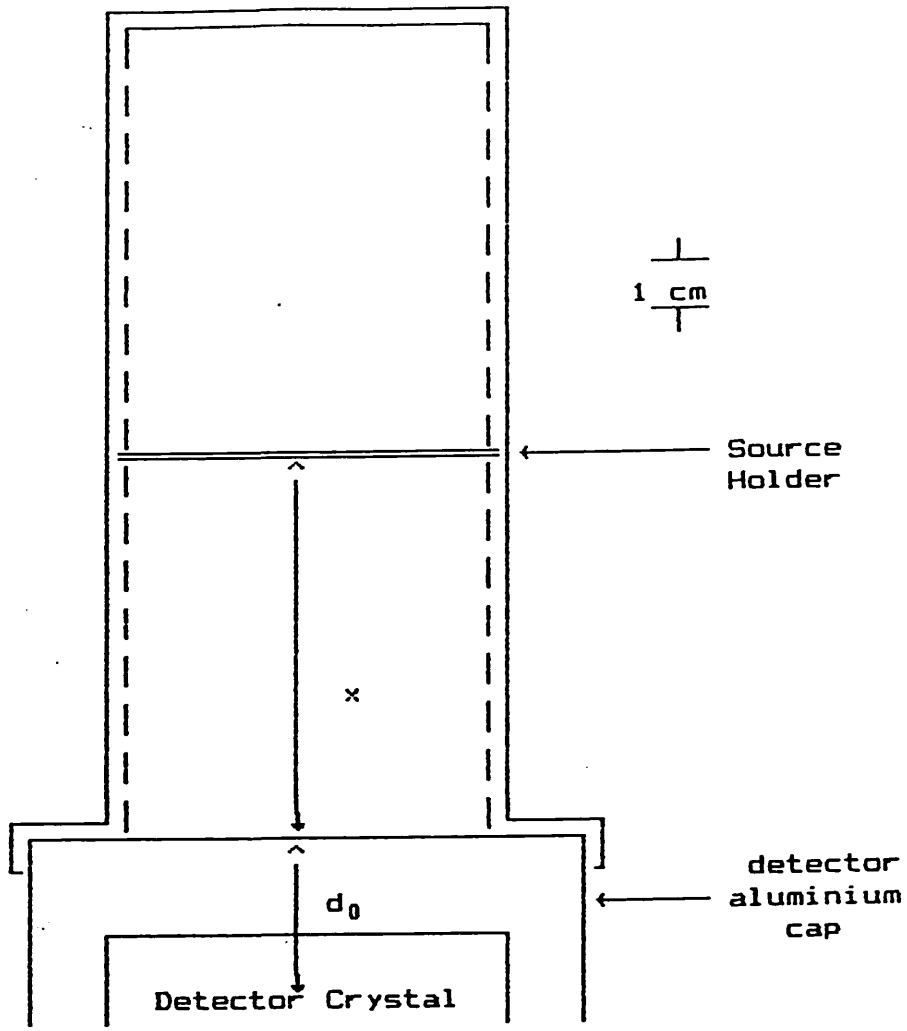

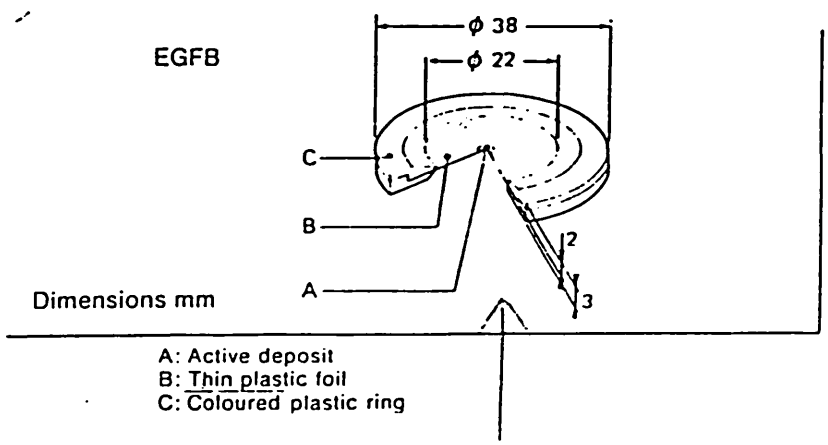

Fig. (3.1b) Source Assembly.

where R = 1.5 mm and H = 0.05 mm and they are the radioactive source radius and thickness respectively. d_0 is the distance of the detector below the aluminum cap as shown in fig 3.1b.

3.3 Limits On The Precision

In developing an empirical function, where the parameter values and their uncertainties depend entirely on some experimental measurements (random variables) and their uncertainties, a careful and accurate assessment of the measurement errors is necessary.

The uncertainty in the photopeak efficiency is calculated from the following relation (see section 2.5):

$$\left(\frac{\sigma_{\epsilon_P}}{\epsilon_P}\right)^2 = \left(\frac{\sigma_{N_C}}{N_C}\right)^2 + \left(\frac{\sigma_{A_0}}{A_0}\right)^2 + \left(\frac{\sigma_{P_\gamma}}{P_\gamma}\right)^2 + \left(\frac{\sigma_D}{D}\right)^2 + \left(\frac{\sigma_C}{C}\right)^2$$

However, since in this part of the work, the variation of efficiency with distance is being investigated, it is also necessary to estimate the uncertainty in the count rate due to uncertainties in determining the source position. These uncertainties arise from three sources which have to be added to the above relation:

(i) the location of the active material within the standard (σ_{sl})

(ii) the location of the standard source within the source holder (σ_{sm})

(iii) the location of the source holder (σ_{sh}).

So the factors to be added to the above equation are (see Appendix A):

$$\left(\frac{\sigma_{sl}}{N_c}\right)^2 + \left(\frac{\sigma_{sh}}{N_c}\right)^2 + \left(\frac{\sigma_{sm}}{N_c}\right)^2 + \left(\frac{\sigma_B}{N_c}\right)^2$$

The general least-square model is used to determine the parameters of the empirical function by minimizing the χ^2 function

$$\chi^2 = (Y-F(p))^T V^{-1} (Y-F(p)) \qquad (3.1)$$

where Y is a vector that contains the experimental measurements

F(p) is a vector containing the parameters that form the predicted measurement.

V is a vector containing the variance-covariance matrix of the experimental measurements

T and -1 refers to transpose and inverse repectively. If no correlation exists between experimental measurements then vector V is a diagonal matrix.

The variance-covariance matrix components are calculated as follows: Let i and r denote the i^{th} and r^{th} gamma-ray energy, j and s denote the source position (distance from the detector cap).

Consider $Cov(\sigma_{\epsilon_p}(ij), \sigma_{\epsilon_p}(rs))$

whenever the same source is used σ_A, σ_λ, $\sigma_{P\gamma}$, σ_{sl} and σ_B will be correlated with $\rho=1$, contributing the components:

$$\left[\frac{\sigma_{A_0}^2}{A_0^2} + \frac{\sigma_{P_\gamma}^2}{P_\gamma^2} + \frac{\sigma_D^2}{D^2} + \frac{\sigma_C^2}{C^2} + \frac{\sigma_{sl}^2}{N_C^2} + \frac{\sigma_B^2}{N_C^2} \right]$$

when the same shelf position (distance) used, the contribution to the covariance is

$$\frac{\sigma_{sh}(i).\sigma_{sh}(r)}{N_c(i).N_c(j)}.$$

The variance-covariance matrix is calculated from the following relation

$$Cov(\ \sigma_{\epsilon_p}(ij),\sigma_{\epsilon_p}(rs)\ ) =$$

$$\epsilon_p(ij).\epsilon_p(rs)\left[\frac{\sigma_{N_c}(ij).\sigma_{N_c}(rs)}{N_c(ij).N_c(rs)}\delta_{ir}.\delta_{js} + \frac{\sigma_{A_0}(ij).\sigma_{A_0}(rs)}{A_0(ij).A_0(rs)}\delta_{ir} + \right.$$

$$\frac{\sigma_D(ij).\sigma_D(rs)}{D(ij).D(rs)}\delta_{ir} + \frac{\sigma_C(ij).\sigma_C(rs)}{C(ij).C(rs)}\delta_{ir} +$$

$$\frac{\sigma_{P_\gamma}(ij).\sigma_{P_\gamma}(rs)}{P_\gamma(ij).P_\gamma(rs)}\delta_{ir} + \frac{\sigma_{sl}(ij).\sigma_{sl}(rs)}{N_c(ij).N_c(rs)}\delta_{ir} +$$

$$\frac{\sigma_B(ij).\sigma_B(rs)}{N_c(ij).N_c(rs)}\delta_{ir} + \frac{\sigma_{sh}(ij).\sigma_{sh}(rs)}{N_c(ij).N_c(rs)}\delta_{js} +$$

$$\left.\frac{\sigma_{sm}(ij).\sigma_{sm}(rs)}{N_c(ij).N_c(rs)}\right]$$

where $\delta_{xy} = \begin{cases} 1 & \text{for } x = y \\ 0 & \text{for } x \neq y \end{cases}$

3.4 Results and Empirical Formula

The measured efficiencies as a function of energy are shown in fig.3.2 for different distances. As can be seen, the variation of efficiency with energy for the same distance is a typical germanium response to gamma-rays, and they can be fitted to curves similar to the ones used in section 2.5 as shown in fig.3.2.

To find a relationship between efficiency and distance, first we consider the idea that a Ge(Li) detector can to some extent be considered as a point detector (the point where the detector can be considered to be concentrated) by introducing the idea of an effective interaction depth d_0 [55,56,57]. The effective interaction depth is defined as distance below the surface of the outside detector mounting can at which a gamma-ray of particular energy appears to interact or gives up all its energy.

This point detector behaviour can be shown by plotting $\epsilon_p^{-\frac{1}{2}}$ against distance x (where x is the measured distance from the top of the detector can). Fig.3.3 shows that behaviour for ^{241}Am (60-keV), ^{137}Cs (661-keV) and ^{65}Zn (1115-keV), except at short source-detector distances [43]. By letting $\epsilon_p \rightarrow \infty$ so that $\epsilon_p^{-\frac{1}{2}} \rightarrow 0$, or by extrapolating the straight lines of fig.3.3 to cut the X-axis, the value of d_0 is that value on the X-axis below the origin where it intercepts. And it can be seen that d_0 varies with energy.

If the point detector behaviour is correct, then the photopeak efficiency for a certain energy E_γ as a function of distance x can be written in terms of $d_0(E_\gamma)$ as:

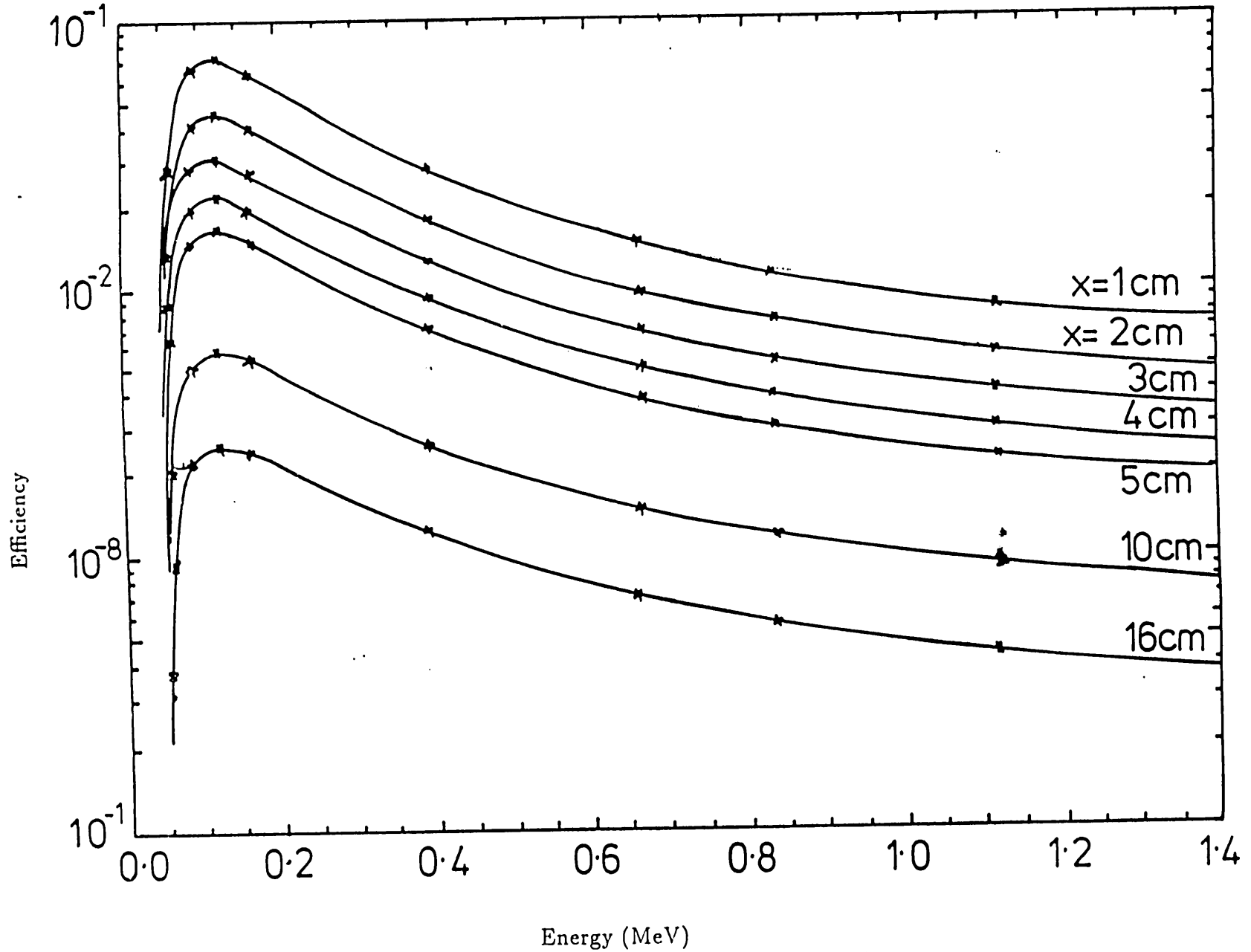

Fig. 3.2 Efficiency of Ge(Li) detector Vs Energy

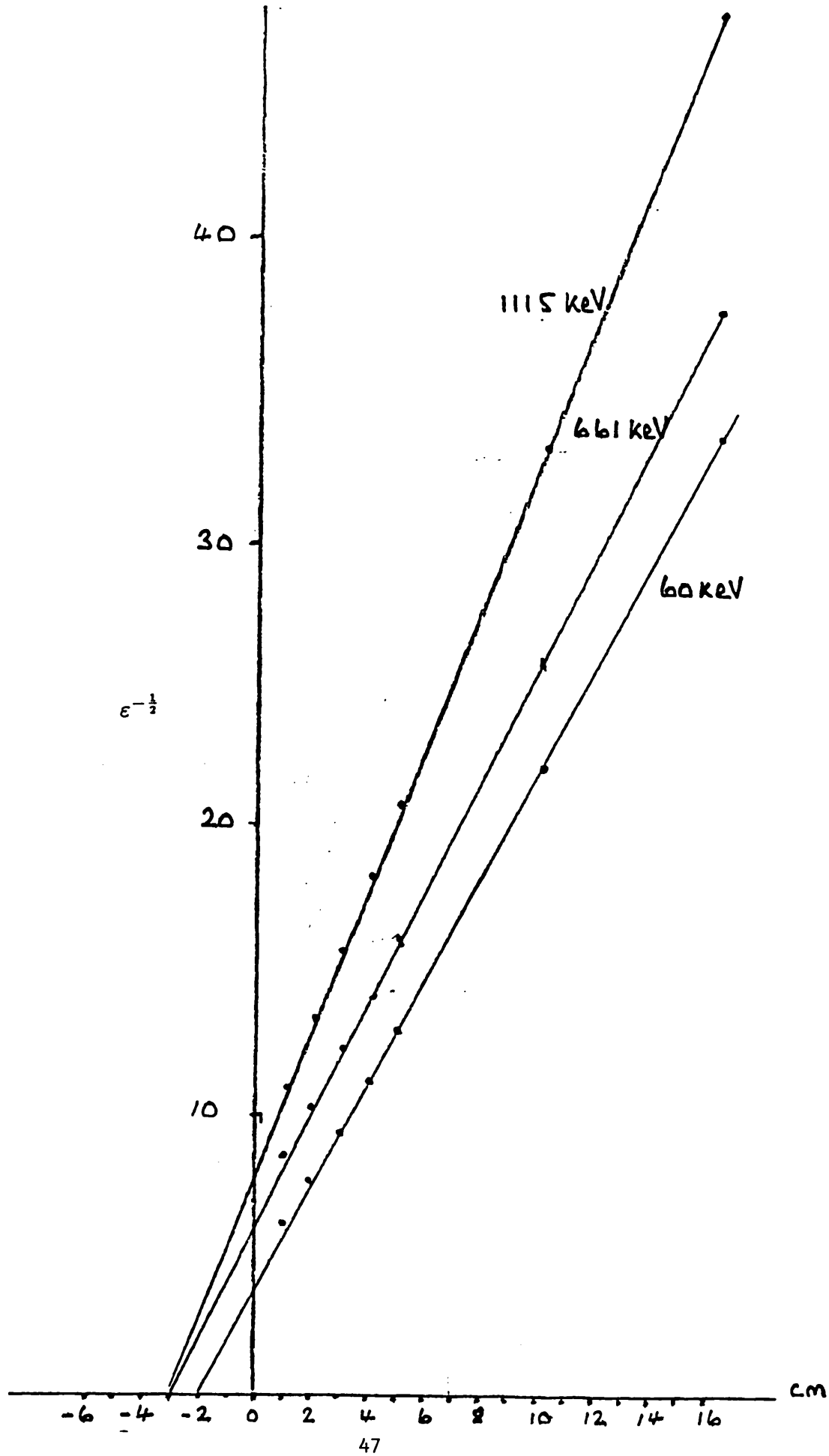

Fig. (3.3) Point Detector Behaviour of Ge crystal.

$$\epsilon_p(x,E_\gamma) \propto \frac{1}{(x+d_0(E_\gamma))^2} . \qquad (3.2)$$

KAWADE et al [57] proposed an energy and distance dependent correction factor on the basis of the point detector model. This is given by:

$$D(x,E_\gamma) = \frac{\epsilon_p(x,E_\gamma)}{\epsilon_p(20,E_\gamma)}$$

where $\epsilon_p(x,E_\gamma)$ and $\epsilon_p(20,E_\gamma)$ are the photopeak efficiencies at distance x and 20 cm respectively. So by knowing the efficiency for a particular energy at 20 cm, then the efficiency for that energy can be calculated for any distance. However, standard sources with energies identical to the ones of interest or under study are not always available.

In order to test the validity of equation (3.2) for representing efficiency as a function of distance, first we consider the Ge(Li) detector as a point detector, and then take into account the deviation from a point detector (at short distances).

The deviation from a point detector behaviour at short distances, is due to the deviation of the gamma-ray beam from a parallel beam [57]. KAWADE et al [57] showed that the deviation from a point detector behaviour at short distances can be represented by the functional form,

$$S(x,E_\gamma) = a(E_\gamma).e^{-b(E_\gamma).x}$$

where $S(x,E_\gamma)$ is the deviation factor for gamma-ray energy E_γ at distance x, and it decreases with increasing distances.

So the following functional form is proposed to

represent the variation of the photopeak efficiency of energy E_γ with distance:

$$\epsilon_p(x,E_\gamma) = \frac{P(E_\gamma)}{(x + d_0(E_\gamma))^2}\,(1 - S(x,E_\gamma)) \qquad (3.3)$$

where P(Eγ) is a geometry independent efficiency parameter.

The measured efficiencies of the same energy, at different distances are fitted to the functional form of equation (3.3). The general least-square method is used to determine the parameter values, and by performing minimization on equation 3.1, the goodness of fit is determined by studying the values of χ^2. The CERN library code MINUIT [32] is used to perform the minimization.

The chi-square values for the individual fits are shown in table 3.1 and the probability distribution of these χ^2 values is shown in fig.3.4. And as it can be seen that the χ^2 values pass the two tail test at 95% level. These results indicate that equation 3.2 is adequate for efficiency representation as a function of distance.

Fig.3.5 shows the measured efficiencies Vs distance for different energies, and the fitted efficiencies using equation 3.3 and the parameters obtained from the individual fittings.

The parameters $P(E_\gamma)$, $d_0(E_\gamma)$, $a(E_\gamma)$, $b(E_\gamma)$ and their errors obtained from fitting measured efficiencies of the same energy but different distances to equation 3.3 are listed in table 3.2. In order to develop an empirical formula from the measured efficiencies, which relates efficiency to energy and distance simultaneously, functional forms which represent these parameter variations with energy are required.

Table 3.1 The χ^2 values per 3 degrees of freedom for individual fits of efficiency versus distance for different energies

Energy in keV	χ^2 value for 3 degrees of freedom
60	5.79
88	3.66
122	1.61
165	2.16
391	3.72
661	1.53
834	2.72
1115	2.51

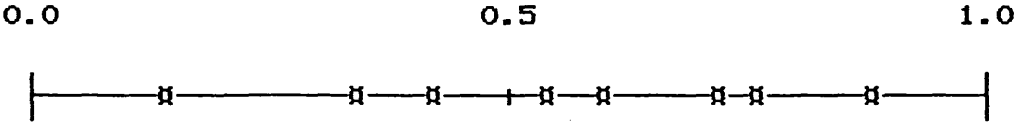

Fig.3.4 Probability distribution of χ^2 values

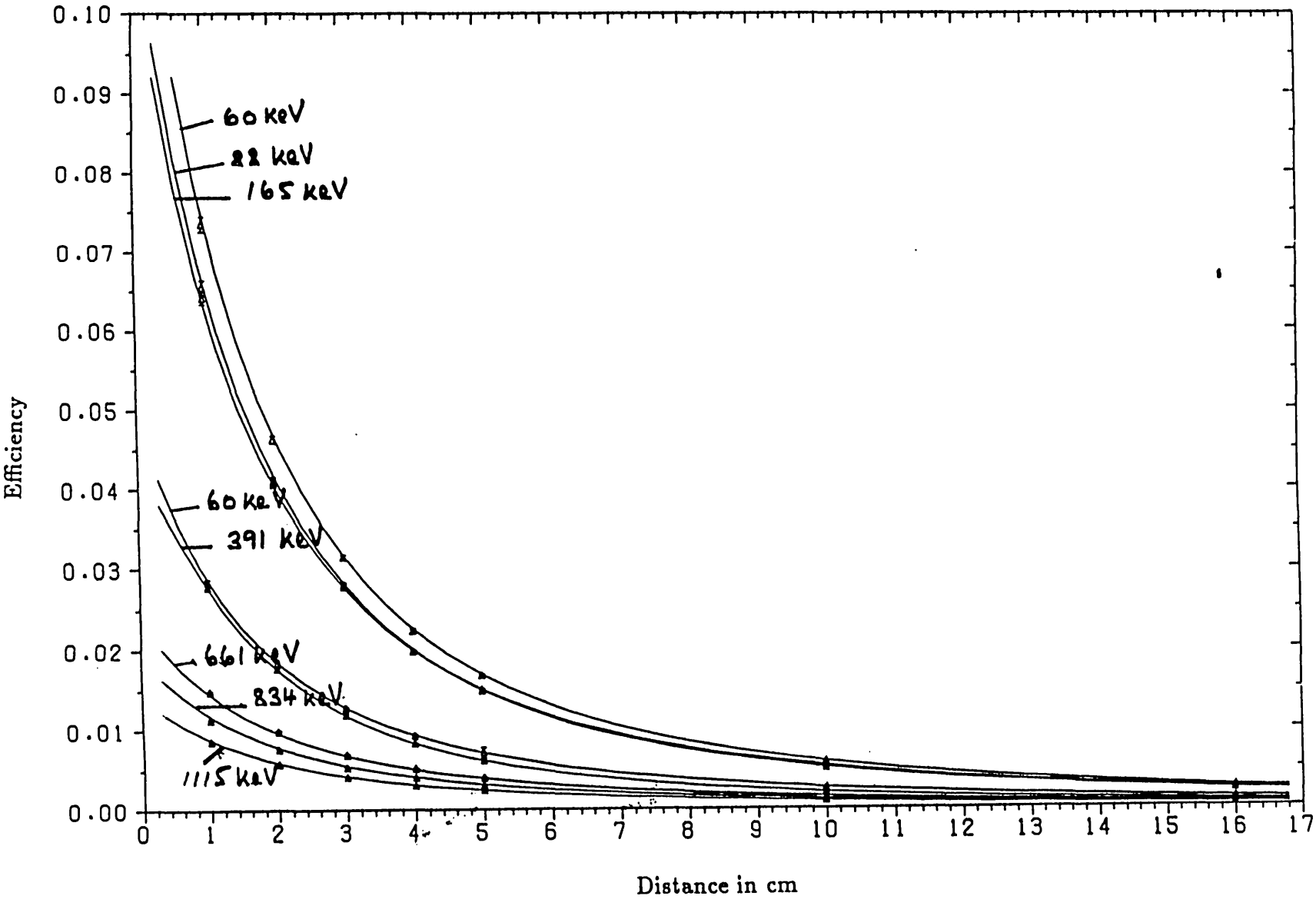

Fig. 3.5 Variation of Efficiency With Distance

Parameter $P(E_\gamma)$ is the inverse of the $(\text{slope})^2$ of the lines in fig.3.3. Different functions are tested to fit the $P(E_\gamma)$ values listed in table 3.2 and the best fit is obtained from the linear function proposed by AHMAD and GRAY [49] which represents the efficiency as a function of energy in the following form:

$$P(E_\gamma) = (p_1+p_2\ell nE_\gamma+p_3(\ell nE_\gamma)^2+p_4(\ell nE_\gamma)^3+p_5(\ell nE_\gamma)^5+p_6(\ell nE_\gamma)^7)/E_\gamma$$

where $p_1 = 0.018$, $p_2 = 0.00192$, $p_3 = 0.00264$, $p_4 = 0.00169$, $p_5 = -0.800\times10^{-6}$, $p_6 = -0.425\times10^{-5}$ and E_γ is in MeV.

The values of $P(E_\gamma)$ from table 3.2 and the above fitted function versus energy are shown in fig.3.6.

The values of the interaction depth parameter $d_0(E_\gamma)$, obtained from fitting the efficiency for each energy against distance and listed in table 3.2 are fitted to a functional form given by:

$$d_0(E_\gamma) = p_7 - p_8e^{-p_9E_\gamma}$$

where $p_7 = 3.26$ cm, $p_8 = 1.76$ cm, $p_9 = 0.00347$ and E_γ in MeV

The values of $d_0(E_\gamma)$ and the above fitted function are shown in fig.3.7. As can be seen from fig.3.7, as the gamma-ray energy $E_\gamma \to 0$, the value of d_0 is equal to p_7-p_8 which is the distance between the surface of the active volume and the outer detector cap. As E_γ goes to ∞ the value of d_0 is equal to p_7 the distance between the outer detector cap and the centre of the active volume. From the above parameters (p_7 and p_8), it suggests that the detector active crystal is of 3.52 cm vertical thickness and mounted 1.5 cm below the top aluminum cap.

Table 3.2 Determined parameter values from individual fitting of efficiency Vs distance for the same energy

Energy in keV	$P(E_\gamma)$	$d_0(E_\gamma)$
60	29.2 ± 0.61	1.82 ± 0.05
88	77.1 ± 1.0	1.96 ± 0.07
122	87.6 ± 1.1	2.14 ± 0.07
165	81.9 ± 1.2	2.32 ± 0.11
391	43.5 ± 0.9	2.79 ± 0.06
661	25.8 ± 0.7	3.11 ± 0.08
834	21.0 ± 0.6	3.12 ± 0.09
1115	17.1 ± 0.7	3.24 ± 0.05
	$a(E_\gamma)$	$b(E_\gamma)$
60	5.15 ± 0.31	0.75 ± 0.11
88	4.05 ± 0.35	0.62 ± 0.10
122	3.15 ± 0.25	0.67 ± 0.13
165	2.75 ± 0.41	0.63 ± 0.11
391	1.21 ± 0.31	0.83 ± 0.16
661	1.15 ± 0.36	0.78 ± 0.13
834	1.15 ± 0.32	0.84 ± 0.15
1115	1.05 ± 0.29	0.88 ± 0.18

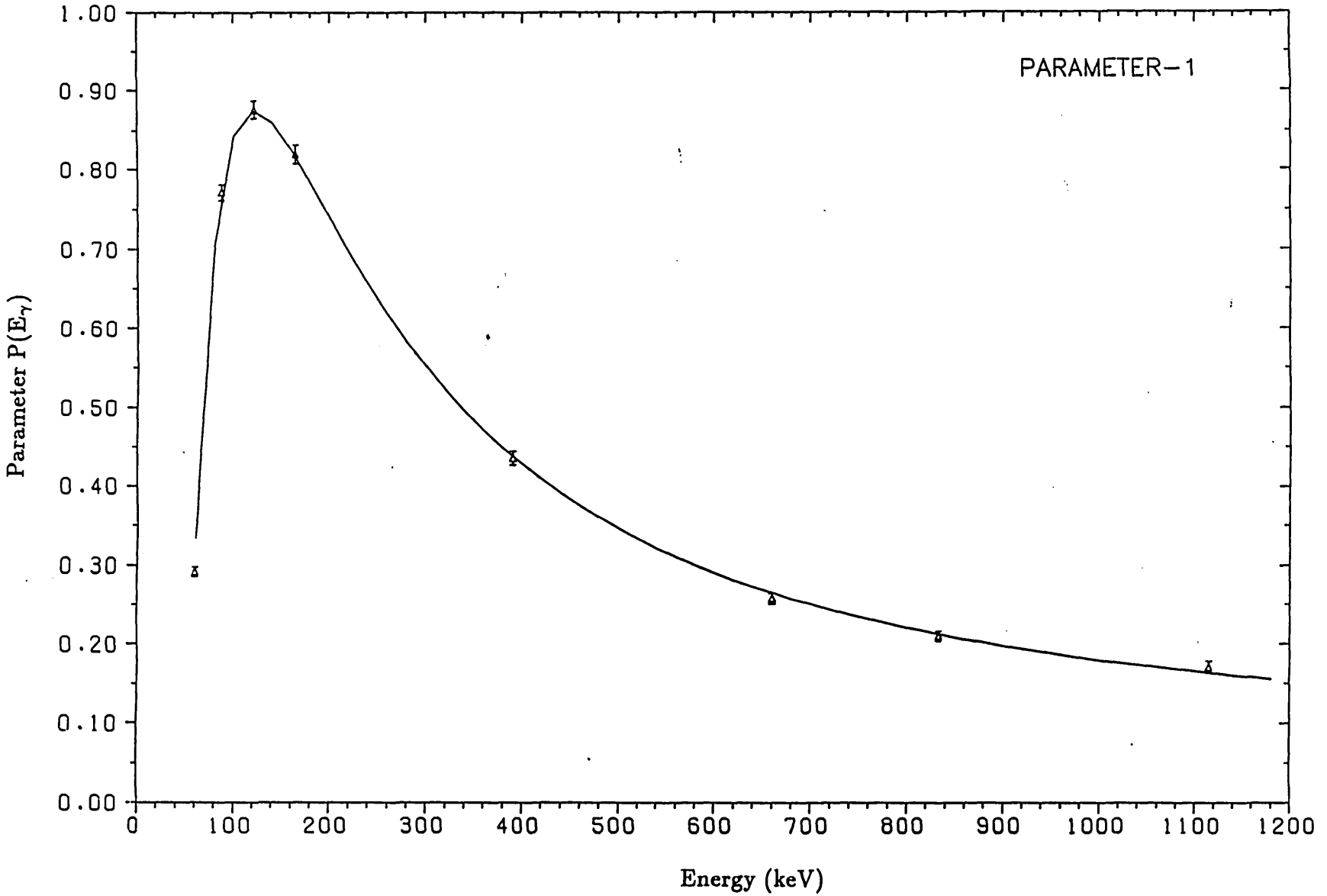

Fig. (3.6) Parameter $P(E_\gamma)$ Vs Energy.

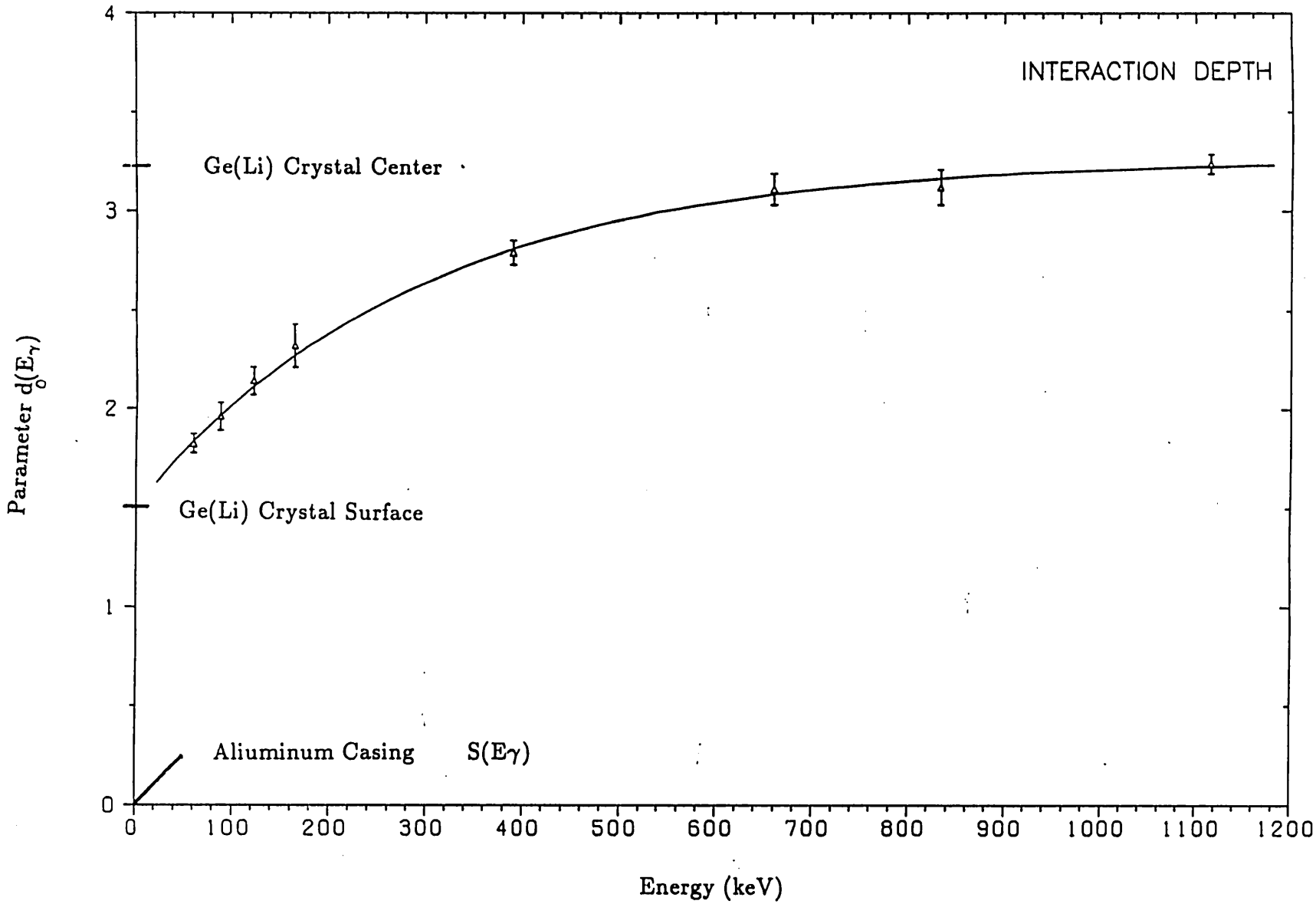

Fig. (3.7) Parameter $d(E_\gamma)$ Vs Energy.

The $a(E_\gamma)$ values are fitted to a function of the form,

$$a(E_\gamma) = p_{10}(E_\gamma.10^3)^{p_{11}}$$

where $p_{10} = 6.61$ and $p_{11} = -0.575$. The values of $a(E_\gamma)$ and the fitted function are shown in fig.3.8.

Due to the large errors on $b(E_\gamma)$ values, a straight line is adequate to represent the $b(E_\gamma)$ variation with energy as shown in fig.3.9, so that,

$$b(E_\gamma) = 0.72 = p_{12}$$

Using all the above relations, the functional form proposed to represent the photopeak efficiency as a function of distance and energy is:

$$\epsilon_p(x,E_\gamma) = \left[\frac{p_1+p_2\ell nE_\gamma+p_3(\ell nE_\gamma)^2+p_4(\ell nE_\gamma)^3+p_5(\ell nE_\gamma)^5+p_6(1\ell nE_\gamma)^7}{E_\gamma.(x + p_7 - p_8e^{-p_9E_\gamma})^2}\right]$$

$$.(1 - (p_{10}(E_\gamma.10^3)^{p_{11}}e^{-p_{12}.x})) \qquad (3.4)$$

This function was tested by fitting the experimental efficiencies of different energies at different distances simultaneously to equation (3.4) using a least-square model and performing minimization on a χ^2 function similar to that of equation (3.1).

The CERN library code MINUIT [32] is used to perform the minimization. The value of χ^2 obtained for 45 degrees of freedom is 54 which passes the chi-square test at 95% level. This is an indication that the photopeak efficiency can be represented by a functional form similar to that of equation

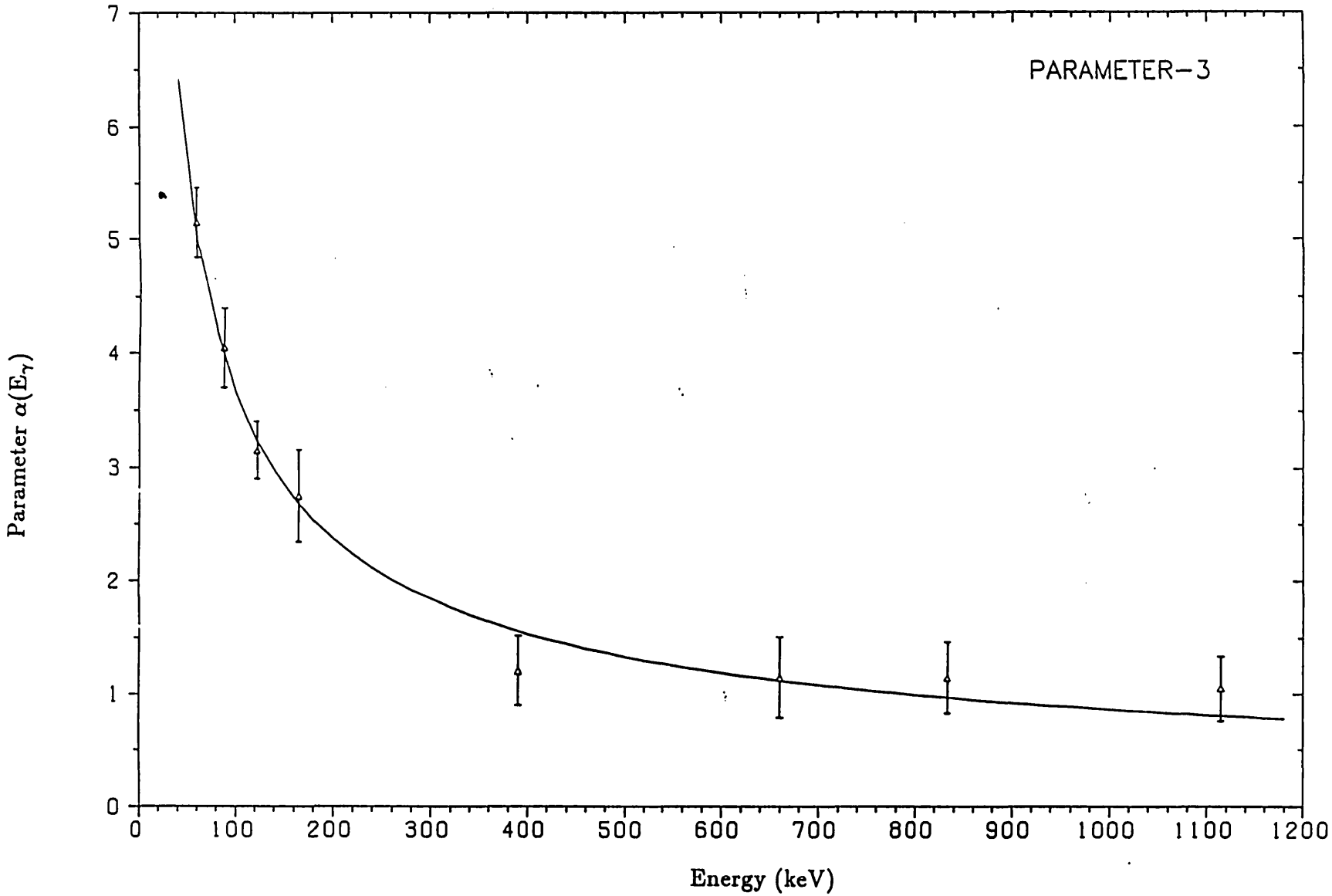

Fig. (3.8) Parameter $\alpha(E_\gamma)$ Vs Energy.

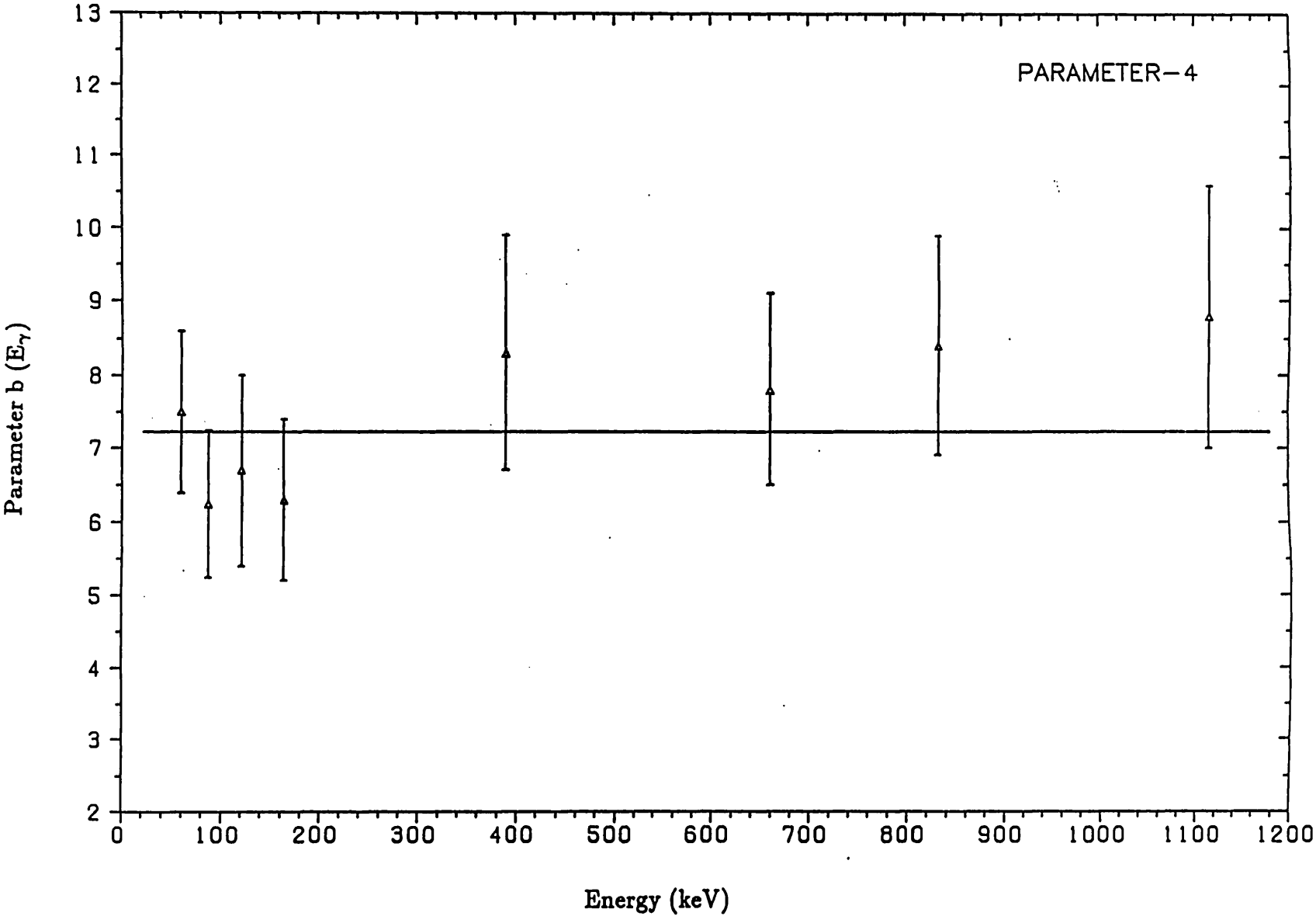

Fig. (3.8) Parameter b (E_γ) VS Energy

(3.4). The 11 parameter values and their standard deviations obtained from the final minimization are listed in table 3.3 and the correlation coefficients matrix which is required for error calculations of the calculated efficiencies is listed in table 3.4.

Table 3.5 shows the measured and calculated efficiencies and their errors. The error on the calculated efficiencies is given by:

$$\sigma^2_{\epsilon_{Pcal}} = \sum_{i=1}^{n} \sum_{j=1}^{n} \frac{\partial \epsilon_{Pcal}}{\partial p_i} \cdot \frac{\partial \epsilon_{Pcal}}{\partial p_j} \cdot \rho(i,j) \cdot \sigma_i \sigma_j$$

where σ_i is error of parameter i

$\rho(i,j)$ is the correlation between σ_i and σ_j and

n is the number of parameters.

3.5 Conclusion

Fig.3.10 shows the calculated deviation factor $S(x,E_\gamma)$ for ^{241}Am (60-keV), ^{57}Co (122-keV) and ^{65}Zn (1115-keV) versus distance. As can be seen this Ge(Li) detector behaves like a point detector for distances above 8 cm. The deviation of the experimental efficiencies from the calculated ones are shown in fig.3.11, where Δ is

$$\Delta = \frac{(\epsilon_{Pcal} - \epsilon_{Pexp})}{\epsilon_{Pexp}}$$

All values of Δ are within 1.5%, and most of them are within 0.8%.

When considering that the experimental efficiencies are measured with errors of 1.5% at short source-detector

distances to about 0.7% at large distances, the empirical function of equation (3.4) is a good representation of photopeak efficiency as a function of distance (one dimension) and energies between 50-1115 keV. The lower limit is due to the use of the linear six parameter function of AHMED and GRAY [49] in the empirical function.

Table 3.3 Determined parameter values from the fitting of efficiency Vs distance and energy simultaneously

parameter	Determined parameter values ± error
P_1	0.17801 ± 0.00012
P_2	$(0.21576 \pm 0.00043) \times 10^{-1}$
P_3	$(0.29003 \pm 0.00015) \times 10^{-1}$
P_4	$(0.15650 \pm 0.00005) \times 10^{-1}$
P_5	$(0.65213 \pm 0.00070) \times 10^{-3}$
P_6	$-(0.96802 \pm 0.00088) \times 10^{-4}$
P_7	3.258 ± 0.006
P_8	1.665 ± 0.013
P_9	3.397 ± 0.055
P_{10}	5.12 ± 0.32
P_{11}	$-.575 \pm 0.005$
P_{12}	0.75 ± 0.05

	1	2	3	4	5	6	7	8	9	10	11
2	.092										
3	-.097	.110									
4	.091	-.106	.111								
5	.092	-.107	.112	-.106	.						
6	.086	-.102	.107	-.100	-.101						
7	-.050	.059	-.062	.058	.059	.056					
8	.020	-.033	.038	-.029	-.029	-.021	.015				
9	-.046	.057	-.061	.055	.055	.050	-.030	.005			
10	-.081	.089	-.092	.091	.092	.090	-.051	.037	-.052		
11	-.067	.079	-.083	.078	.079	.074	-.043	.020	-.040	-.068	
12	.071	-.082	.086	-.082	-.082	-.078	.046	-.023	.043	.070	.061

Table (3.4) Correction coefficients of the determined parameters.

Table 3.5 Measured and calculated efficiebcies

Energgy (keV)	Efficiency (Measured)	Efficiency (calculatted)
60	$(0.278 \pm 0.004)\times10^{-1}$	$(0.281 \pm 0.006)\times10^{-1}$
88	$(0.177 \pm 0.002)\times10^{-1}$	$(0.175 \pm 0.002)\times10^{-1}$
122	$(0.735 \pm 0.009)\times10^{-1}$	$(0.738 \pm 0.008)\times10^{-1}$
165	$(0.647 \pm 0.008)\times10^{-1}$	$(0.655 \pm 0.006)\times10^{-1}$
391	$(0.261 \pm 0.004)\times10^{-1}$	$(0.257 \pm 0.002)\times10^{-1}$
661	$(0.148 \pm 0.002)\times10^{-1}$	$(0.148 \pm 0.001)\times10^{-1}$
834	$(0.116 \pm 0.001)\times10^{-1}$	$(0.115 \pm 0.001)\times10^{-1}$
1115	$(0.869 \pm 0.009)\times10^{-2}$	$(0.871 \pm 0.003)\times10^{-2}$
1 cm Source-Detector Distance		
60	$(0.178 \pm 0.002)\times10^{-1}$	$(0.180 \pm 0.003)\times10^{-1}$
88	$(0.411 \pm 0.005)\times10^{-1}$	$(0.409 \pm 0.003)\times10^{-1}$
122	$(0.463 \pm 0.005)\times10^{-1}$	$(0.466 \pm 0.003)\times10^{-1}$
165	$(0.410 \pm 0.004)\times10^{-1}$	$(0.416 \pm 0.003)\times10^{-1}$
391	$(0.178 \pm 0.002)\times10^{-1}$	$(0.180 \pm 0.001)\times10^{-1}$
661	$(0.988 \pm 0.009)\times10^{-2}$	$(0.984 \pm 0.004)\times10^{-2}$
834	$(0.767 \pm 0.008)\times10^{-2}$	$(0.769 \pm 0.003)\times10^{-2}$
1115	$(0.580 \pm 0.006)\times10^{-2}$	$(0.583 \pm 0.002)\times10^{-2}$
2 cm Source-Detector distance		

Table 3.5 Continued

60	$(0.120 \pm 0.001)\times10^{-1}$	$(0.122 \pm 0.002)\times10^{-1}$
88	$(0.282 \pm 0.003)\times10^{-1}$	$(.285 \pm .002)\times10^{-1}$
122	$(0.316 \pm 0.003)\times10^{-1}$	$(0.315 \pm 0.002)\times10^{-1}$
165	$(0.279 \pm 0.003)\times10^{-1}$	$(0.283 \pm 0.002)\times10^{-1}$
391	$(0.128 \pm 0.001)\times10^{-1}$	$(0.126 \pm 0.001)\times10^{-1}$
661	$(0.697 \pm 0.004)\times10^{-2}$	$(0.697 \pm 0.002)\times10^{-2}$
834	$(0.541 \pm 0.005)\times10^{-2}$	$(0.547 \pm 0.002)\times10^{-2}$
1115	$(0.417 \pm 0.003)\times10^{-2}$	$(0.414 \pm 0.001)\times10^{-2}$
3 cm Source-Detector distance		

60	$(0.851 \pm 0.008)\times10^{-2}$	$(0.863 \pm 0.012)\times10^{-2}$
88	$(0.198 \pm 0.002)\times10^{-1}$	$(0.197 \pm 0.001)\times10^{-1}$
122	$(0.225 \pm 0.002)\times10^{-1}$	$(0.225 \pm 0.001)\times10^{-1}$
165	$(0.201 \pm 0.002)\times10^{-1}$	$(0.204 \pm 0.001)\times10^{-1}$
391	$(0.935 \pm 0.011)\times10^{-2}$	$(0.928 \pm 0.003)\times10^{-2}$
661	$(0.519 \pm 0.004)\times10^{-2}$	$(0.518 \pm 0.002)\times10^{-2}$
834	$(0.404 \pm 0.004)\times10^{-2}$	$(0.407 \pm 0.001)\times10^{-2}$
1115	$(0.310 \pm 0.003)\times10^{-2}$	$(0.309 \pm 0.001)\times10^{-2}$
4 cm Source-Detector distance		

Table 3.5 Continued

60	$(0.631 \pm 0.006)\times10^{-2}$	$(0.639 \pm 0.008)\times10^{-2}$
88	$(0.149 \pm 0.001)\times10^{-1}$	$(.1481 \pm .0005)\times10^{-1}$
122	$(0.166 \pm 0.001)\times10^{-1}$	$(0.168 \pm 0.001)\times10^{-1}$
165	$(0.151 \pm 0.001)\times10^{-1}$	$(0.153 \pm 0.001)\times10^{-1}$
391	$(0.717 \pm 0.007)\times10^{-2}$	$(0.709 \pm 0.002)\times10^{-2}$
661	$(0.399 \pm 0.003)\times10^{-2}$	$(0.399 \pm 0.001)\times10^{-2}$
834	$(0.311 \pm 0.002)\times10^{-2}$	$(0.314 \pm 0.001)\times10^{-2}$
1115	$(0.239 \pm 0.002)\times10^{-2}$	$(0.239 \pm 0.001)\times10^{-2}$
5 cm Source-Detector distance		

60	$(0.215 \pm 0.002)\times10^{-2}$	$(0.217 \pm 0.002)\times10^{-2}$
88	$(0.513 \pm 0.004)\times10^{-2}$	$(0.511 \pm 0.002)\times10^{-2}$
122	$(0.592 \pm 0.004)\times10^{-2}$	$(0.588 \pm 0.002)\times10^{-2}$
165	$(0.539 \pm 0.005)\times10^{-2}$	$(0.542 \pm 0.001)\times10^{-2}$
391	$(0.265 \pm 0.002)\times10^{-2}$	$(0.265 \pm 0.001)\times10^{-2}$
661	$(0.153 \pm 0.001)\times10^{-2}$	$(0.1527 \pm 0.0003)\times10^{-2}$
834	$(0.120 \pm 0.001)\times10^{-2}$	$(0.1211 \pm 0.0002)\times10^{-2}$
1115	$(0.931 \pm 0.007)\times10^{-3}$	$(.927 \pm .001)\times10^{-3}$
10 cm Source-Detector distance		

Table 3.5 Continued

60	$(0.953 \pm 0.007)\times10^{-3}$	$(0.961 \pm 0.011)\times10^{-3}$
88	$(0.228 \pm 0.002)\times10^{-2}$	$(0.227 \pm 0.001)\times10^{-2}$
122	$(0.265 \pm 0.002)\times10^{-2}$	$(0.263 \pm 0.001)\times10^{-2}$
165	$(0.242 \pm 0.002)\times10^{-2}$	$(0.245 \pm 0.001)\times10^{-2}$
391	$(0.124 \pm 0.001)\times10^{-2}$	$(0.1227 \pm 0.0002)\times10^{-2}$
661	$(0.718 \pm 0.005)\times10^{-3}$	$(0.718 \pm 0.001)\times10^{-3}$
834	$(0.566 \pm 0.004)\times10^{-3}$	$(0.571 \pm 0.001)\times10^{-3}$
1115	$(0.441 \pm 0.003)\times10^{-3}$	$(0.439 \pm 0.001)\times10^{-3}$
16 cm Source-Detector distance		

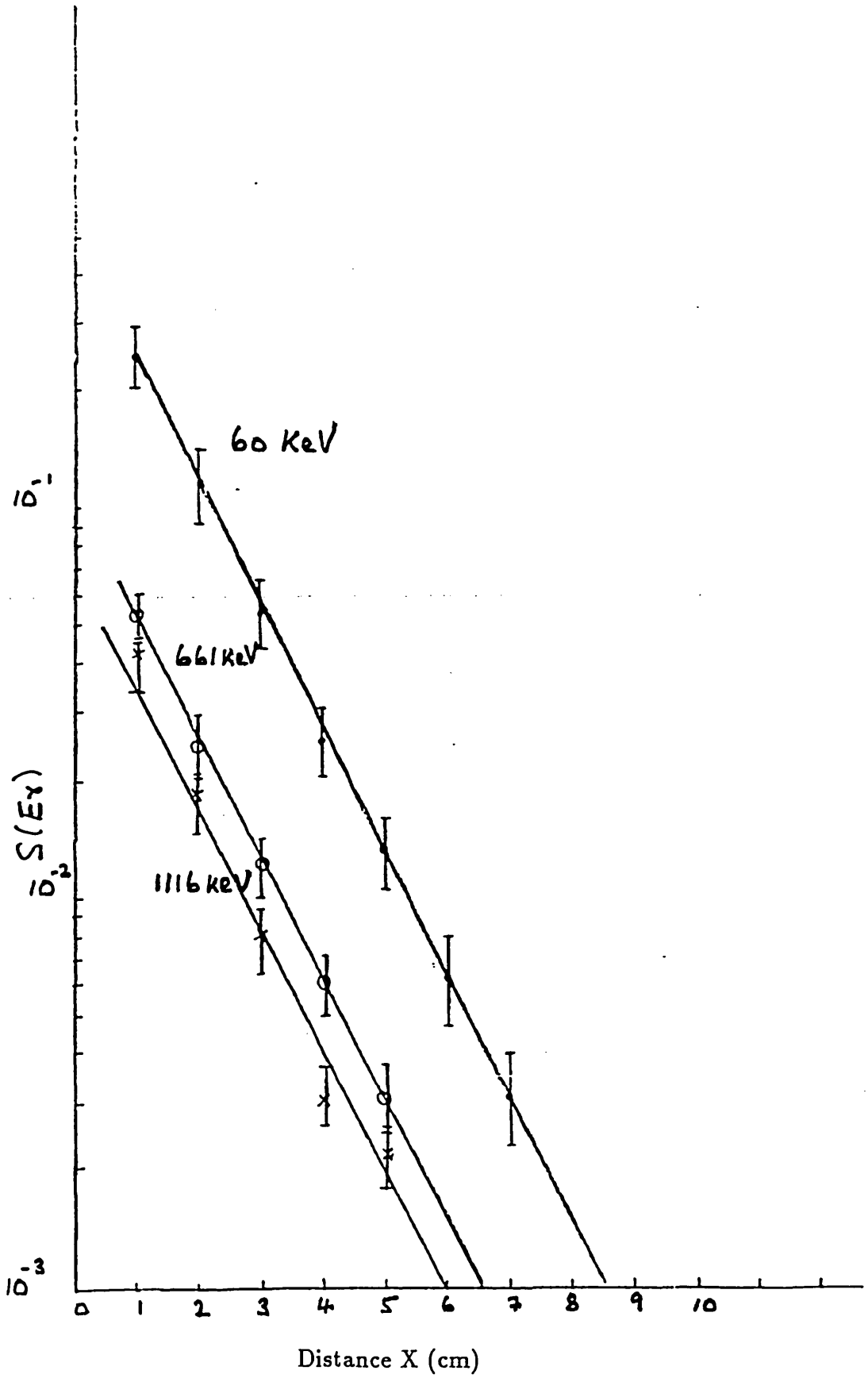

Fig. (3.10) S(Eγ) for various gamma-ray energies as a function of source-dtector distance.

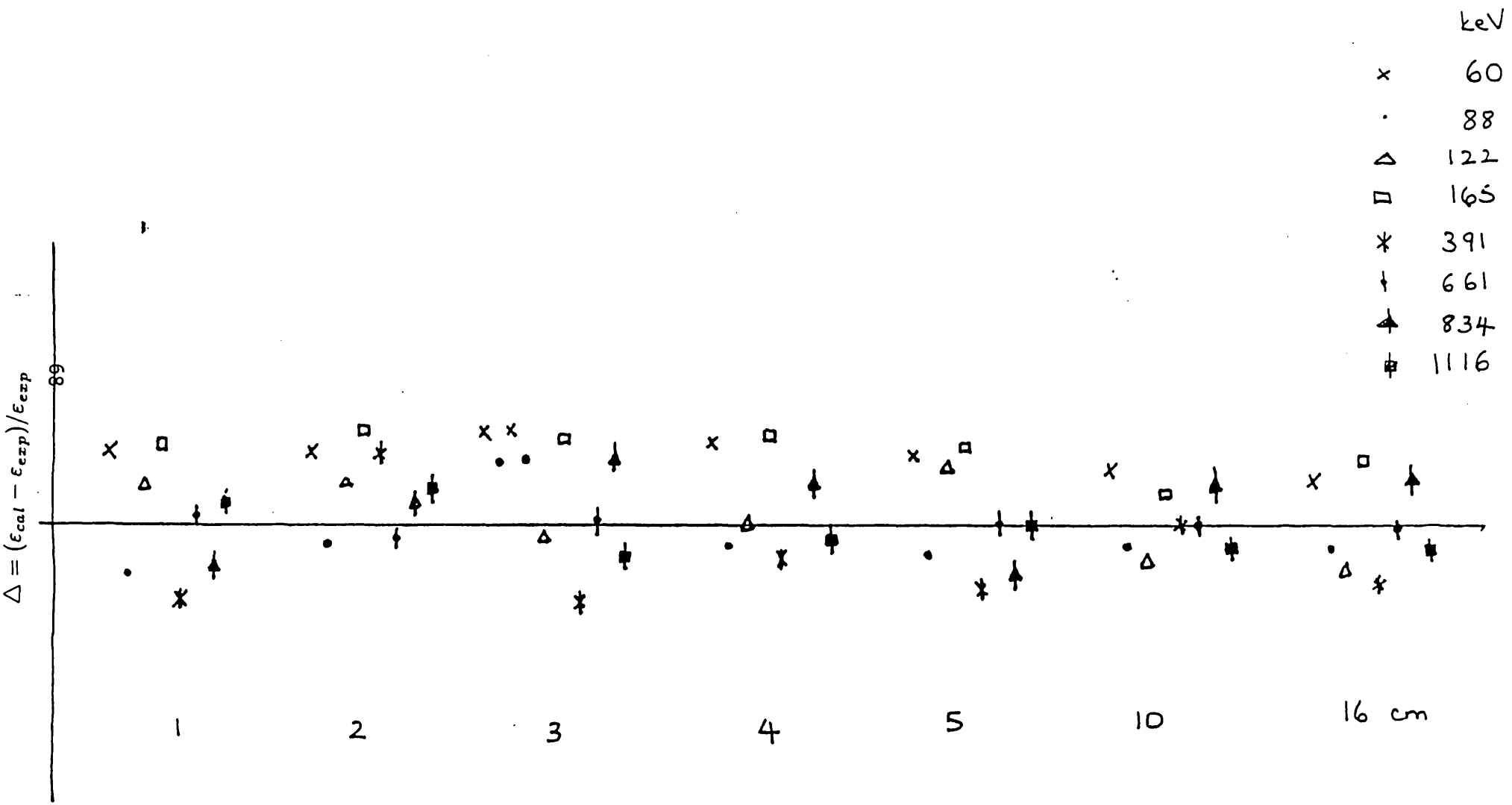

Fig. (3.11) Comparison of caculated efficiencies with experimental ones.

CHAPTER FOUR

FLUX PARAMETERIZATION

In almost all cases, when measuring the neutron flux spectra or when using neutron activation analysis, the quantity which is measured is the reaction rate. By definition the reaction rate per target atom of a given type is given by the product of the flux per unit energy interval, f(E), times the microscopic cross-section, $\sigma(E)$, integrated over all possible energies

$$= \int_0^{\infty} \sigma(E) f(E) dE.$$

The purpose of a neutron flux convention is to simplify the calculation of reaction rates in typical reactor spectra in which both thermal and epithermal neutron contributions are significant, hence enabling the unfolding of different information concerning the neutron flux and the nuclear data of the irradiated isotopes from the measured reaction rates.

4.1 Resonance Integral Convention

If the neutron absorption can be formulated in terms of resonance absorption at certain distinct energies, then the cross-section for absorption due to resonances (providing the resonances are not too close together) is considered to be the sum of single Breit-Wigner terms [2]

$$\sigma(E) = \sum_{i=1}^{N} \sigma_i(E) \qquad (4.1)$$

where i refers to the ith resonance

and $$\sigma_i(E) = \sigma_{ri} \left[\frac{E_{ri}}{E} \right]^{1/2} \left[\frac{\Gamma_i \Gamma_{\gamma i}}{\Gamma_i^2 + 4(E - E_{ri})^2} \right] \qquad (4.1a)$$

and E_{ri} is the energy of the ith resonance,

Γ_i is the full width of the ith resonance,

$\Gamma_{\gamma i}$ is the partial width of the ith resonance for radiative capture

σ_{ri} is the peak cross-section at that resonance energy.

It can be seen that when the resonance energy E_r is much greater than the neutron kinetic energy E, or asymptotically, as $E \to 0$ then

$$\sigma_i(E) \to \sigma_{ri} \left[\frac{E_{ri}}{E} \right]^{1/2} \left[\frac{\Gamma_i \Gamma_{\gamma i}}{\Gamma_i^2 + 4E_{ri}^2} \right]$$

and the cross-section essentially varies as (1/v), and hence the 1/v tail at low energies.

It also can be seen that above the resonance energy E_r as the neutron energy $E \to \infty$ then

$$\sigma_i(E) \to \frac{\sigma_{ri} E_{ri}^{1/2} \Gamma_i \Gamma_{\gamma i}}{4E^{5/2}}$$

the cross-section varies as the -5/2 power of the neutron energy. Because of this great variation with energy above a resonance [2], isotopes with resonances near the thermal

region are used as absorbers (e.g., cadmium) which will absorb all neutrons below a particular energy and transmit all those above it.

The integration of equation 4.1 between the energy limits $E_1 \rightarrow E_2$, is known as the resonance integral I_0 and is given by:

$$I_0 = \int_{E_1}^{E_2} \sigma(E) \frac{dE}{E}$$

and the reduced resonance integral I' is defined by:

$$I' = \int_{E_1}^{E_2} \sigma_R(E) \frac{dE}{E}$$

where $\sigma(E) = \sigma_R(E) + \sigma_{1/v}$ (4.1b)

the second term on the right hand side is the 1/v contribution to the resonance cross-section.

The upper limit of the integration, E_2 is normally taken as 1 Mev or infinity but the difference it makes to the integral value is not significant, but this is not true in the case of the lower limit E_1. STOUGHTON and HALPERIN [2] defined the resonance integral as:

$$I_0 = \int_{\mu kT}^{1\ Mev} \sigma(E) \frac{dE}{E}$$

and another convention used by HOGDAHL [3] defined the resonance integral as:

$$I_0 = \int_{E_{Cd}}^{1\ Mev} \sigma(E)\ \frac{dE}{E} \qquad (4.2)$$

where E_{Cd} is the cadmium cut-off energy and is defined below in section 4.5.

The most commonly used convention in activation analysis is that of equation (4.2) with a variation in the upper limit which is set to infinity. So the resonance integral is defined here as:

$$I_0 = \int_{E_{Cd}}^{\infty} \sigma(E)\ \frac{dE}{E} \qquad (4.3)$$

The cadmium cut-off energy E_{Cd} has been set at 0.55 eV for a cylindrical cadmium box with a uniform wall thickness of 1 mm as reported by GOLDSTEIN et al [58].

4.2 Neutron Flux Convention

The neutron flux convention adopted in this work is taken from AHMAD [15] and is similar to that used by BEREZNAI and MACMAHON [8] and also has features in common with that of DE CORTE et al [9]. The flux convention is reproduced here for the sake of clarity.

The reaction rate, or saturated activity per target

atom for an (n, γ) type of reaction is given by:

$$A = \Phi_{th}\,\sigma_{th} + \Phi_e\, I_0(\alpha) \qquad (4.4)$$

where Φ_{th} is the conventional Maxwellian thermal flux equal to $n_{th}v_0$, the product of the thermal neutron density, and the reference speed of 2200 m/s.

σ_{th} is the effective activation cross-section for cadmium absorbable neutrons, and it is given by:

$$\sigma_{th} = g\sigma_o + \frac{\Phi_e}{\Phi_{th}} \int_{\mu kT}^{E_{Cd}} \sigma(E)\, \frac{E_i^{\alpha}}{E^{i+\alpha}}\, dE \qquad (4.5)$$

where μkT is the energy dividing the thermal region from the epithermal region. The second term on the right hand side corresponds to the cross-section for neutrons in the energy interval between μkT and E_{Cd}

Φ_e is the epithermal flux per unit ℓnE at energy E_i, which is an arbitrary energy chosen for convenience to be 1eV. i.e

$$f_e(E) = \Phi_e \frac{E_i^{\alpha}}{E^{i+\alpha}} \quad \text{for } (E \geq \mu kT) \qquad (4.6)$$

where $f_e(E)$ is the epithermal neutron flux density, assumed proportional to $1/E^{i+\alpha}$, and

$I_0(\alpha)$ is the effective resonance integral in a non-1/E spectrum, defined similarly to equation (4.3), but it depends on the value of α:

$$I_0(\alpha) = \int_{E_{Cd}}^{\infty} \sigma(E) \frac{E_i^{\alpha}}{E^{i+\alpha}} dE \qquad (4.7)$$

To deal with the integral from μkT to E_{Cd} which appears in equation 4.5, the dimensionless quantity $W'(\alpha)$ is introduced, and it is given by:

$$W'(\alpha) = \frac{1}{\sigma_0} \int_{\mu kT}^{E_{Cd}} \left[\sigma(E) - \frac{g\sigma_0 v_0}{v} \right] \frac{E_i^{\alpha}}{E^{i+\alpha}} dE \qquad (4.8)$$

The factor g, is the well known Westcott g-factor that allows for deviations from a 1/v cross-section in the thermal region, and for 1/v cross-section g = 1. W' is the factor allowing for deviation from a 1/v cross-section between μkT and E_{Cd}, and for a 1/v cross-section $W' = 0$.

Combining equations 4.4, 4.5 and 4.8 gives:

$$A = \Phi_{th} g\sigma_0 + \Phi_e \left[\sigma_0 W'(\alpha) + g\sigma_0 f_i(\alpha) + I_0(\alpha) \right] \qquad (4.9)$$

where $$f_i(\alpha) = \int_{\mu kT}^{E_{Cd}} \frac{v_0}{v} \frac{E_i^{\alpha}}{E^{i+\alpha}} dE \qquad (4.10)$$

which can be easily evaluated for any value of α.

$I_0(\alpha)$ is not a nuclear constant because of its dependence on α, and in order to evaluate it from available nuclear data, use is made of the concept of the effective

resonance energy $\bar{E}_r$ introduced by RYVES and PAUL [6] and defined as "The energy of a single resonance which gives the same resonance activation effect as the actual resonances for the isotope". It is given by:

$$\frac{E_i^{\alpha}}{\bar{E}_r^{\alpha}} = \frac{I'(\alpha)}{I'(0)} = \frac{(I_0(\alpha) - g\sigma_0 f_2(\alpha))}{(I_0 - g\sigma_0 f_2(0))} \qquad (4.11)$$

where $f_2(\alpha)$ is the 1/v contribution to the resonance integral and is given by:

$$f_2(\alpha) = \int_{E_{Cd}}^{\infty} \frac{v_0}{v} \frac{E_i^{\alpha}}{E^{i+\alpha}} \, dE \qquad (4.12)$$

and by rearranging equation 4.11 we get

$$I_0(\alpha) = g\sigma_0 \left[\left(\frac{E_i}{\bar{E}_r} \right)^{\alpha} \left(\frac{I_0}{g\sigma_0} - f_2(0) \right) + f_2(\alpha) \right] \qquad (4.13)$$

Combining equations (4.9) and (4.13) gives

$$A = \Phi_{th} g\sigma_0 + \Phi_e g\sigma_0 \left[\frac{W'(\alpha)}{g} + f_1(\alpha) + \left(\frac{E_i}{\bar{E}_r}\right)^{\alpha} \left(\frac{I_0}{g\sigma_0} - f_2(0)\right) + f_2(\alpha) \right] \qquad (4.14)$$

In neutron activation analysis, when an element is irradiated in a neutron flux, then counted on a gamma-ray spectrometer the saturated activity per target atom is given by:

$$A = \frac{N_C M}{N_{AV} \theta P_\gamma m \epsilon_\gamma S D C t_C} \qquad (4.15)$$

where N_C is the net peak area in the gamma ray spectrum corrected for losses due to deadtime, pulse pile-up and coincidence summing.

M is the atomic mass of the target isotope

N_{AV} is Avogadro's number

θ is the natural isotopic abundance

P_γ is the gamma-ray emission probability

ϵ_γ is the gamma-ray photopeak efficiency

m is the element mass

S is the correction factor for saturation during irradiation

$$= (1 - e^{-\lambda t_i})$$

D is the correction factor for decay between irradiation and gamma-ray counting, as defined in chapter two

C is the correction factor for decay during counting, as defined in chapter two

t_C is the clock counting time.

When equating equations (4.14) and (4.15) the four items of nuclear data (θ, P_γ, M and $g\sigma_0$) which appear as a product are treated as a single compound nuclear constant, η, where

$$\eta = \theta P_\gamma g \sigma_0 M^{-1} \qquad (4.16)$$

and the advantage of η as a constant [11] is that, although the individual components of the nuclear data may not be known

precisely, the η constants themselves can be determined from reaction rate measurements with a precision greater than that of the individual compoments. SIMONITS et al [59] used a nuclear constant $K_{0,Au}$ where

$$K_{0,Au} = \frac{\theta P_\gamma g \sigma_0 M^{-1}}{(\theta P_\gamma g \sigma_0 M^{-1})_{Au}} = \frac{\eta}{\eta_{Au}} \qquad (4.17)$$

Combining equation 4.14, 4.15, 4.16 and letting E_i = 1eV gives

$$N_S = N_{AV}\eta \{\Phi_{th} + \Phi_e\left[\frac{W'(\alpha)}{g} + f_1(\alpha) + \bar{E}_r^{-\alpha}\left(\frac{I_0}{g\sigma_0} - f_2(0)\right) + f_2(\alpha)\right]\} \qquad (4.18)$$

where $N_s = N(mSDCt_c)^{-1}$

Its equivalent for cadmium covered activity is given by:

$$N_{Cd} = N_{AV}\eta \Phi_e\{(\bar{E}_r)^{-\alpha}\left[\frac{I_0}{g\sigma_0} - f_2(0)\right] + f_2(\alpha)\} \qquad (4.19)$$

and for the cadmium ratio ($R_{Cd} = \frac{N_S}{N_{Cd}}$)

$$R_{Cd}^{-1} = \frac{\Phi_{th}/\Phi_e + W'(\alpha)/g + f_1(\alpha)}{(\bar{E}_r)^{-\alpha}\left[\frac{I_0}{g\sigma_0} - f_2(0)\right] + f_2(\alpha)} \qquad (4.20)$$

Then in order to use the above equations in neutron activation analysis, it is necessary to know:

(1) five items of nuclear data, $\frac{W'(\alpha)}{g}$, η, λ, $\bar{E}_r$ and $\frac{I_0}{g\sigma_0}$

(2) two cut-off energies, μkT and E_{Cd}

(3) three neutron flux parameters, α, ϕ_{th} and ϕ_e

4.3 The Calculation of W'(α)

The non-1/v part of the resonance activity produced by neutrons with energies between the cadmium cut-off energy E_{Cd} and the epithermal cut-off energy μkT, is given by the quantity W'(α). It was shown by AHMAD [11] that W' is weakly dependent on α, and so it is justified to replace W'(α) by W' (i.e. for α = 0) and then W' is given by:

$$W' = \frac{1}{\sigma_0} \int_{\mu kT}^{E_{Cd}} \left[\sigma(E) - g\sigma_0 \left(\frac{E_0}{E} \right)^{1/2} \right] \frac{dE}{E} \qquad (4.21)$$

It is assumed that only the lowest principal resonance departs from the 1/v dependence between the limits of integration [60]. Using the Breit-Wigner formula of equation (4.1) for this resonance, the integral can be evaluated numerically using the Simpson rule technique [10], or one can use values of W' tabulated by RYVES and ZIEBA [60], which are shown in chapter six.

4.4 Calculation of $\bar{E}_r$

The effective resonance energy concept first introduced by RYVES and PAUL [6] then redefined later by L.MOENS et al [61] as:

$$(\bar{E}_r)^{-\alpha} = \frac{I_0'(\alpha)}{I_0'(0)} \qquad (4.22)$$

From equation (4.22) the effective resonance energy is a function of α, and thus in principle, is not a nuclear constant for a given isotope.

If the reduced resonance integrals in equation (4.22) are replaced by the summation of the integrated Breit-Wigner terms for all resonances, and it is assumed that the resonance peaks are narrow [61] then it can be shown that [61]:

$$(\bar{E}_r)^{-\alpha} = \frac{\sum_i \frac{\pi}{2} \frac{\sigma_i \Gamma_{\gamma i}}{E_{ri}} E_{ri}^{-\alpha}}{\sum_i \frac{\pi}{2} \frac{\sigma_i \Gamma_{\gamma i}}{E_{ri}}} \qquad (4.23)$$

where i refers to the i^{th} resonance and the other terms have the usual meanings.

When expanding $(E_r)^{-\alpha}$ in a series, the higher order terms can be omitted for sufficiently low E_r and/or low α-values such that

$$(E_r)^{-\alpha} = e^{-\alpha \ln E_r} = (1 - \alpha \ln E_r). \qquad (4.24)$$

Introducing the expression of equation (4.24) for E_r and E_{ri} into equation (4.23), and after some rearrangement [58] we obtain an expression for the effective resonance energy independent of α :

$$\ln\bar{E}_r = \frac{\sum_i \frac{\sigma_i \Gamma_{\gamma i}}{E_{ri}} \ln E_{ri}}{\sum_i \frac{\sigma_i \Gamma_{\gamma i}}{E_{ri}}} \qquad (4.25)$$

L.MOENS et.al [61], showed that the error introduced by the above approximation even for values of E_r as high as 4000ev and values of α as high as 0.1 is not more than 1.6%.

In the tabulated values of E_r by L.MOENS et al [62], resonances below the cadmium cut-off energy were not taken into account when calculating I_0' and $I_0'(\alpha)$. However since only few isotopes show resonances below that energy (e.g ^{176}Lu), these values are adequate for most isotopes.

4.5 Cadmium Cut-off Energy E_{Cd}

The 'effective cadmium cut-off' as defined in the IAEA report [63] is the energy E_{Cd} associated with a perfect filter (infinite absorption below the cut-off, and zero absorption above it) under which an irradiated material would have the same reaction rate as under a cadmium cover.

Because of the wide range of values of the cadmium cut-off energy E_{cd} reported in the literature, the European American Nuclear Data Committee recommended a value of E_{Cd} = 0.55 ev for a cylindrical cadmium filter with uniform wall thickness of 1mm and height/diameter ratio = 2. Details of the conditions are reported in GOLDSTEIN et al [58].

Resonance integrals are defined with a lower limit set at 0.55 eV, so it will be interesting to see the effect of using a different value say x, on the resonance integral I_0, so the change in I_o is

$$\Delta I_0 = \int_x^{0.55} \sigma(E) \frac{dE}{E} \qquad (4.26)$$

For these purposes we will assume that $\sigma(E) = g\sigma_0(E_0/E)^{1/2}$, and then equation (4.26) becomes

$$\Delta I_0 = 2g\sigma_0 E_0^{-1/2} \left[(x)^{-1/2} - (0.55)^{-1/2} \right] \qquad (4.27)$$

Since the quantity measured here is $I_0/g\sigma_0$ (see chapter six) rather then the resonance integrals then $\Delta(I_0/g\sigma_0)$ can be approximately expressed as a fraction of $I_0/g\sigma_0$ by the following expression:

$$\frac{\Delta(I_0/g\sigma_0)}{I_0/g\sigma_0} = \frac{0.318}{I_0/g\sigma_0} \left[(x)^{-1/2} - (0.55)^{-1/2} \right] \qquad (4.28)$$

for $E_0 = 0.0253$ ev.

A correct cadmium cut-off energy is needed as it can be seen from equation (4.28) specially at low $I_0/g\sigma_0$ ratio. For example consider the case of a 1/v detector with no resonance in the epithermal region, then $I_0/g\sigma_0 = 0.429$. Using equation (4.28), it is easily shown that for values of $x = 0.4$ and 0.7, $\frac{\Delta(I_0/g\sigma_0)}{I_0/g\sigma_0}$ varies between 17.25% and -11.35% respectively, and it decreases with increasing values of $I_0/g\sigma_0$ and becomes less sensitive to the accuracy of the cut-off energy E_{Cd}

For the thermal cut-off energy μkT, which divides the Maxwellian from the 1/E region, Westcott [1] suggested that the epithermal flux goes to zero at five times the energy

corresponding to the Maxwellian temperature T, i.e 5kT, where k is Boltzmann's constant. HUGHES [64] suggested a cut-off at the point where the Maxwellian flux is equal to that of the 1/E spectrum. This cut-off point turns out to be 0.17 ev for a graphite reactor [61]. STOUGHTON and HALPERN [2] concluded that the 5kT cut-off energy (i.e. approximately 0.13 ev) of WESTCOTT is a more appropriate choice, since the actual cut-off energy of HUGHES [64] will be more difficult to determine.

In non ideal spectra where the flux varies as $1/E^{1+\alpha}$, AHMAD [11] showed that the cut-off energies E_{Cd} and μkT slightly depend on α, but that these changes will have a negligible effect on $I_0/g\sigma_0$.

4.6 Determination of Flux Parameters

Methods of finding the flux parameters fall into three categories involving the measurement of

(a) Absolute activities of at least three isotopes to obtain the three parameters Φ_{th}, Φ_e and α

(b) cadmium covered absolute activities of at least two isotopes to estimate Φ_e and α

(c) cadmium ratios of two or more isotopes to estimate Φ_{th}/Φ_e and α.

Examples of the use of these methods are described in BEREZANI and MACMAHON [8] and DE CORTE et al [9,65]. The basis of these methods involves finding values of the parameters which satisfy equations 4.18, 4.19 and 4.20

Equation 4.18 can be used to find a unique set of flux parameters in an irradiation site by measuring the reaction rates in that site for three isotopes. The results will be

biased because of inadquate knowledge of the nuclear data especially for $I_0/g\sigma_0$ and η, and because of the errors in the measurements. The same reasoning is true for cadmium covered absolute activities and cadmium ratio, when measuring the reaction rates of two isotopes.

For this reason, the number of reaction rates to be used should be more than the number of flux parameters to be determined, hence producing an over determined system in order to reduce the biases and to obtain direct information on the size of the uncertainties in the results. This technique, known as the generalized least-square technique (MARTIN [66]), was first applied to this type of problem by AHMAD [11], with reference to bare irradiations using equation (4.18), but the same principles are applicable in the other two methods.

In a bare irradiation, for example , when more than three reaction rates are measured no one set of values ϕ_{th}, ϕ_e and α can be found which will excatly reproduce the measured values when applied in equation (4.18). This is because of the presence of uncertainties or errors in all measured quantities which must be taken into account when seeking the values of ϕ_{th}, ϕ_e and α which minimize the appropriate weighted square deviations between measured and calculated values. Since the nuclear data are also based on measurements with uncertainties, the best values must not be assumed equal to the values evaluated from the literature. AHMAD [11] and JEFFERIES [10] applied this technique with the above flux convention to determine values of the nuclear data (η and $I_0/g\sigma_0$) and the flux parameters simultaneously by evaluating the best values of η and $I_0/g\sigma_0$ from the reported literature values and then using these values as input measurements, then

obtaining values with improved uncertainties (see Ahmad [15] for more details). The same technique is used by GHURBAL [13], in which he provided simultaneously determination of reduced resonance integrals and effective resonance energies.

For some isotopes there are not enough literature data to perform any sort of statistical evaluation of the best values, to be used as input measurements. Instead new values for the nuclear data ($I_0/g\sigma_0$, and η) should be determined together with the flux parameters which will best fit equation 4.18 or equation 4.19 and 4.20 depending on measuring technique.

In order to determine the flux parameters Φ_{th}, Φ_e and α and the nuclear data $I_0/g\sigma_0$ and η simultanuosly, they are considered as unknown parameters to be determined by measuring the saturated activities for n isotopes at m different channels so that for bare irradiation the minimum number of measurements required to solve equation (4.18) is

$$= 3m + 2n$$

and for cadmium covered irradiation the minimum number of measurements is

$$= 2m + 2n$$

When estimating a number of different parameters simultaneously by the least square method [66], it implies that the estimates of the parameters are statistics having a multivariant normal distribution. The probability distribution function for such a distribution involves not only the means and the variances of each parameter but also the covariances between each pair of parameters. An estimate

of the set of these quantities for each parameter constitutes a complete specification of the probability distribution function of the parameters, which can be used in any subsequent calculation to provide a proper estimate of errors.

The function to be minimized in order to find the least-square estimates of the flux parameters and the nuclear data is

$$\chi^2 = \left[E - C \right]^T \left[V_e \right]^{-1} \left[E - C \right]$$

where E is the vector of experimental reaction rates

C is the vector of calculated reaction rates (which is a function of the parameters ϕ_{th}, ϕ_e, α, $I_0/g\sigma_0$ and η)

V_e is the variance-covariance matrix of the experimental reaction rates.

All the quantities in square brackets are matrices, and T indicates the transpose of a matrix and -1 the inverse.

This technique is applied in chapter six to determine new nuclear data values (η and $I_0/g\sigma_0$) for some isotopes and providing a test for the flux model in predicting these nuclear data from measured saturated activities alone.

CHAPTER FIVE

FLUX NORMALIZATION

The use of any method in neutron activation analysis (NAA) makes use of the assumption that all samples are irradiated in the same flux. However since the irradiation of the standards and samples are usually done at different times, unless the flux is constant a method for flux normalization is required to obtain any meaningful results.

A method for studying the extent of flux variation in the Imperial College reactor and its effect on the reaction rates is proposed and used to reduce the uncertainty due to flux perturbation.

5.1 Normalization Method

The standard method for flux normalization [10] is to record the number of counts accumulated in a neutron counter at that irradiation site, during the same irradiation time of each sample or using the (n,γ) reaction from the same element irradiated with each sample, then gamma counted and then all measurements are normalized to a mean count rate.

However, in a thermal reactor where both thermal and epithermal neutron contributions to the reaction rate are significant, the measurements have to be normalized to a mean thermal and epithermal flux. Since the thermal flux is characterized by temperature while the epithermal flux is characterized by energy (see chapter four for details), their variations with time are expected to be independent of each other.

If an isotope is irradiated in constant thermal and epithermal fluxes, for a time t, then the activity induced in the isotope at the end of the irradiation is given by:

$$A = m \left[\alpha \Phi_{th} + \beta \Phi_e \right] (1 - e^{-\lambda t}) \qquad (5.1)$$

where α and β are constants of the irradiated isotope and the irradiation position, m is the isotope mass and the factor $(1-e^{-\lambda t})$ is the build-up factor of the activity during irradiation.

Consider the activity due to thermal neutrons only, it will be given by:

$$A_{th} = m \alpha \Phi_{th}(1 - e^{-\lambda t}) \qquad (5.2)$$

and the activity due to epithermal neutrons only is,

$$A_e = m \beta \Phi_e(1 - e^{-\lambda t}) \qquad (5.3)$$

Let the factor δ_1 account for deviation of the thermal flux from an otherwise constant flux and δ_2 account for deviation of the epithermal flux from a constant flux. Equations (5.2) and (5.3) now become:

$$A_{th} = \delta_1 m \alpha \Phi_{th}(1 - e^{-\lambda t}) \qquad (5.4)$$

$$A_e = \delta_2 m \beta \Phi_e(1 - e^{-\lambda t}) \qquad (5.5)$$

For constant thermal and epithermal fluxes, then $\delta_1=\delta_2=1$ For variable fluxes, but variable in the sense that $\delta_1=\delta_2\neq1$, then the standard normalization method [10] can be used. For variable fluxes, so that, $\delta_1 \neq\delta_2 \neq1$, then the method to be used

is to normalize all measurements to a mean thermal and epithermal flux.

So in order to decide on the normalization method, the variations of δ_1 and δ_2 are to be monitored with time. Also it is the number of reactions induced in purely thermal and purely epithermal detectors respectively.

5.2 Experimental Procedure and Method

The irradiation site is in the Imperial College Reactor, which is a tank type reactor. The fuel is 80% enriched ^{235}U and the moderator is light water, which acts also as coolant. The reactor has facilities for many samples to be irradiated in different irradiation channels at the same time. The irradiation channel used for this work is known as I.C.I.S, the in core irradiation system, and has a ratio of thermal to epithermal flux of $\simeq$ 17.

An ionization chamber is installed in the core and is used to monitor the power output. The power output is kept at 100 kW by means of raising and lowering of a fine control rod positioned near the centre of the core, also the temperature of the water outlet from the core is monitored by a thermocouple positioned above the core.

In order to find δ_1 and δ_2, an isotope which is mainly sensitive to thermal neutrons and another mainly sensitive to epithermal neutrons are to be irradiated together at the same position for a short period during which Φ_{th} and Φ_e can be considered constant. This procedure is repeated at different times in order to cover a wide range of factors (different reactor operators, different samples in the core, etc).

A combination of isotopes satisfying the requirements to find δ_1 and δ_2, is found in the element lutetium. This element has one stable isotope, ^{175}Lu, and one, ^{176}Lu which for practical purposes is also stable since it has a half-life of 10^{10} years. Neutron capture in lutetium produces two radioactive nuclides, ^{176m}Lu and ^{177}Lu (the m indicates that the decay proceeds from a metastable level or excited state of the ^{176}Lu nucleus rather than from the ground state). Both nuclides beta decay to excited states of hafnium isotopes which, in turn, decay to their ground states by gamma-ray emission. The $^{175}Lu(n,\gamma)^{176m}Lu$ reaction is used to monitor the epithermal flux because of its high epithermal to thermal cross-section, and $^{176}Lu(n,\gamma)^{177}Lu$ reaction to monitor the thermal flux because the thermal to epithermal ratio in I.C.I.S is $\simeq$ 17 and the epithermal to thermal cross-section of ^{177}Lu is $\simeq$ 1, so that the main contribution to the reaction rate will be due to thermal neutrons.

Two thin foils (7 mm diameter) of aluminium with 1% lutetium are positioned back to back in a polythene capsule and then irradiated in I.C.I.S for 5 min. The same procedure is repeated with two foils of Al.1%.Lu irradiated for the same length of time at the same irradiation position at different times of the day and different times of the week, and then each foil is gamma counted on a Ge(Li) detector (for details of the gamma spectroscopy system see chapter 3) for 2000 sec. The 88-keV gamma-ray from ^{176m}Lu and the 208-keV from ^{177}Lu are used to measure the number of reactions in the corresponding isotope. For each measurement the outlet temperature of the coolant was recorded.

5.3 Results and Discussion

The results, in number of counts in 2000 sec per unit mass from each foil for ^{176m}Lu and ^{177}Lu, are shown in fig.5.1 and fig.5.2 respectively. The means from each measurement are shown in fig.5.3 and 5.4 respectively. The contributions to the calculated uncertainty are from counting statistics and weighing errors. Using the mean-square deviation, the means from fig.5.3 and 5.4 gave a χ^2 values of 132 and 232 respectively for 24 degrees of freedom which are very large, and they failed the χ^2 test at 99.9% level. This suggests a definite variation in the number of reactions greater than the measured uncertainties. To find from these results whether the main source of variation in the measurements is due to counting and weighing statistics or flux perturbation, the analysis of variance and expected mean squares for the one-way classification (ANOVA) [67] is applied assuming all measurements have the same counting and weighing errors. This test gives an idea of the variation within each group of measurements compared to the variation between groups, and it has an F distribuion [67].

For the results of ^{176m}Lu and ^{177}Lu from fig.5.1 and 5.2 for 24 independent groups of measurements and two measurements in each group, the recorded F-values of 4.94 and 7.13 respectively fail the F-test at .999 probability level which indicates a variation in the measurements due mainly to flux perturbation.

To find the variation of the thermal flux with respect to the epithermal flux or δ_1/δ_2, the ratio of the number of reactions from $^{176m}Lu/^{177}Lu$ of the same foil is plotted in fig.5.5 for different measurements. Applying the

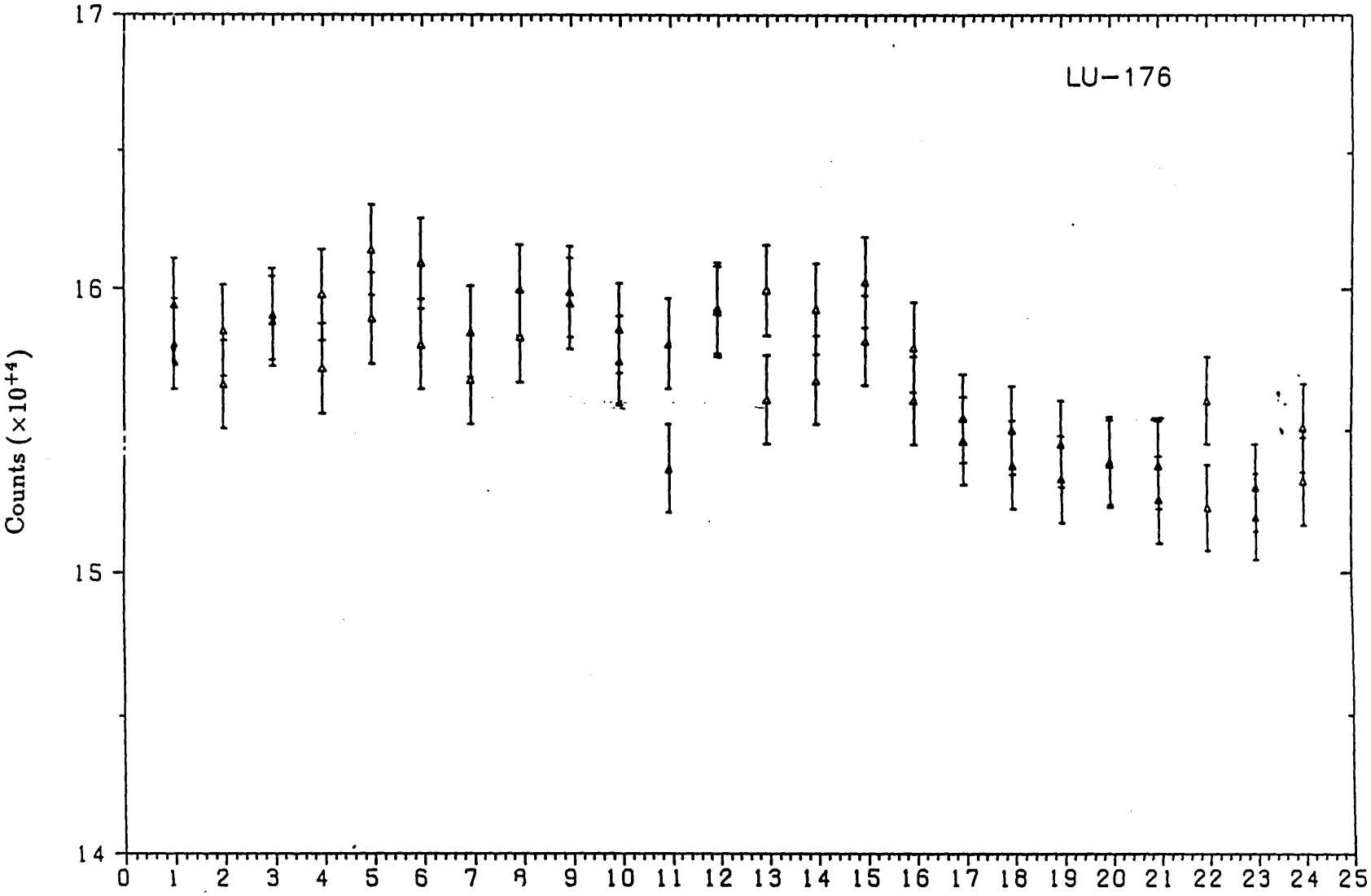

Fig. (5.1) Result of ^{176}Lu.

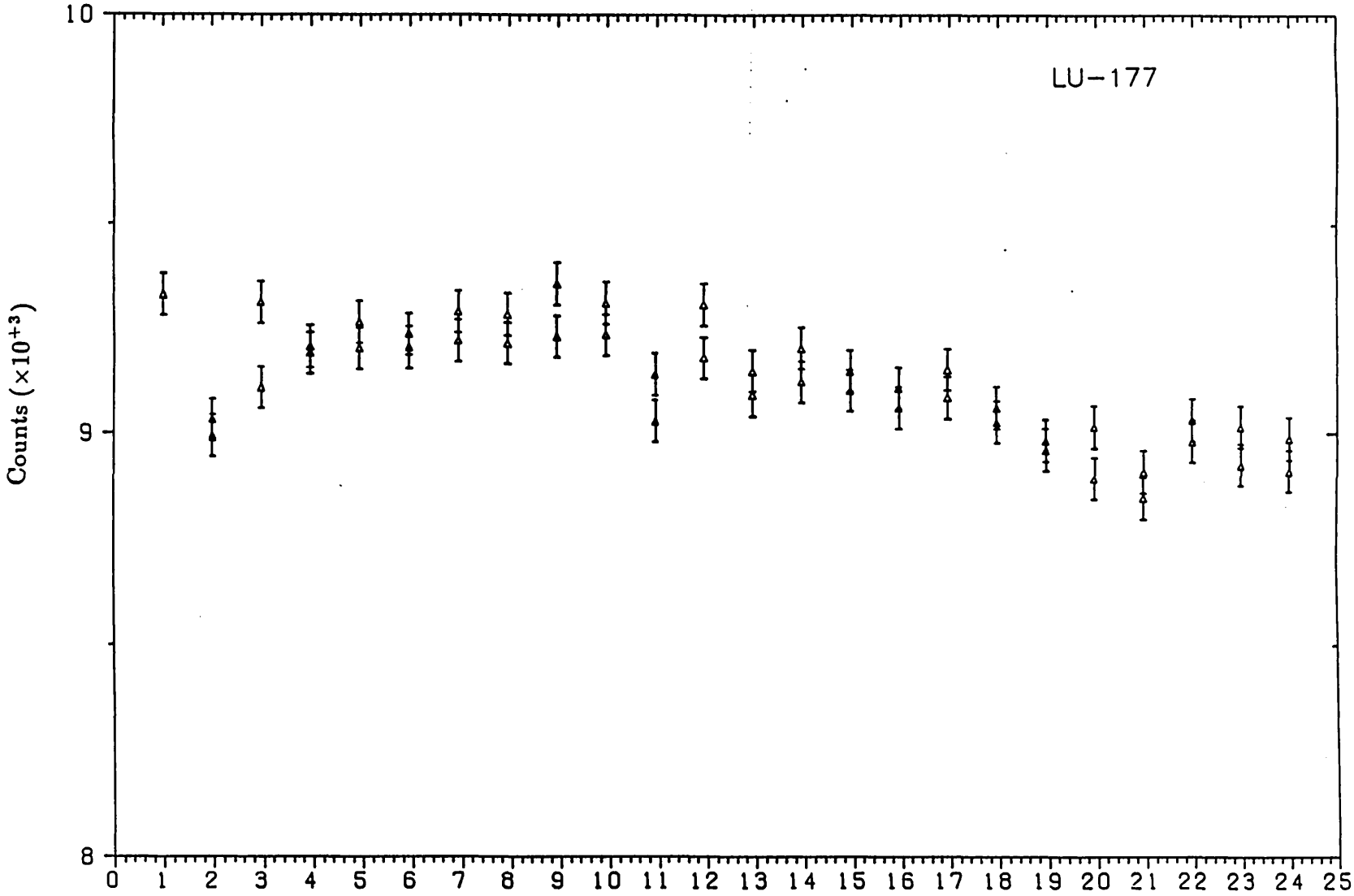

Fig. (5.2) Result of ^{177}Lu.

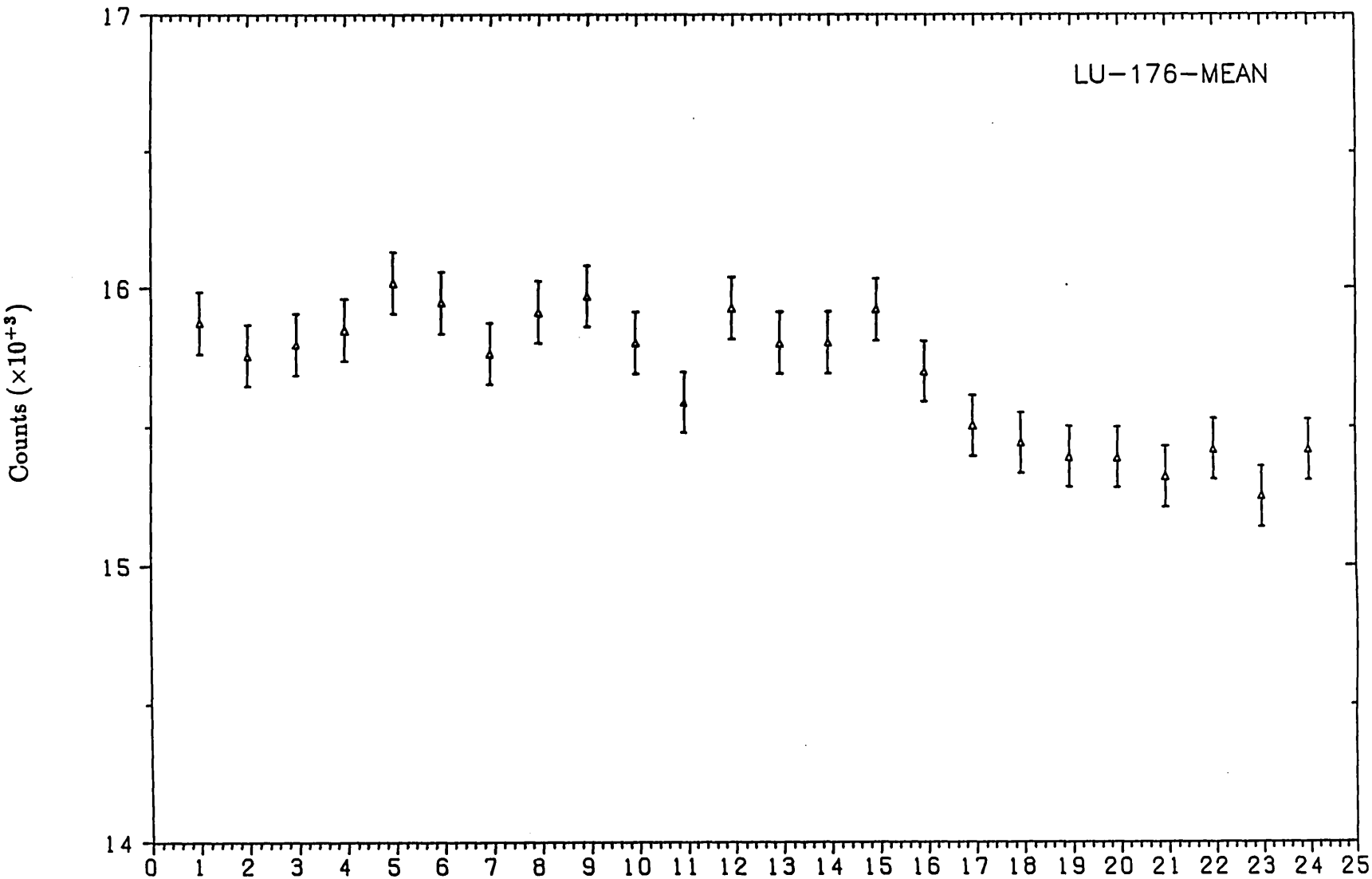

Fig. (5.3) Result of ^{176}Lu (mean).

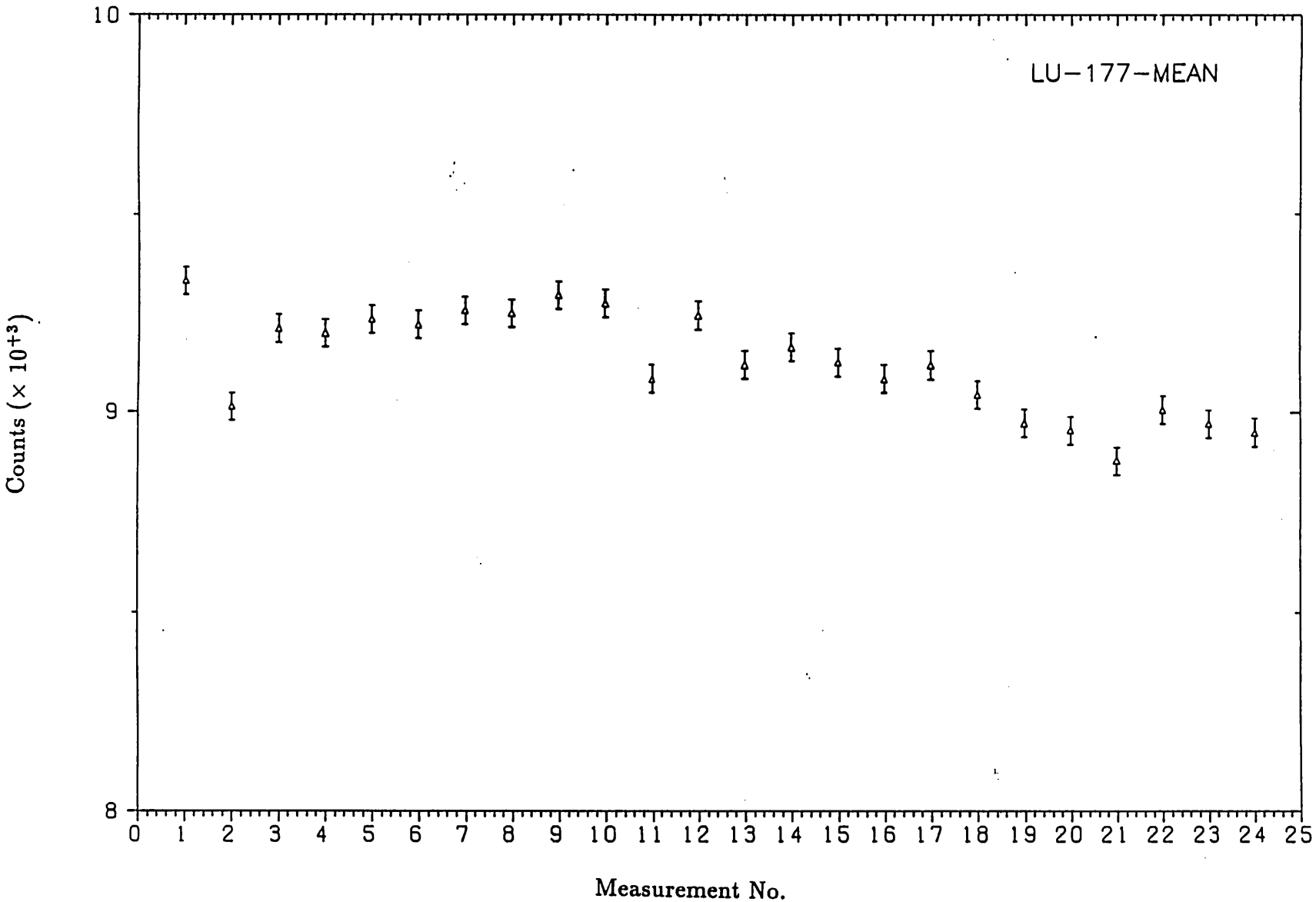

Fig. (5.4) Results of ^{177}Lu (mean).

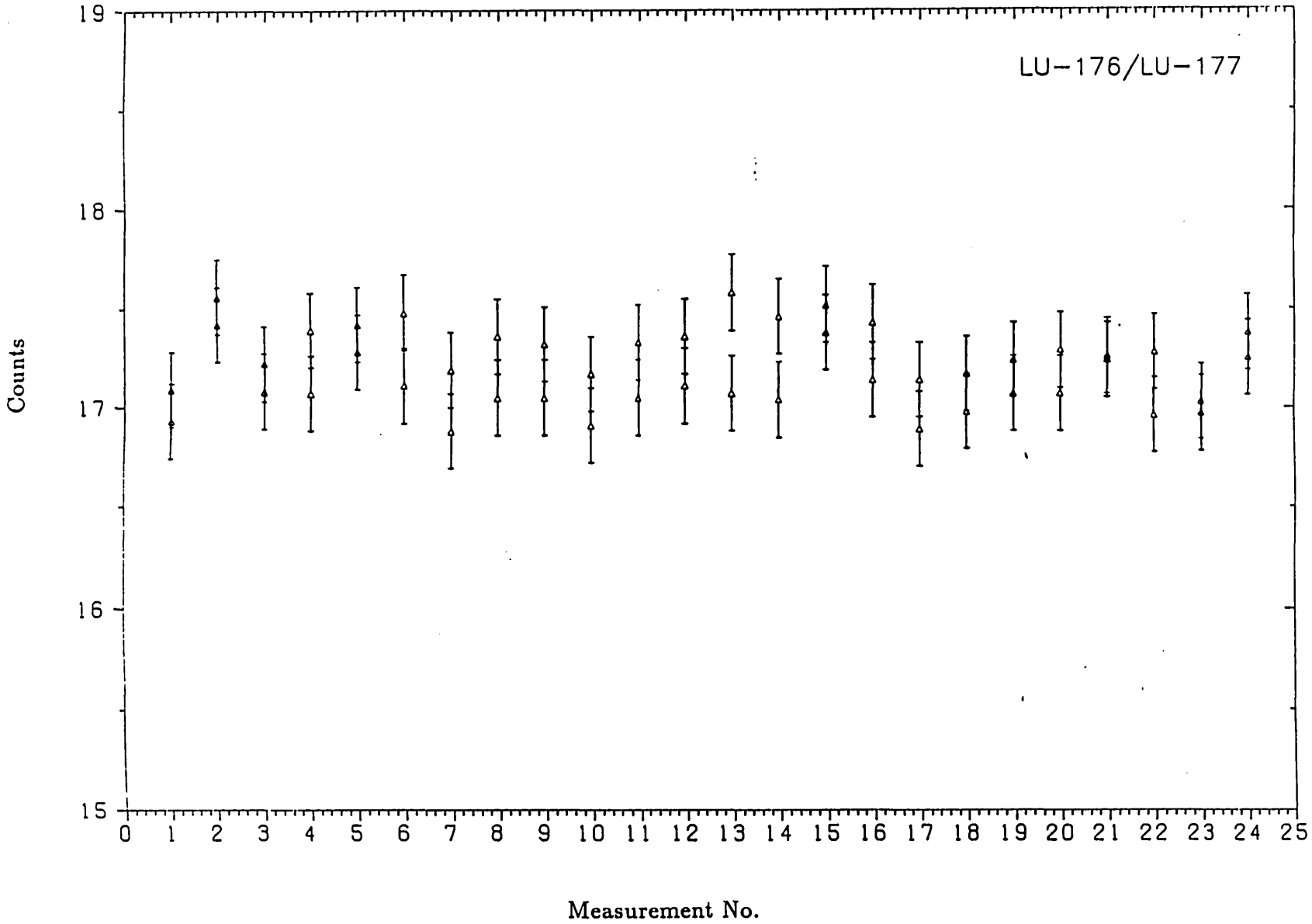

Fig. (5.5) Results of the ratio of ^{176}Lu to ^{177}Lu.

(ANOVA) analysis the F-value obtained from the ratio results is .91 and it passes the F-test at the .90 probability level. This indicates that the reaction rates from ^{176m}Lu and ^{177}Lu are affected by the flux perturbation in the same manner and at the same rate, and hence the ratio of epithermal to thermal flux or δ_1/δ_2 can be assumed constant. Hence the flux can be normalized by irradiating a single monitor with each sample and then all measurements are normalized to a mean number of reactions produced in the monitor.

To find if the temperature of the coolant outlet can be used as an indicator of the flux variations, the mean of each group of measurements from fig.5.3 and 5.4 are plotted with the recorded temperature of the coolant outlet above the core during that particular irradiation in fig.5.6 and 5.7 respectively. To determine if there is any correlation between recorded temperatures and the number of reactions, the percentage points distribution of the correlation coefficient when $\rho = 0$ [67] is used, and the values of r obtained from ^{176m}Lu and ^{177}Lu are .79 and .71 respectively and both fail at the .005 two tail test. Hence a definite correlation exists between the coolant outlet temperature and the flux.

To find whether this correlation or rate of change of thermal and epithermal flux with temperature is similar, the number of reactions from ^{176m}Lu and ^{177}Lu per unit mass Vs temperature are plotted in fig.5.8 and 5.9 respectively, and it can be seen that there is a pattern of decrease in the number of reactions with increase in the coolant outlet temperature in both isotopes, and to measure the rate of decrease of the number of reactions from both isotopes, assume that the number of reactions per unit mass is given by:

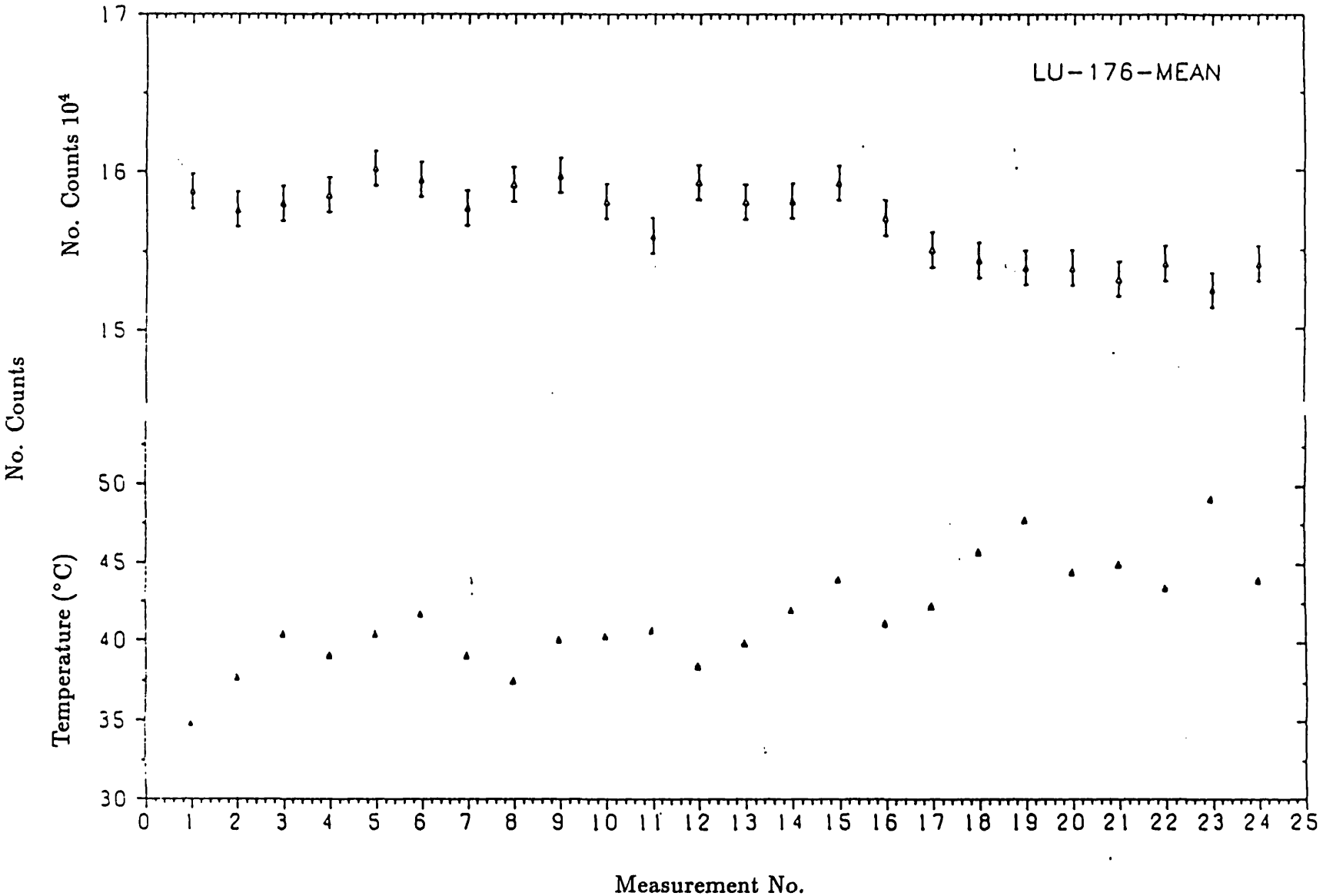

Fig. (5.6) Reseults of ^{176}Lu (mean).

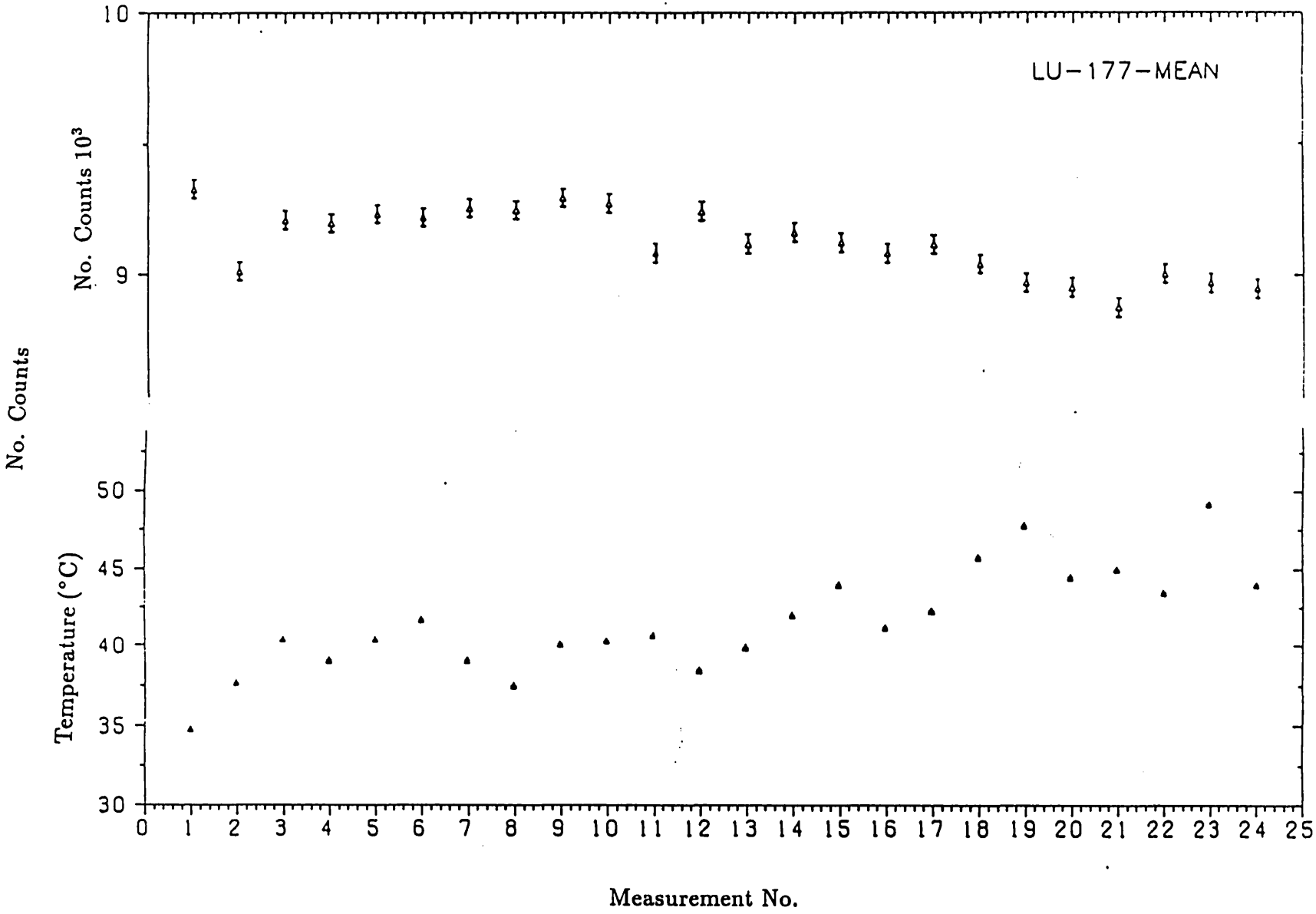

Fig. (5.7) Results of ^{177}Lu (mean).

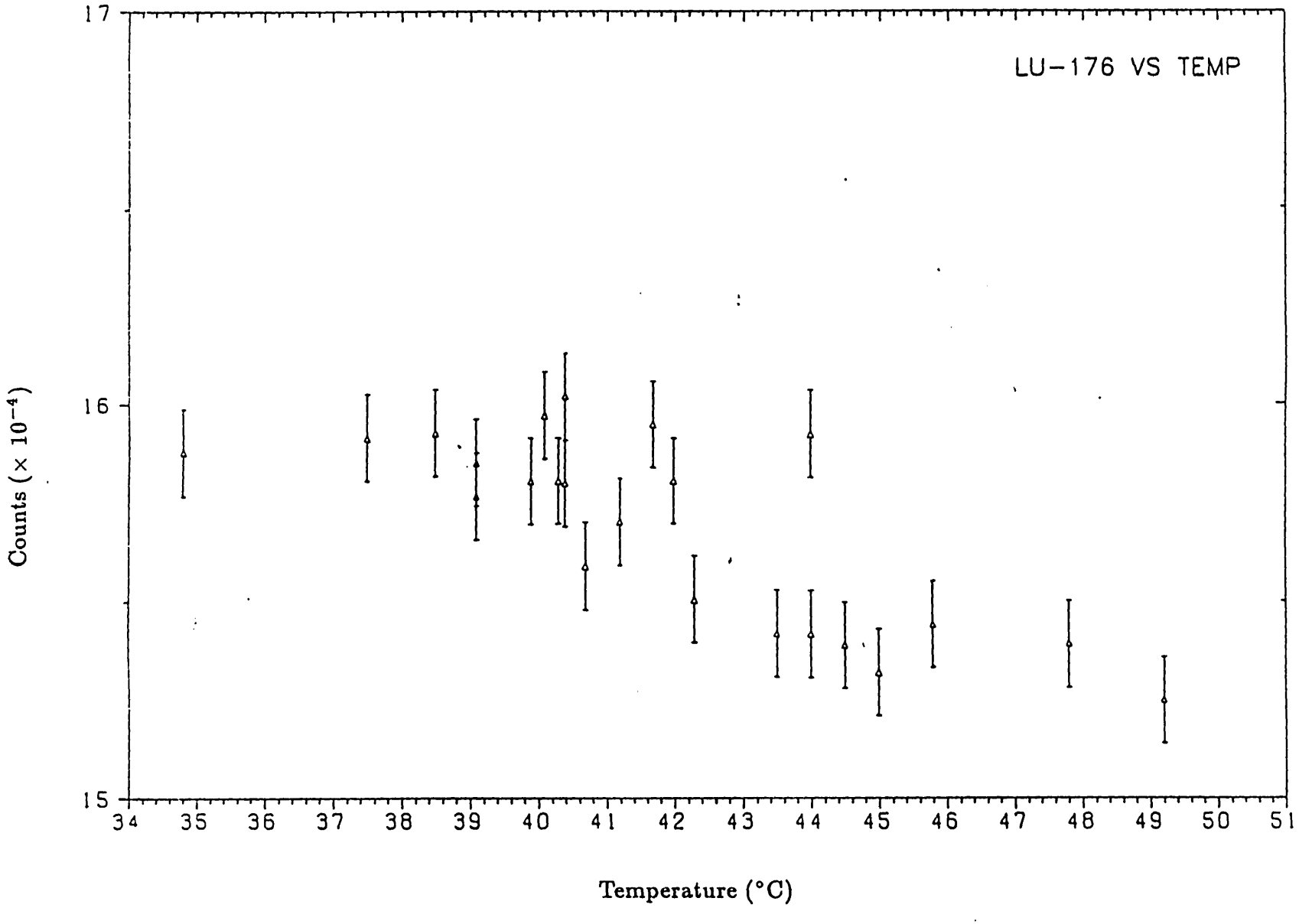

Fig. (5.8) ^{176}Lu (mean) Vs outlet Temperature.

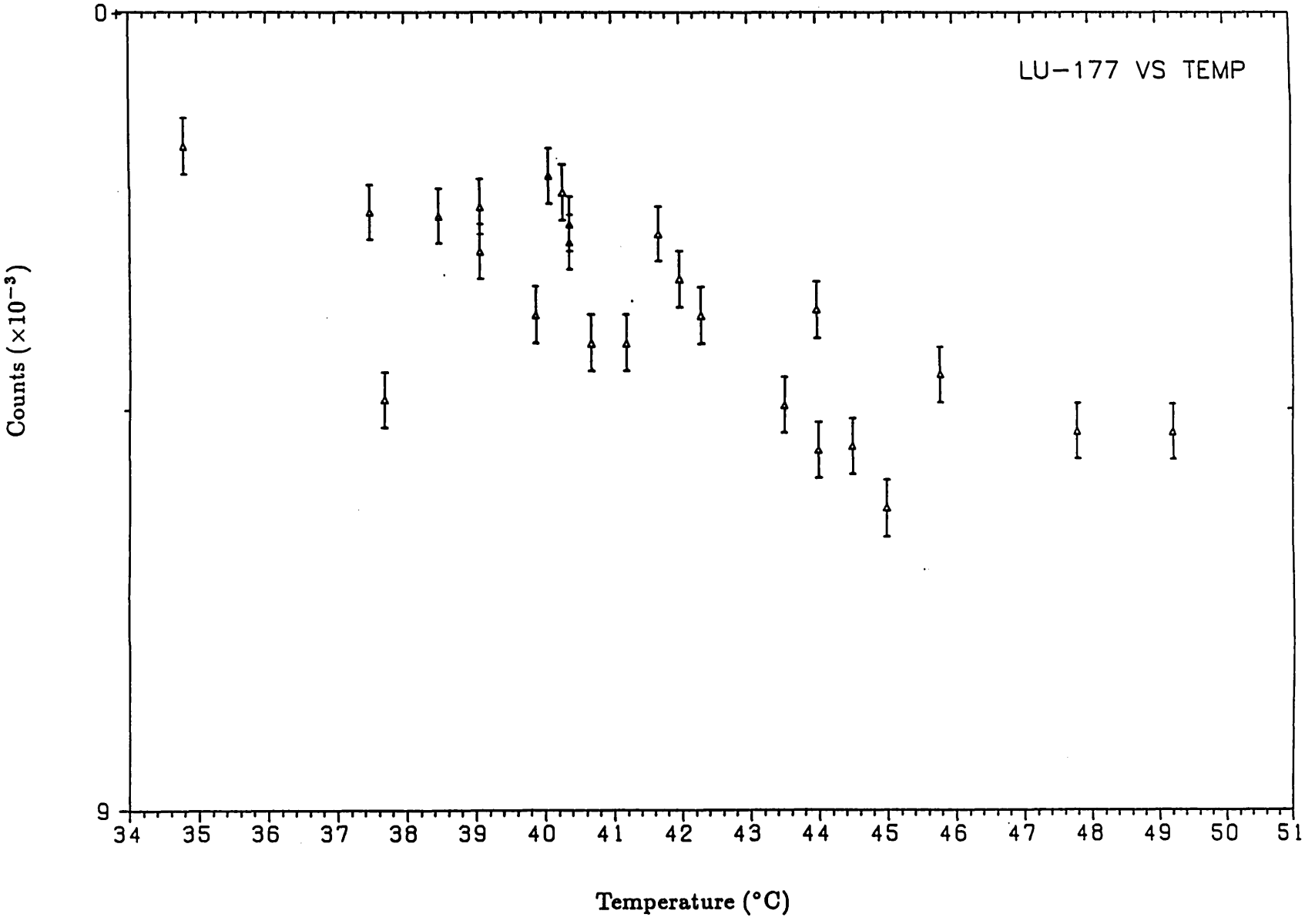

Fig. (5.9) ^{177}Lu (mean) Vs outlet Temperature.

$$Y = MX + C$$

where X is the temperature for Y reactions, M is the slope, and C is the number of reactions at X = 0. M is given by:

$$M = \frac{\sum_{i}^{n} (X_i - \bar{X})(Y_i - \bar{Y})}{\sum_{i}^{n} (X_i - \bar{X})^2}$$

where i refers to the group number. The M value for ^{176m}Lu is $-(0.062 \pm 0.010)\times10^{4}$ and $-(0.033 \pm 0.008)\times10^{3}$ for ^{177}Lu. To find if these slopes are significant, a student t-test [68] is used with the assumption that M=0 and T-values of 5.74 and 6.04 were found for ^{176m}Lu and ^{177}Lu respectively and both failed at the 0.995 probability level indicating that $M \neq 0$ and there is a definite decrease of the thermal and epithermal fluxes with an increase in the coolant outlet temperature.

The rate of change of number of counts with the outlet temperature for ^{176m}Lu and ^{177}Lu are $-(0.395 \pm 0.065)\%$ and $-(0.351 \pm 0.085)\%$ per degree respectively. Both percentage rates of change are within one standard deviation so a mean rate of change is taken to be $-(0.38 \pm 0.04)\%$ per degree of the coolant outlet temperature.

Correcting all measurements to a mean coolant outlet temperature, the results of fig.5.3 and 5.4 are plotted again in fig.5.10 and 5.11 respectively. The χ^2 values for the means in fig.5.10 and 5.11 are 41 and 70 respectively which still fail the χ^2 test at .95 probability level but show a factor of three reduction from the results before normalizing all measurements to a mean temperature. So an error due to

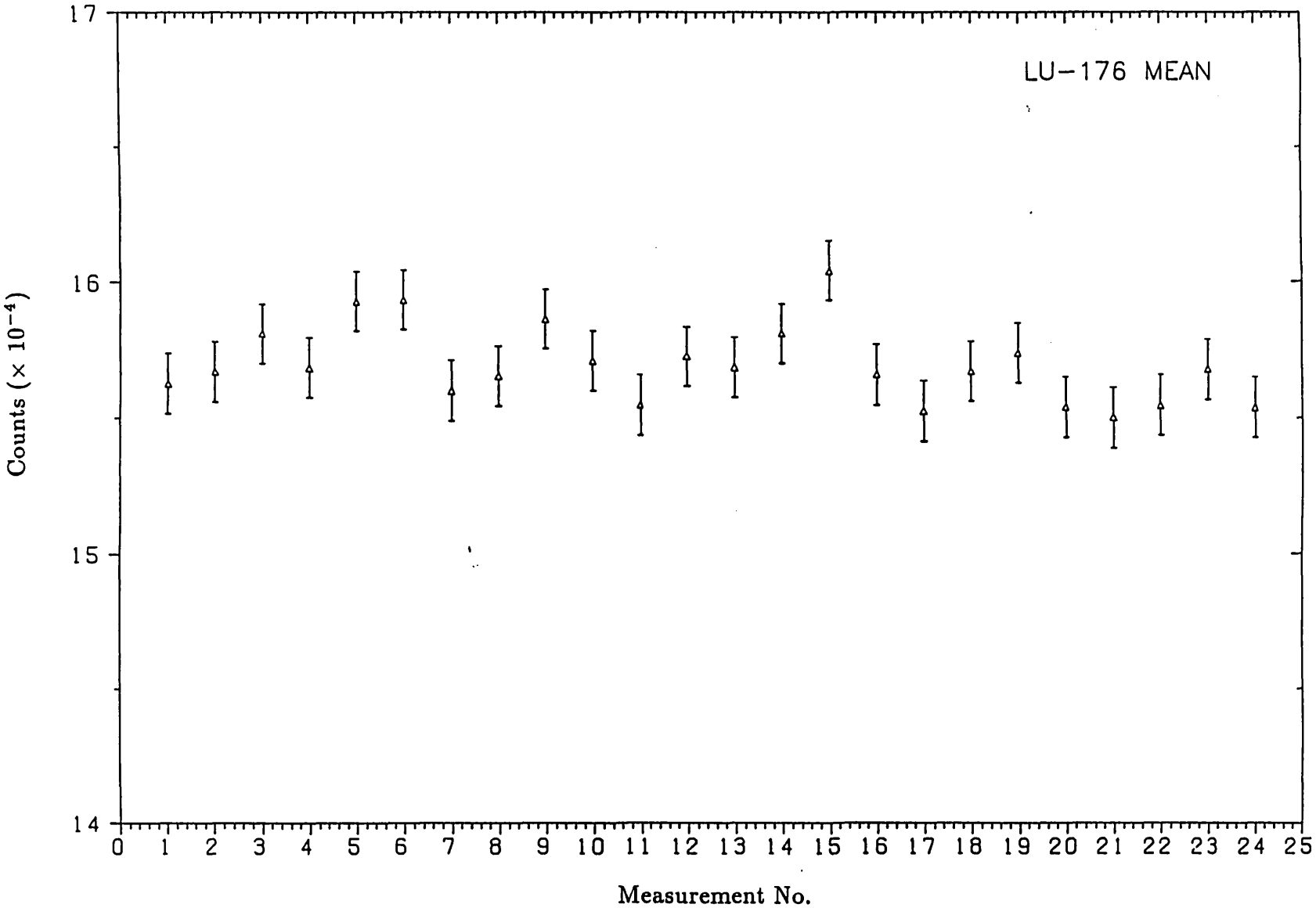

Fig. (5.10) Results of ^{176}Lu (mean) normalized to a mean outlet temperature.

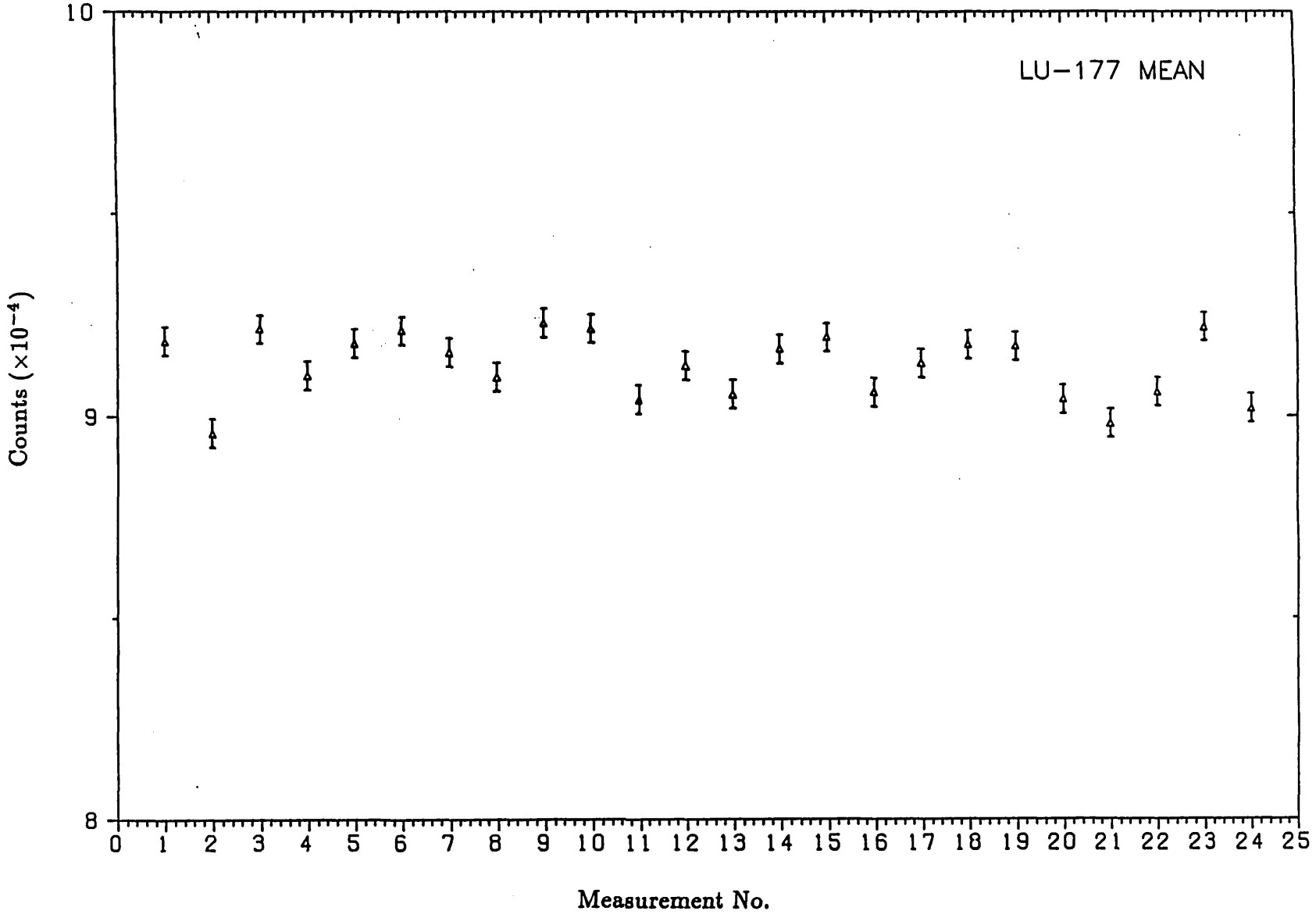

Fig. (5.11) Result of ^{177}Lu (mean) normalized to a mean outlet temperature.

flux perturbation still exists and to find from the results an estimation of that error in the form of an additive standard deviation, the true variance is given by:

$$\sigma^2_{\bar{X}} = \frac{(X_i - \bar{X})^2}{n - 1}$$

where $\sigma^2_{\bar{X}} = \sigma^2_s + \sigma^2_f$

where subscript s refers to the statistical error due to counting and weighing and f refers to flux perturbation. The standard deviations σ_s for ^{176m}Lu and ^{177}Lu are 0.7% and 0.6% respectively and σ_f is 0.7%.

Applying the (ANOVA) [67] test again for the measurements in fig.5.10 and 5.11, the F-value obtained for the ^{176m}Lu passes the F-test at .90 probability level while the F-value for ^{177}Lu is 3.13 which fails.

5.4 Conclusion

The results indicate a variation or perturbation of the thermal and epithermal fluxes with time even with keeping the output power at 100 kW by raising or lowering of the control rod to compensate for flux variations. Because the indication of power comes from a single position in the core where the ionization chamber is positioned, the flux at other locations may not be the same.

Both thermal and epithermal fluxes at the irradiation position used, vary in the same manner with time and at the same rate so only a single monitor need to be irradiated with each sample, then gamma counted so that all measurements can

be normalized to a mean flux, by normalizing to a mean number of counts per sec produced by the monitor. Alternatively, by recording the outlet temperature of the coolant during each measurement and then correcting all measurements to a mean temperature and adding an error of 0.7%, a reasonable normalization can be achieved. The 0.7% represents the factors mentioned above (different reactor operators, different samples, etc)

CHAPTER SIX

EXPERIMENTAL DETERMINATION OF RESONANCE INTEGRALS AND NUCLEAR DATA

6.1 Choice of Isotopes

It was shown in section 4.4 that in order to predict the measured gamma emission rates, five items of nuclear data are required. They are W'/g, η, λ, E_r and $I_0/g\sigma_0$. In an ideal situation these items would be known exactly so that the solution for the flux parameters and their variance-covariance matrix could be correctly determined from the measured saturated activities and their uncertainties. In practice reported values for all the above items carry uncertainties and hence influence the solution for the flux parameters. According to AHMAD [11] the flux parameters to be estimated are not sensitive to changes in W'/g and E_r, but this is not true for η and $I_0/g\sigma_0$. σ_0 which appears in η and basically determines the reaction rate in mainly thermal neutron spectra has uncertainties of 5 to 10%. As far as I_0 is concerned, the uncertainties may be as much as a factor of 10 greater than for σ_0. The scatter in resonance integrals is well illustrated in the compilation of GRYNTAKIS and KIM [12].

In 1982 AHMAD [11], 1983 JEFFERIES [10] used values of η and $I_0/g\sigma_0$ evaluated from reported literature values of I_0, σ_0 and the components of η. Then from the measured activities, new and improved values of η and $I_0/g\sigma_0$ are predicted. Unfortunately, for some isotopes, the number of reported values is too small (or non existent) to perform any

sort of best value evaluation. For this reason it was decided to consider η and $I_0/g\sigma_0$ as unknown parameters to be estimated with the flux parameters from the measured saturated activities and their uncertainties, also providing a test of the flux model of chapter four.

In using the bare irradiation technique, where the saturated activity per target atom per second is predicted by the following relation (equation 4.18):

$$N_s = N_{AV}\eta \left[\Phi_{th} + \Phi_e\left[\frac{W'}{g} + f_1(\alpha) + \bar{E}_r^{-\alpha}\left[\frac{I_0}{g\sigma_0} - f_2(\alpha)\right] + f_2(\alpha)\right]\right],$$

most of the reactions induced in the irradiated detector are due to thermal neutrons. In other words, the information carried in that measurement is mainly about σ_0 of that isotope, and Φ_{th}. In order to use the above relation to gain enough information about all the five parameters, the ratio $I_0/g\sigma_0$ should be large, or comparable with Φ_{th}/Φ_e, hence ensuring that enough information about the epithermal flux in that position and the resonance integrals of the irradiated isotopes are obtained.

If using the cadmium covered technique, the saturated activity per target atom per second is predicted by the following relation (equation 4.19):

$$N_{Cd} = N_{AV}\eta\,\Phi_e\left[\bar{E}_r^{-\alpha}\left[\frac{I_0}{g\sigma_0} - f_2(0)\right] + f_2(\alpha)\right]$$

where the measured reaction rate in the irradiated detector is purely due to epicadmium neutrons. Hence, the best information about the resonance integral for that particular

isotope is obtained.

However, when using the cadmium covered technique the cadmium cut-off energy E_{Cd} is set equal to .55 eV for a cadmium box of 1 mm uniform wall thickness with a ratio of height/diameter = 2 [58]. But in some practical situations, these conditions may prove difficult to meet and may effect the true cut-off energy E_{Cd}. It was shown in section 4.8, that the higher the ratio of $I_0/g\sigma_0$ the less sensitive it is to variations in the cadmium cut-off energy. Taking into account the above points, and the choice of irradiation channels available in the reactor, in our opinion the flux model can best be used to provide new values of η and $I_0/g\sigma_0$, with resonable uncertainties from measured reaction rates, for isotopes with high $I_0/g\sigma_0$ ratios.

In the latest compilation of $K_{0,Au}$ (η/η_{Au}), Q_0 (I_0/σ_0) and related nuclear data in 1986 by F.DE CORTE et al [62], they indicated that for some isotopes, a more accurate determinations of nuclear data are desirable. The isotopes chosen for this work and the reactions of interest are listed in table 6.1

6.2 Neutron Self-Shielding

When the neutron activation method is used, some assessment of the effect of neutron self-shielding occuring in some of the materials used as detectors, must be included. Although the use of a thin sample generally causes a negligible perturbation in the neutron flux in the medium surrounding the sample, the flux may be greatly depressed in the sample itself due to shielding by its outer regions. This will occur mainly at neutron resonance energies, when the

Table 6.1 Isotopes chosen for this work and the reactions of interest

$^{71}Ga(n,\gamma)^{72}Ga$
$^{75}As(n,\gamma)^{76}As$
$^{81}Br(n,\gamma)^{82}Br$
$^{86}Sr(n,\gamma)^{87m}Sr$
$^{115}In(n,\gamma)^{116m}In$
$^{121}Sb(n,\gamma)^{122}Sb$
$^{133}Cs(n,\gamma)^{134m}Cs$
$^{152}Sm(n,\gamma)^{153}Sm$
$^{158}Gd(n,\gamma)^{159}Gd$
$^{159}Tb(n,\gamma)^{160}Tb$
$^{165}Ho(n,\gamma)^{166}Ho$
$^{169}Tm(n,\gamma)^{170}Tm$
$^{175}Lu(n,\gamma)^{176m}Lu$
$^{179}Hf(n,\gamma)^{180m}Hf$
$^{181}Ta(n,\gamma)^{182}Ta$
$^{186}W(n,\gamma)^{187}W$
$^{197}Au(n,\gamma)^{198}Au$
$^{238}U(n,\gamma)^{239}U$

collision mean-free-path becomes comparable to, or small compared with, the sample dimensions.

The self-shielding factor, G for a detector is defined as the ratio of the experimental activation to the theoretically expected activation without self-shielding. Several authors have already [69-72] studied these self-shielding factors for a number of isotopes and have also provided some useful formulae to calculate these factors.

For all the material used in this work (Au, In, W etc.), the reported literature values [63,75] indicate negligible self-shielding factors, i.e. G is nearly 1, at low enough concentration. To neglect the effect of self-shielding in the samples, the thickness of each element is kept below 0.1 mg/cm^2.

6.3 Epi-cadmium flux depression

When using the cadmium cover technique, the presence of a cadmium box in the irradiation media causes a fractional change in the flux due to its high thermal absorption cross-section. In a multiplying medium this leads to a reduction in the fission rate in the medium surrounding the cadmium box.

In order to reduce the above effect, also due to limitation on the amount of cadmium allowed in the reactor, the cadmium boxes used are of 0.5 mm wall thickness and 3 cm^2 surface area.

The saturated activity for an isotope irradiated under cadmium cover is given by [73]:

$$N_{Cd} = \frac{N_C}{F_{Cd}\epsilon_\gamma SDC} \qquad (6.1)$$

where N_C is the corrected count in the net peak area (as defined in chapter four) and F_{Cd} is the cadmium epithermal neutron transmission factor, which accounts for the fact that the epicadmium activation of cadmium covered irradiated isotope is, in some cases, significantly different from that of a bare irradiated isotope. F_{Cd} is defined as [73]:

$$F_{Cd} = \left[\frac{N_{Cd}}{N_s} \right]_{\text{for epicadmium neutrons}} \qquad (6.2)$$

Usually F_{Cd} factors do not differ from unity for most isotopes. However, when the resonance of Cd and of the Cd-covered isotope partially overlap, F_{Cd} can be markedly lower than unity. This is the case for [73] $^{186}W(n,\gamma)^{187}W$, where there is an overlap between the ^{113}Cd: 18.4 eV resonance and the ^{186}W: 18.84eV resonance. Moreover, for isotopes with large resonances in the 1-10 eV range, F_{cd} can also be lower than unity due to the high energy tailing of the dominant 0.178 eV ^{113}Cd resonance (e.g $^{115}In(n,\gamma)^{116m}In$, resonance at 1.457 eV and $^{197}Au(n,\gamma)^{198}Au$, resonance at 4.906 eV). Also, F_{Cd} can be higher than unity if neutrons, which are resonance scattered in cadmium, enter the correct energy band to be resonantly captured in the cadmium covered isotope (e.g $^{65}Cu(n,\gamma)^{66}Cu$).

When using the cadmium cover technique, the cut-off energy E_{Cd} is a function of cadmium thickness. For the cadmium boxes with 0.5 mm wall thickness used in this work the cut-off energy is taken to be 0.4 eV. To account for the

extra activity induced in the sample due to a lower cut-off energy E_{Cd} compared to that of 1.0 mm thick Cd, equation 4.19 is modified as follows:

$$N_{Cd} = N_{AV}\eta\phi_e\left[\frac{W''}{g} + f_1'(\alpha) + \bar{E}_r^{-\alpha}\left[\frac{I_0}{g\sigma_0} - f_2(0)\right] + f_2(\alpha)\right] \qquad (6.3)$$

where $$W'' = \frac{1}{\sigma_0}\int_{0.4}^{0.55}\left[\sigma(E) - g\sigma_0\left(\frac{E_0}{E}\right)^{1/2}\right]\frac{dE}{E^{1+\alpha}} \qquad (6.4)$$

and $$f_1'(\alpha) = \int_{0.4}^{0.55}\left[\left(\frac{E_0}{E}\right)^{1/2}\right]\frac{dE}{E^{1+\alpha}} \qquad (6.5)$$

6.4 Input Data

In order to determine the flux parameters of the irradiation position and the nuclear data (η and $I_0/g\sigma_0$) of the measured isotopes simultaneously, the items, λ, E_r, g, W' and F_{Cd} are considered constants. These items, for each detector are listed in table 6.2.

For the values of the decay constant λ, the half-lives for the different isotopes used in this work were taken from the 1986 compilation by DE.CORTE et al [62], the effective resonance energy values E_r were taken from S.JOVANOVIC et al [77]. The Westcott g factors were taken from C.H. WESTCOTT [74], and only the g value for gold, indium and uranium were found to differ from 1.0.

Table 6.2. Detector characteristics and nuclear constants

Target Element	Reaction of Interest	Mass (µg)	Gamma Energy (keV)	half Life
^{71}Ga	$^{71}Ga(n,\gamma)^{72}Ga$	19.65	834	14.1 h
^{75}As	$^{75}As(n,\gamma)^{76}As$	35.92	559	26.32 h
^{81}Br	$^{81}Br(n,\gamma)^{82}Br$	30.00	554	35.3 h
^{86}Sr	$^{86}Sr(n,\gamma)^{87m}Sr$	40.00	388	2.805 h
^{115}In	$^{115}In(n,\gamma)^{116m}In$	0.326	417	54.15 h
^{121}Sb	$^{121}Sb(n,\gamma)^{122}Sb$	6.95	564	2.70 d
^{133}Cs	$^{133}Cs(n,\gamma)^{134m}Cs$	30.00	127	2.91 h
^{152}Sm	$^{152}Sm(n,\gamma)^{153}Sm$	25.51	103	46.7 h
^{158}Gd	$^{158}Gd(n,\gamma)^{159}Gd$	21.21	363	18.56 h
^{159}Tb	$^{159}Tb(n,\gamma)^{160}Tb$	37.81	87	72.1 d
^{165}Ho	$^{165}Ho(n,\gamma)^{166}Ho$	23.06	80	26.8 h
^{169}Tm	$^{169}Tm(n,\gamma)^{170}Tm$	30.61	84	128.6 d
^{175}Lu	$^{175}Lu(n,\gamma)^{176m}Lu$	3.06	88	3.635 h
^{179}Hf	$^{179}Hf(n,\gamma)^{180m}Hf$	40.00	332	5.519 h
^{181}Ta	$^{181}Ta(n,\gamma)^{182}Ta$	40.00	152	114.43d
^{186}W	$^{186}W(n,\gamma)^{187}W$	3.93	134	23.9 h
^{197}Au	$^{197}Au(n,\gamma)^{198}Au$	10.61	412	2.695 d
^{238}U	$^{238}U(n,\gamma)^{239}U$	3.32	74	23.50 m

Table 6.2. Continued

Target Element	effective resonance energy $\bar{E}_r$ (eV)	W'	g	F_{Cd}
^{71}Ga	154	0	1.0	1.0
^{75}As	106	0	1.0	1.0
^{81}Br	152	0	1.0	1.0
^{86}Sr	795	0	1.0	1.0
^{115}In	1.56	0.2953	1.0195	0.961
^{121}Sb	13.1	0.0268	1.0	0.982
^{133}Cs	9.27	0.0255	1.0	1.0
^{152}Sm	8.53	0.0151	1.0	0.991
^{158}Gd	48.2	0	1.0	1.0
^{159}Tb	18.1	0.0121	1.0	0.988
^{165}Ho	12.3	0.0134	1.0	0.975
^{169}Tm	4.80	0.0519	1.0	1.0
^{175}Lu	16.1	0.0198	1.0	0.991
^{179}Hf	16.2	0.0253	1.0	1.0
^{181}Ta	10.4	0.0171	1.0	1.0
^{186}W	20.5	0	1.0	0.983
^{197}Au	5.65	0.0501	1.0053	0.996
^{238}U	16.9	0.0126	1.0017	0.977

For the factor W', which accounts for deviation of the cross-section from 1/v law in the region between μkT and E_{Cd}, the values were calculated using the RYVES [60] method. The reported literature values of the cadmium transmission factors F_{Cd}, for a 0.5 mm thick cadmium box for the isotopes used in this work, were difficult to find since most of the reported values are for 1 mm thick cadmium covers. In order to make use of the recommended values by ELNIMR [73,78], the relation between F_{Cd} and cadmium thickness is considered to be of the following form [13]:

$$F_{Cd} = e^{-\delta_i t} \qquad (6.6)$$

where t is cadmium thickness and δ_i cadmium attenuation for isotope i. The F_{Cd} for .5 mm are calculated as follows:

$$(F_{Cd})_{0.5} = e^{\ln(F_{Cd})_i \times 0.5} \qquad (6.7)$$

where the subscripts i and 0.5 correspond to the cadmium cover thickness. The F_{Cd} values for ^{158}Gd and ^{181}Ta are given by ELNIMR [73] as 1.0, although they are expected to be lower due to low energy resonances (1-10 eV.)

6.5 Sample Preparation

Since most of the isotopes chosen for this work are not available commercially in the form of dilute foils, and because of the long time involved, if the isotopes were to be irradiated individually, the samples are prepared in the form of multielement standards, to simulate a practical situation and save time.

In preparing a multielement standard, for the

calibration of irradiation facilities, the multielement components can be chosen to satisfy the following requirements:

(i) Minimum interference or overlapping between gamma-ray peaks of the product isotopes, in order to make the peak area evaluation reasonably easy.

(ii) The product isotope should not appear as a product of any of the other isotopes in the same sample.

(iii) The isotopes forming the sample, should have a combination of half-lives and activation cross-sections, so that a reasonable activity from the product nuclides is obtained after the chosen time of irradiation.

Taking the above points into account, the eighteen isotopes were divided over three samples.

All these elements are available in the form of standard solutions (10^3 or 10^4 parts per million). To prepare the samples, the standard solution of each element was diluted down to the appropriate concentration, then a drop of 10µl was deposited on a 7mm diameter filter paper placed on a sticky tape. The filter papers are then placed in an oven at low temperature to dry, then sealed by another tape on the top. A list of the elements

in each sample is shown in table 6.3.

The depositing of the 10µl solution was done by a micropipette. The accuracy and reproducibality of the same volume was evaluated by, weighing 10µl of water using the same micropipette and then repeating the same procedure N times, then the error in reproducing 10µl is given by:

Table 6.3. The components of each sample plus the element mass, target isoptope and the gamma-ray of interest.

TARGET ELEMENT	NUCLIDE of INTEREST
Au	^{197}Au
U	^{238}U
Ho	^{165}Ho
Lu	^{175}Lu
Sm	^{152}Sm
Cs	^{133}Cs
In	^{115}In
SAMPLE - 1 -	

Ga	^{71}Ga
As	^{75}As
Sr	^{86}Sr
Gd	^{158}Gd
Hf	^{179}Hf
W	^{186}W
Tm	^{169}Tm
SAMPLE - 2 -	

Tb	^{159}Tb
Ta	^{181}Ta
Br	^{81}Br
Sb	^{121}Sb
SAMPLE - 3 -	

$$\sigma_v^2 = \frac{\sum_{i=1}^{N} (W_i - \bar{W})^2}{(N - 1)} \qquad (6.8)$$

where σ_v^2 is the variance due to the micropipette and is found to be (2.0%)

W_i the weight of the i^{th} measurement

$\bar{W}$ the mean of N measurements and is found to be 9.7 µg.

The gamma spectra of samples type 1, 2 and 3 are shown in figs. 6.1, 6.2 and 6.3 respectively.

6.6 Dead Time Correction

The correction factor for the decay of a nuclide with decay constant λ, during counting C, is defined as

$$C = \int_0^{t_c} \tau(t)\, e^{-\lambda t}\, dt \qquad (6.9)$$

where t_c is the count period (clock or real time) and $\tau(t)$ the ratio of real to live counting times. If t_c is short compared with the nuclide half-life, then $\tau(t)$ is constant during the counting period $0-t_c$ and equation (6.9) becomes

$$C = \tau \left[\frac{1 - e^{-\lambda t_c}}{\lambda} \right] \qquad (6.10)$$

If the counting period is longer than, or comparable with, the nuclide half life, then the above correction factor is not applicable because the factor $\tau(t)$ varies with time. But during a short interval Δt (short compared with the

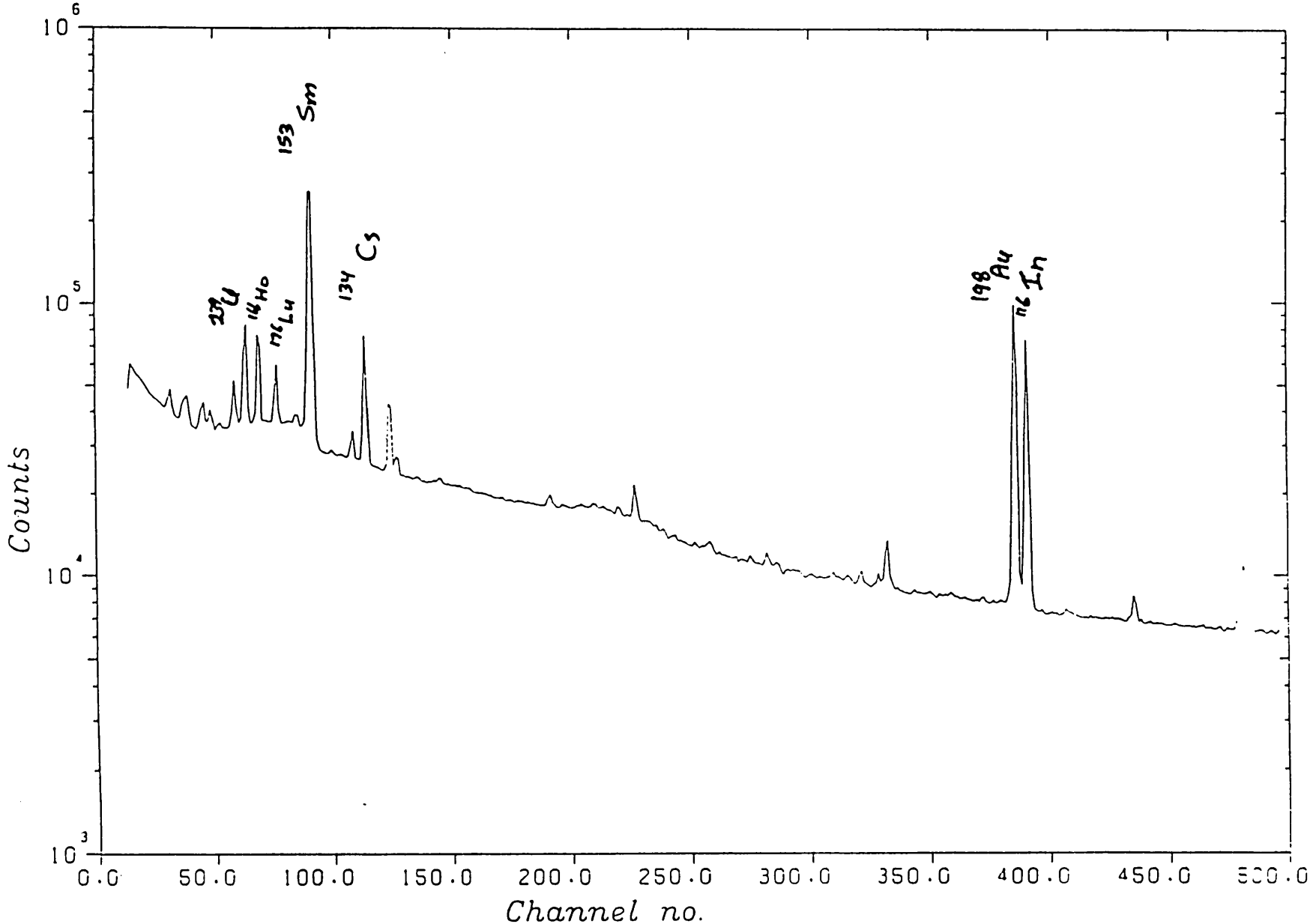

Fig. 6.1 Gamma Spectrum of Sample Type 1

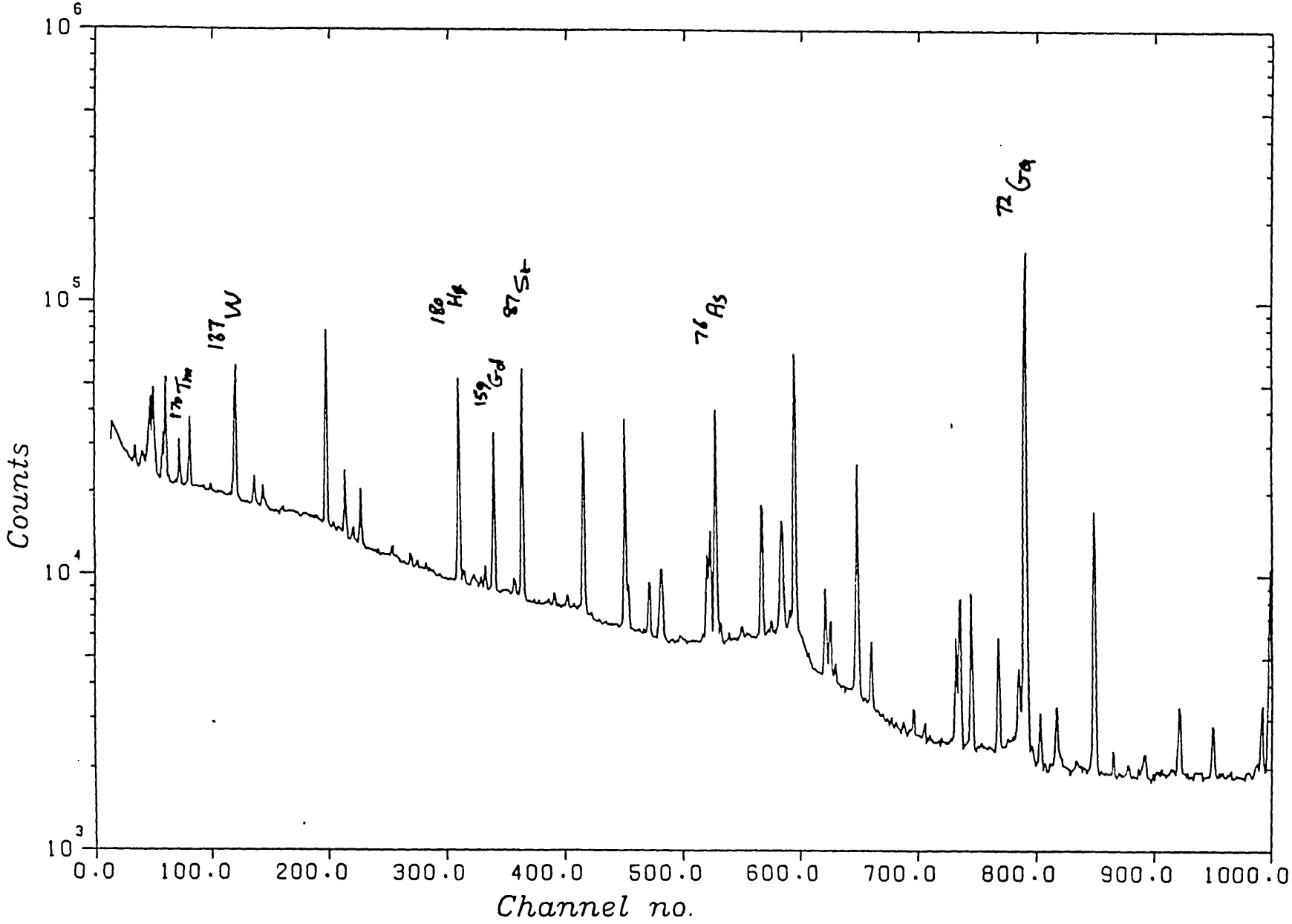

Fig. 6.2 Gamma Spectrum of Sample Type 2

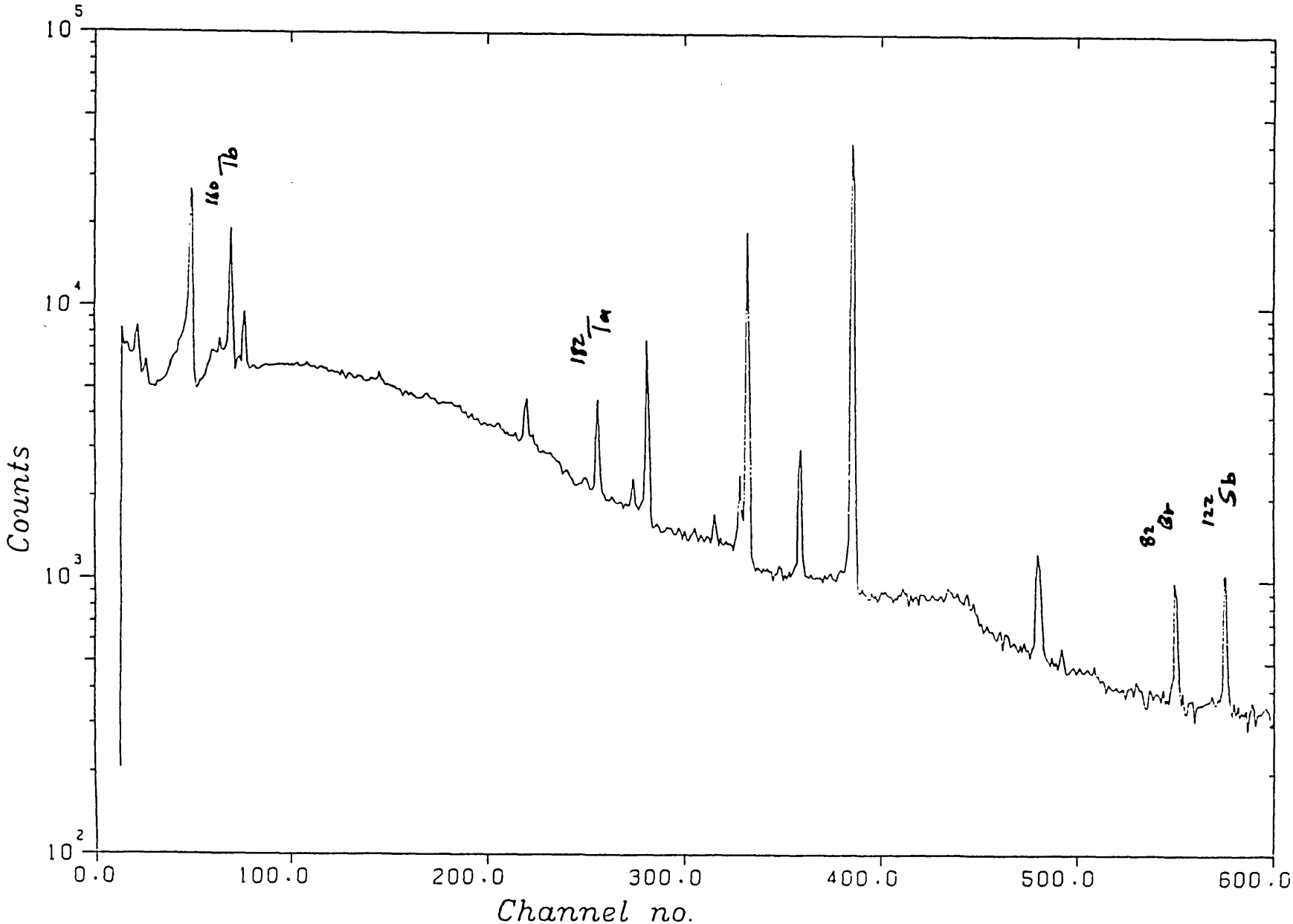

Fig. 6.3 Gamma Spectrum of Sample Type 3

nuclide half-life), the dead-time can be considered constant, then the true number of counts in the i^{th} spectrum during that interval is given by

$$N_i = A_{0i} C_i = A_{0i} \tau_i \left[\frac{1 - e^{-\lambda \Delta t}}{\lambda} \right] \qquad (6.11)$$

where $A_{0i} = A_0 e^{-(i-1)\lambda \Delta t}$

A_0 = initial count rate

and after n spectra, the correct number of counts are given by

$$N = \sum_{i=1}^{n} N_i = A_0 \left[\frac{1 - e^{-\lambda \Delta t}}{\lambda} \right] \sum_{i=1}^{n} \tau_i \, e^{-(i-1)\lambda \Delta t} \qquad (6.12)$$

To satisfy the above equation, the data acquisition is done as follows:

Consider the decaying of an isotope with time, between t_1 and t_2 as shown in fig.6.4. The data is acquired during the time intervals t_r, then corrected for dead-time and stored during intervals t_a. The total time is given by

$$t_2 - t_1 = n(t_r + t_a) \qquad (6.13)$$

and

$$t_a = \frac{(t_2 - t_1)}{n} - t_r \qquad (6.14)$$

In an interval (t_i, t_j) the corrected number of counts due to the peak of a nuclide with decay constant λ is given by

$$\int_{t_i}^{t_j} A_{0i} e^{-\lambda t}\, dt = -\frac{A_{0i}}{\lambda} e^{-\lambda t} \Big|_{t_i}^{t_j} \qquad (6.15)$$

$$= \frac{A_{0i}}{\lambda} \left[e^{-\lambda t_i} - e^{-\lambda t_j} \right] \qquad (6.16)$$

Given n spectra, for spectrum i the number of counts is

$$N_i = \frac{A_0}{\lambda} \left[1 - e^{-\lambda t_r} \right] e^{-\lambda (i-1)(t_r+t_a)} \; ; \; i=1,n \qquad (6.17)$$

and the correct number of counts from n spectra is

$$N = \sum_{i=1}^{n} N_i$$

$$= \frac{A_0}{\lambda} \left[1 - e^{-\lambda t_r} \right] \sum_{j=0}^{n-1} e^{-j(\lambda (t_r+t_a))} \qquad (6.18)$$

$$= \frac{A_0}{\lambda} \left[1 - e^{-\lambda t_r} \right] \frac{\left(1 - e^{-\lambda (t_r+t_a) n} \right)}{\left(1 - e^{-\lambda (t_r+t_a)} \right)} \qquad (6.19)$$

the true count rate at time t_i of a nuclide with a decay constant λ is given by:

$$A_0 = \frac{N \lambda \left[1 - e^{-\lambda (t_2-t_1)/n} \right]}{\left[1 - e^{-\lambda t_r} \right] \left[1 - e^{-\lambda (t_2-t_1)} \right]} \qquad (6.20)$$

$$A_0 = \frac{N\lambda\left[1 - e^{-\lambda T}\right]}{\left[1 - e^{-\lambda t_r}\right]\left[1 - e^{-\lambda T}\right]} = \frac{N}{C} \qquad (6.21)$$

where $T = t_2 - t_1$. The correction for decay during counting in this case is given by:

$$C = \frac{\left[1 - e^{-\lambda t_r}\right]\left[1 - e^{-\lambda T/n}\right]}{\lambda\left[1 - e^{-\lambda T/n}\right]} \qquad (6.22)$$

and the variance in C, σ^2_{C/C^2} is given by:

$$\left[\frac{1}{\lambda}\left(-\right) + \left(\frac{t_r\, e^{-\lambda t_r}}{1-e^{-\lambda t_r}}\right) + \left(\frac{T\, e^{-\lambda T}}{1-e^{-\lambda T}}\right) + \left(\frac{T/n\, e^{-\lambda T/n}}{1-e^{-\lambda T/n}}\right)\right]^2 \sigma^2_{\lambda} \qquad (6.23)$$

assuming negligible error in t_r and T

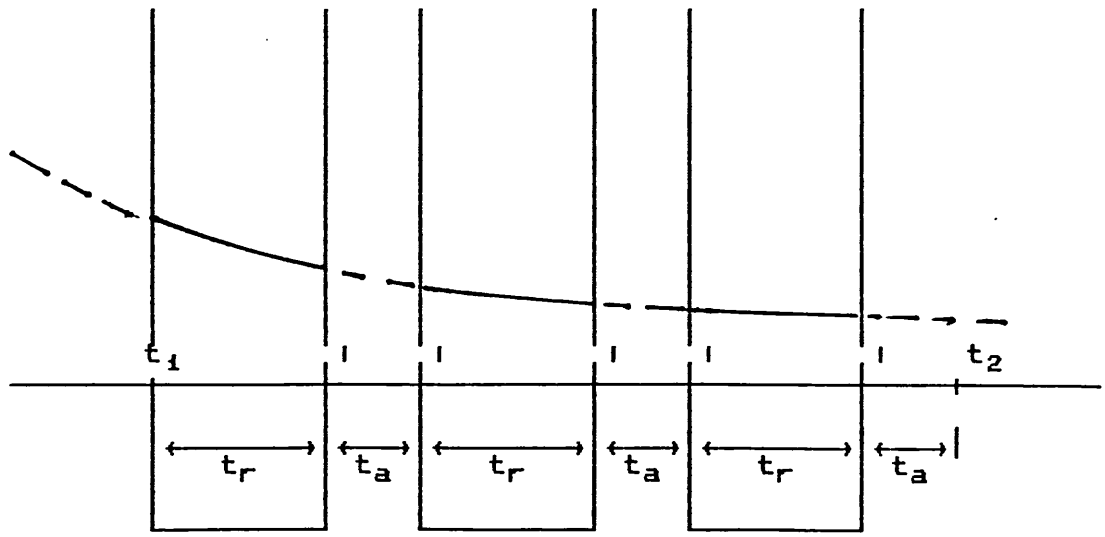

Fig 6.4 Decay of a radioactive isotope with time

The spectrum was accumulated after each interval t_r, then each channel in that spectrum is corrected for dead time during interval t_r, then stored. The same procedure is repeated for each interval then added to the other intervals.

The intervals t_r are chosen to be small compared with shortest half-life.

6.7 Experimental Procedure

In order to measure with any accuracy, the flux parameters Φ_{th}, Φ_e and α for an irradiation position simultaneously with the nuclear data η and $I_0/g\sigma_0$ for the isotopes listed in table 6.1, it is necessary to measure the reaction rates for these isotopes in at least 3 irradiation sites so as to provide an over determined set of solutions to equation 4.18

Taking into account the above point, three irradiation positions were chosen in the Imperial College reactor, and they are shown in fig.6.5. The positions are:

(1) C.A.S aluminium tube, the Cyclic Activation System. This facility is installed just inside the core boundaries, where samples can be loaded for irradiation in an aluminium tube.

(2) C.A.S cadmium tube, which is positioned next to system (1) but samples are irradiated in a cadmium tube.

(3) I.C.I.S tube, the In-Core Irradiation System. This facility is installed at the centre of the core.

Samples were irradiated individually to reduce the effect of any perturbation in the flux due to neighbouring nuclides. For each irradiation, the sample was placed in a

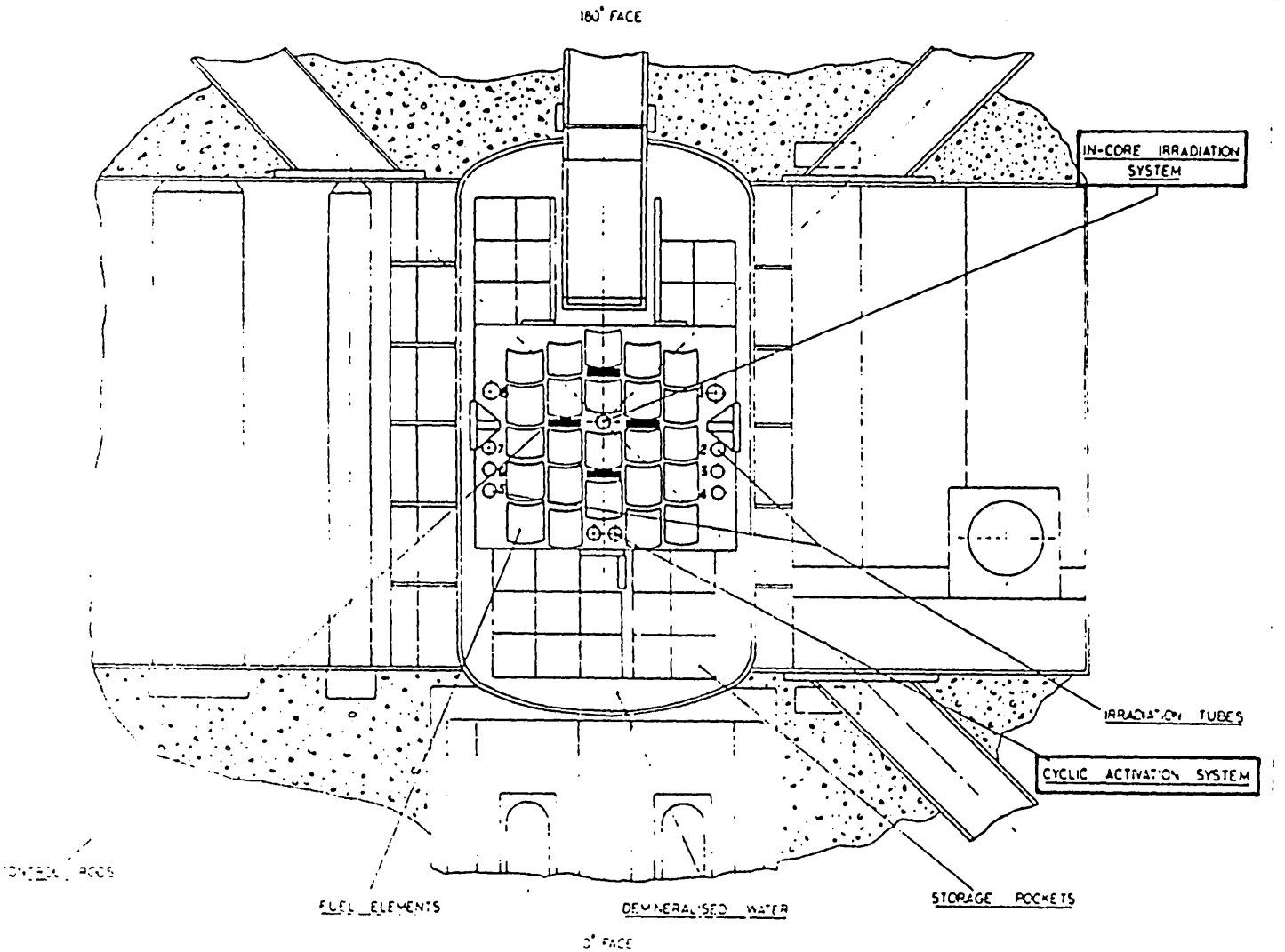

Fig 4.5 REACTOR CORE (PLAN)

polythene capsule. Bare irradiation was performed in C.A.S aluminium and I.C.I.S, and the irradiation in C.A.S cadmium was considered bare since some neutrons are getting thermalized when passing through the polythene capsule.

Cadmium covered irradiation was performed in I.C.I.S by placing the sample in a cadmium box of 0.5mm wall thickness then placing the cadmium box in the polythene capsule. The capsules for C.A.S are too small in diameter to allow a cadmium box to be irradiated.

In preparing the samples, an extra error is introduced due to pipetting and slight precipitation in some of the standard solutions (Au, W, U). To reduce the bias in the experimental measurements due to that extra error which can be reflected in the prediction of the flux parameters and nuclear data, five duplicates of each sample were irradiated at each position then gamma counted on the gamma-ray spectroscopy system listed below. The temperature of the coolant output was recorded for each measurement and then all measurements are normalized to a mean temperature in order to reduce the effect of flux variation over time (for details of the flux normalization method see Chapter four). The weighted mean value of the corrected net peak area and the variance of the mean were calculated using equation 6.24. and 6.25. or 6.26. (whichever gave the larger value) respectively:

$$\bar{N}_c = \frac{\sum_{i=1}^{n} \frac{N_{c_i}}{\sigma_i^2}}{\sum_{i=1}^{n} \frac{1}{\sigma_i^2}} \qquad (6.24)$$

$$\sigma_{\mu}^{2} = \frac{1}{\sum_{i=1}^{n} \frac{1}{\sigma_i^2}} \qquad (6.25)$$

$$\sigma_{s}^{2} = \frac{\sum_{i=1}^{n} (N_{c_i} - \bar{N}_c)^2}{n(n-1)} \qquad (6.26)$$

where N_{c_i} is the i^{th} net peak area

σ_i is the error in N_{c_i}

n is the number of measurements

The σ_i's were determined from the errors on

a) The gamma-ray net-peak area,

b) The correction factors described in Chapter two. Except for dead-time correction for a multielement which is dealt with in section 6.6,

c) The uncertainties in the weighing σ_{ω} and concentration σ_c of the standard solutions and

d) The correction due to flux variation σ_f as described in Chapter four.

Equations 6.25 and 6.26 are sometimes referred to as the internal and external errors respectively.

Detector and Associated Electronics

Detector:	closed-end HARSAW Ge(Li) model AC066 with 70 c.c crystal.
H.T supply:	Ortec model 459.
Amplifier:	Ortec 472.
Multiplexer:	Ortec 476-4.
ADCAM:	Ortec 918 (multichannel buffer).
M.C.A:	IBM-PC-XT.

6.8 Analysis Method

If n observations (measurements) of saturated activities are written as a vector E with its associated variance matrix V_e of the order (n x n), the predictions of the model, the flux model containing the flux and nuclear parameters, forms the vector C. What is required is to find a set of flux and nuclear parameters, and their associated variance-covariance matrix, which minimize the difference between the observations in vector E and the predictions in vector C to within the errors of matrix V_e.

The method used to estimate the flux and nuclear parameters is the generalized least-square method. Since the model used is non linear with respect to the parameters, an iteration procedure is necessary in order to estimate these parameters. The parameters are found such that the function,

$$\chi^2 = (E - C)^T V_e^{-1} (E - C) \qquad (6.27)$$

is minimized. The solution for the parameters is given by [66]

$$P = (D^T V_e^{-1} D)^{-1} D V_e^{-1} E. \qquad (6.28)$$

and with a variance matrix

$$Var(P) = (D^T V_e^{-1} D)^{-1} \qquad (6.29)$$

where D is known as the design matrix that contains the differentials of the model with respect to the parameters. The minimization is performed by the CERN library code MINUIT [32].

The variance of the saturated activities is

calcul[illegible]

$$\sigma^2_{N_S} = N_S^2 \left[\left(\frac{\sigma_{N_C}}{N_C} \right)^2 + \left(\frac{\sigma_{\epsilon_p}}{\epsilon_p} \right)^2 + \left(\frac{\sigma_S}{S} \right)^2 + \left(\frac{\sigma_D}{D} \right)^2 + \left(\frac{\sigma_C}{C} \right)^2 \right] \qquad (6.30)$$

where $\frac{\sigma_{N_C}}{N_C}$ is the error in the peak area (eqn 6.25 or 6.26)

$\frac{\sigma_{\epsilon_p}}{\epsilon_p}$ error in the interpolated efficiency

$\frac{\sigma_S}{S}$ error due to the correction for saturation during irradiation, and it is given by

$$\left[\left(\frac{t_I \, e^{-\lambda_i t_I}}{1 - e^{-\lambda_i t_I}} \right) \right] \sigma_{\lambda_i} \qquad (6.31)$$

neglecting any error in t_I the irradiation time.

$\frac{\sigma_D}{D}$ error due to delay correction factor between irradiation and counting (see chapter two).

$\frac{\sigma_C}{C}$ error due to correction for decay during counting.

Due to using the same standard solutions and efficiency function, the measurements are correlated for example, when using the same element irradiated in different channels σ_ϵ , σ_C and σ_λ are correlated.

ϵ c λ

When using any element irradiated in any channel then all the σ_ϵ are correlated.

In general the off-diagonal components of the matrix V_e are calculated as follows:

$$\mathrm{Cov}(\sigma_{N_s}(ijk),\sigma_{N_s}(rsl)) =$$

$$N_s(ijk).N_s(rsl)\left[\frac{\mathrm{Cov}(\sigma_{\epsilon_p}(ijk),\sigma_{p\epsilon}(rsl))}{\epsilon_p(ijk).\epsilon_p(rsl)} + \frac{\sigma_c(ijk).\sigma_c(rsl)}{c(ijk).c(rsl)}\delta_{ir} + \right.$$

$$\frac{\sigma_S(ijk)_S\sigma(rsl)}{S(ijk).S(rsl)}\delta_{ir} + \frac{\sigma_D(ijk).\sigma_D(rsl)}{D(ijk).D(rsl)}\delta_{ir} +$$

$$\left.\frac{\sigma_C(ijk).\sigma_C(rsl)}{C(ijk).C(rsl)}\delta_{ir}\right] \qquad (6.32)$$

where i and r are two isotopes

j and s are two samples

k and l are two irradiation channels

i.e $N_s(ijk)$ is the net peak area measured for isotope i in sample j irradiated in channel k, and

$$\delta_{xy} = \begin{cases} 1 & \text{for } x = y \\ 0 & \text{for } x \neq y \end{cases}$$

6.9 Results and Discussion

When the least-square model was applied to predict the parameters listed in table 6.4 simultaneously, from the 72

Table 6.4. List of the parameters and parameter numbers

No.	Parameter	No.	Parameter	No.	Parameter
1.	^{198}Au	19.	^{198}Au	37.	Φ_{th}
2.	^{239}U	20.	^{239}U	38.	Φ_e CAS (Al)
3.	^{166}Ho	21.	^{166}Ho	39.	α
4.	^{176}Lu	22.	^{176}Lu	40.	Φ_{th}
5.	^{153}Sm	23.	^{183}Sm	41.	Φ_e CAS (Cd)
6.	^{134}Cs	24.	^{134}Cs	42.	α
7.	^{116}In	25.	^{116}In	43.	Φ_{th}
8.	^{72}Ga	26.	^{72}Ga	44.	Φ_e ICIS
9.	^{76}As	27.	^{76}As	45.	α
10.	^{87}Sr η	28.	^{87}Sr $\frac{I_0}{g\sigma_0}$		
11.	^{159}Gd	29.	^{159}Gd		
12.	^{180}Hf	30.	^{180}Hf		
13.	^{187}W	31.	^{187}W		
14.	^{170}Tm	32.	^{170}Tm		
15.	^{160}Tb	33.	^{160}Tb		
16.	^{182}Ta	34.	^{182}Ta		
17.	^{82}Br	35.	^{82}Br		
18.	^{122}Sb	36.	^{122}Sb		

measured saturated activities and their variance-covariances, the value of the χ^2 obtained is 34 for 27 degrees of freedoms which passed the two-tailed test at 90% confidence level. The solution values for $I_0/g\sigma_0$ are listed in table 6.5 together with values of $Q_0 (= I_0/\sigma_0)$ taken from the 1986 compilation by F.DE.CORTE et al [62]. All values are obtained with errors less than 2% except for ^{170}Tm and ^{238}U. The large errors in these parameters are due to an error in the dilution of Tm standard solution, and precipitation in the uranium solution on the container walls which led to an error in the weight of this element. In general there is a good agreement between the results of this work $(I_0/g\sigma_0)$ and the Q_0 values of SIMONITS [75,76] reported in DE.CORTE et al. 1986 compilation [62]. For ^{153}Sm there is a difference of 4 standard deviations between the value obtained in this work and the value of SIMONITS [75,76], 7 std for ^{160}Tb and 4 std for ^{187}W. So more independent measurements are needed for these isotopes.

The nuclear constant η values obtained in this work are listed in table 6.6. All values are obtained with errors less than the individual components (θ, p_γ and σ_0), for example ^{159}Gd the error in p_γ is 38% where η_{Gd} is obtained with a combined error of 1.6%. The $K_{0,Au}$ values reported by DE.CORTE et al [62] are converted to η values by multiplying the $K_{0,Au}$ by $(p_\gamma\theta g\sigma_0/M)_{Au}$. The low errors of DE.CORTE et al. [62] are due to neglecting errors in the flux and nuclear data.

The values of the flux parameters (Φ_{th}, Φ_e , α) determined simultaneously with nuclear data are listed in table 6.7. All three positions have negative α-value. The

Table 6.5. Results of $I_0/g\sigma_0$ values compared with the reported literature values.

product Nuclide	This Work (± errors)	Reported Values by DE CORTE et al. (± errors)
^{72}Ga	6.85 ± 0.12	6.63 ± 0.35
^{76}As	15.12 ± 0.32	13.6 ± (-)
^{82}Br	19.83 ± 0.37	19.3 ± 0.6
^{87}Sr	4.32 ± 0.10	4.11 ± 0.07
^{116m}In	16.33 ± 0.32	16.8 ± 0.3
^{122}Sb	33.65 ± 0.60	33 ± 1
^{134}Cs	12.26 ± 0.25	11.8 ± 0.6
^{153}Sm	13.43 ± 0.24	14.4 ± 0.3
^{159}Gd	32.91 ± 0.63	31 ± 1
^{160}Tb	20.88 ± 0.48	17.9 ± 0.7
^{166}Ho	10.49 ± 0.21	10.9 ± 0.3
^{170}Tm	16.9 ± 1.6	14.5 ± (-)
^{176}Lu	34.79 ± 0.64	34.8 ± 1.1
^{180}Hf	14.10 ± 0.26	14.4 ± 0.4
^{187}W	12.78 ± 0.23	13.7 ± 0.3
^{182}Ta	30.0 ± 0.5	33.3 ± (-)
^{198}Au	15.52 ± 0.12	15.71 ± 0.28
^{239}U	111 ± 12	103.4 ± 1.3

Table 6.6. Results of η values compared with the reported literature values.

product Nuclide	This Work (% errors)	Values Derived from DE CORTE et al. (% errors)
^{72}Ga	2.48×10^{-2} (1.4)	2.5×10^{-2} (0.6)
^{76}As	2.28×10^{-2} (1.6)	2.37×10^{-2} (0.6)
^{82}Br	1.16×10^{-2} (1.5)	1.14×10^{-2} (1.1)
^{87}Sr	7.28×10^{-4} (1.5)	7.12×10^{-4} (0.5)
^{116m}In	3.70×10^{-1} (1.5)	3.60×10^{-1} (1.1)
^{122}Sb	1.90×10^{-2} (1.4)	2.09×10^{-2} (1.5)
^{134}Cs	2.60×10^{-3} (1.3)	2.62×10^{-3} (1.7)
^{153}Sm	1.12×10^{-1} (1.5)	1.10×10^{-1} (0.4)
^{159}Gd	3.51×10^{-4} (1.6)	3.95×10^{-4} (-)
^{160}Tb	1.63×10^{-2} (1.7)	2.01×10^{-2} (1.1)
^{166}Ho	2.48×10^{-2} (1.6)	2.61×10^{-2} (1.6)
^{170}Tm	2.01×10^{-2} (1.6)	2.06×10^{-2} (-)
^{176}Lu	8.39×10^{-3} (1.2)	8.26×10^{-3} (1.5)
^{180}Hf	2.91×10^{-4} (1.4)	2.82×10^{-4} (1.5)
^{187}W	5.56×10^{-3} (1.3)	5.4×10^{-3} (0.7)
^{182}Ta	8.25×10^{-3} (1.4)	7.69×10^{-3} (0.7)
^{198}Au	4.80×10^{-1} (3.8)	4.785×10^{-1} (0)
^{239}U	5.16×10^{-3} (1.5)	———

Table 6.7. Flux Parameters of the irradiation positions

Irradiation position	Flux parameter	measured values
CAS Aluminium	Φ_{th}	$(1.36 \pm 0.02) \times 10^{12}$
	Φ_{e}	$(0.686 \pm 0.009) \times 10^{11}$
	α	-0.035 ± 0.005
CAS Cadmium	Φ_{th}	$(0.573 \pm 0.463) \times 10^{10}$
	Φ_{e}	$(0.510 \pm 0.003) \times 10^{11}$
	α	-0.027 ± 0.002
I.C.I.S	Φ_{th}	$(2.31 \pm 0.03) \times 10^{12}$
	Φ_{e}	$(1.347 \pm 0.007) \times 10^{11}$
	α	$-.034 \pm 0.002$

Fig. 6.8

CORRELATION COEFFICIENTS

INT.	1	2	3	4	5	6	7	8	9	10	11	12	13	14	15	16	17	18
2	-.012																	
3	.000	-.001																
4	.013	.016	.000															
5	.031	.036	.000	-.035														
6	.025	.037	-.001	-.025	-.065													
7	-.003	-.009	.001	.002	.006	-.002												
8	-.024	-.030	.000	.026	.066	.048	-.003											
9	-.030	-.046	.001	.029	.077	.045	.004	-.056										
10	-.007	-.010	.000	.006	.016	.009	.001	-.012	-.010									
11	.000	-.006	.001	-.002	-.003	-.010	.005	.004	.013	.003								
12	.004	.005	.000	-.005	-.012	-.009	.001	.009	.011	.002	.000							
13	.008	.009	.000	-.010	-.024	-.019	.002	.018	.022	.005	.000	-.003						
14	.010	.011	.000	-.011	-.027	-.020	.002	.020	.024	.005	-.001	-.004	-.007					
15	-.003	-.023	.002	-.003	-.001	-.024	.016	.006	.032	.008	.016	.000	.002	-.001				
16	.010	.017	.000	-.010	-.026	-.013	-.003	.018	.014	.003	-.005	-.004	-.008	-.008	-.015			
17	.007	.010	.000	-.007	-.013	-.011	.000	.013	.013	.003	-.002	-.002	-.005	-.005	-.005	-.004		
18	.007	.009	.000	-.008	-.020	-.014	.001	.015	.016	.003	-.001	-.003	-.005	-.006	-.002	-.005	-.004	
19	.011	.021	-.001	-.009	-.025	-.008	-.006	.017	.008	.001	-.009	-.004	-.008	-.003	-.025	-.001	-.003	-.005
20	-.012	-.040	.002	.004	.019	-.017	.021	-.008	.026	.007	.023	.003	.008	.006	.074	-.015	-.003	.002
21	.001	.002	.000	-.001	-.002	.000	-.001	.001	.000	.000	-.001	.000	-.001	-.001	-.003	.000	.000	.000
22	.012	.021	-.001	-.011	-.029	-.014	-.004	.021	.015	.003	-.007	-.004	-.009	-.009	-.020	-.004	-.004	-.006
23	.027	.053	-.002	-.022	-.063	-.023	-.014	.043	.021	.003	-.021	-.009	-.020	-.019	-.061	-.002	-.007	-.013
24	.026	.041	-.001	-.025	-.066	-.038	-.005	.048	.042	.008	-.012	-.009	-.020	-.020	-.031	-.012	-.011	-.014
25	-.004	.000	.000	.006	.013	.015	-.005	-.011	-.019	-.004	-.003	.002	.003	.004	-.012	.007	.004	.003
26	-.020	-.053	.003	.010	.036	-.009	.024	-.020	.018	.006	.028	.006	.014	.011	.087	-.013	-.001	.006
27	-.029	-.043	.001	.029	.074	.045	.003	-.054	-.050	-.010	.011	.010	.022	.023	.028	.015	.013	.016
28	-.005	-.008	.000	.005	.014	.009	.000	-.010	-.010	-.002	.002	.002	.004	.004	.005	.003	.002	.003
29	-.001	.003	.000	.003	.006	.011	-.005	-.006	-.014	-.003	-.004	.001	.001	.002	-.013	.006	.003	.002
30	.007	.011	.000	-.006	-.017	-.008	-.002	.012	.009	.002	-.004	-.002	-.005	-.005	-.010	-.002	-.002	-.004
31	.009	.015	-.001	-.007	-.020	-.008	-.004	.014	.008	.001	-.006	-.003	-.006	-.006	-.017	-.001	-.003	-.004
32	.011	.019	-.001	-.010	-.027	-.013	-.003	.019	.014	.003	-.006	-.004	-.003	-.003	-.017	-.004	-.004	-.006
33	[illegible]	[illegible]	-.001	.015	.033	.042	-.014	-.029	-.053	-.012	-.011	.004	.007	.010	-.040	.021	.011	.009
34	.012	.015	.000	-.012	-.031	-.021	.001	.023	.025	[illegible]	[illegible]	-.004	-.009	-.010	-.006	-.003	-.006	-.007
35	.007	.011	[illegible]	-.007	-.013	-.010	-.002	[illegible]	.011	[illegible]	[illegible]	[illegible]	-.005	-.005	-.009	-.003	-.003	-.004
36	[illegible]	[illegible]	.000	-.007	-.018	[illegible]	[illegible]	[illegible]	.009	[illegible]	[illegible]	[illegible]	-.006	-.006	-.013	-.002	-.003	-.004
37	[illegible]	-.011	.000	.005	.014	.005	[illegible]	[illegible]	-.005	-.001	.004	[illegible]	.004	.004	.012	.001	.002	.003
38	[illegible]	-.013	.000	[illegible]	.019	[illegible]	.002	-.013	-.010	-.002	.004	[illegible]	.006	.006	.012	.002	.003	.004
39	.009	.010	.000	-.010	-.025	-.020	.002	.019	.023	[illegible]	[illegible]	-.003	-.007	[illegible]	.002	-.003	-.005	-.006
40	.018	.016	.000	-.021	-.051	-.044	.007	.040	.053	.012	.002	-.007	-.014	-.016	.012	-.019	-.012	-.012
41	.017	.018	.000	-.019	-.048	-.033	.005	.037	.045	.010	.000	-.005	-.013	-.015	.004	-.015	-.010	-.011
42	-.016	-.020	.000	.017	.043	.030	-.001	-.032	-.035	-.007	.003	.006	.012	.013	.006	.011	.008	.010
43	.000	-.009	.001	-.003	-.005	-.014	.008	.006	.013	.004	.007	.000	.000	-.001	.024	-.008	-.003	-.002
44	.014	.016	.000	-.015	-.038	-.029	.003	.029	.034	.007	-.002	-.005	-.011	-.012	-.001	-.011	-.008	-.009
45	-.014	-.016	.000	.016	.039	.030	-.003	-.030	-.035	-.007	.001	.005	.011	.013	.000	.012	.003	.009

INT.	Columns 19 onward (in order)
20	-.029
21	.001 -.004
22	.000 -.020 .000
23	.010 -.069 .002 .000
24	-.005 -.027 .000 -.012 -.015
25	.009 -.020 .001 .009 .023 .017
26	-.029 .111 -.004 -.018 -.070 -.020 -.026
27	.009 .021 .000 .016 .024 .042 -.018 .013
28	.002 .003 .000 .003 .005 .008 -.003 .001 -.010
29	.008 -.020 .001 .007 .020 .013 .002 -.025 -.012 -.002
30	.000 -.010 .000 -.002 -.001 -.007 .005 -.009 .009 .002 .004
31	.002 -.019 .000 -.001 .004 -.006 .007 -.019 .009 .002 .006 -.001
32	.000 -.017 .000 -.003 -.001 -.011 .008 -.016 .015 .003 .006 -.002 -.001
33	.028 -.063 .003 .026 .070 [illegible] .004 -.079 -.049 -.029 .008 .014 .021 .023
34	-.007 .000 -.001 -.009 -.017 -.021 .006 .005 .024 .005 .004 -.005 -.006 [illegible] .016
35	-.001 -.009 .000 -.003 -.003 -.009 .005 -.007 .011 .002 .004 -.002 -.001 [illegible] .014 -.006
36	.001 -.013 .000 -.002 .001 -.007 .006 -.012 .009 .002 .005 -.001 [illegible] -.002 .016 -.005 -.002
37	-.002 .013 .000 [illegible] -.003 [illegible] -.005 .014 -.006 [illegible] [illegible] .001 -.014 [illegible] .001 .000 [illegible] [illegible]
38	.000 .012 .000 .002 .001 [illegible] -.005 .010 -.010 -.002 -.004 .001 .001 -.002 -.016 .006 .002 .001 .000
39	-.008 .008 -.001 -.009 -.021 -.020 .003 .014 .023 .004 .001 -.005 -.006 -.003 .006 -.009 -.005 -.006 .004 .006
40	-.021 .029 -.002 -.022 -.052 -.047 .005 .043 .051 .009 .001 -.012 -.016 -.020 .010 -.020 -.013 -.014 .011 .014 -.014
41	-.016 .017 -.002 -.013 -.040 -.039 .006 .023 .044 .008 .002 -.010 -.013 -.016 .015 -.018 -.011 -.011 .009 .011 -.014 -.027
42	.010 -.002 .001 .013 .025 .030 -.003 -.009 -.034 -.006 -.005 .007 .003 .012 -.021 .015 .008 .002 -.006 -.008 .013 .027 .024
43	-.012 .034 -.002 -.010 -.030 -.017 -.005 .041 .016 .003 -.006 -.005 -.009 -.009 -.016 -.004 -.005 -.007 .006 .006 .000 .003 .000 .005
44	-.011 .005 -.001 -.013 -.028 -.029 .006 .016 .033 .006 .003 -.007 -.009 -.012 .015 -.014 -.008 -.008 .006 .008 -.011 -.023 -.021 .019 -.002
45	.011 -.009 .001 .013 .027 .030 -.006 -.017 -.034 -.006 -.003 .008 .009 .012 -.015 .014 .003 .003 -.006 -.009 .011 .023 .021 -.019 .002 .017

corresponding matrix of correlation coefficients of the parameters is shown in table 6.8. These correlation coefficients are important when calculating the propagation of error for the calculated saturated activities using two or more of the parameters in tables 6.5, 6.6 and 6.7.

Using the values obtained of the $(I_0/g\sigma_0)$, η and their variance-covariance matrix and values of θ and P_γ from [62], I_0 values are calculated and listed in table 6.9. All values of I_0 are obtained with improved uncertainties, or an improvement in the information of the listed I_0 values (except for ^{238}U and ^{170}Tm for the reasons stated above).

Using reported values of σ_0, g, θ, M and their uncertainties the η values can be unfolded and new, in some cases more improved, values of P_γ can be obtained. Table 6.10 shows the calculated P_γ values for some elements compared with values from ERDTMANN [80].

The calculated value (using σ_0 of 162.3 (0.43%) [72]) of P_γ for ^{116m}In 417 keV is 27.4% (1.6%), which agrees with the value of 27.8% (4%) reported by JEFFERIES [11]. This indicates an agreement with the conclusion of JEFFERIES that the branching ratio of the indium 417 keV gamma may not be as well known as it is claimed to be [81].

In the case of ^{159}Gd where ERDTMANN's [80] P_γ for the 363 keV gamma line is 8% (38%) the value obtained from this work, using $\sigma_0(^{158}Gd)$ of 2.2 (9.1%) reported by MUGHABGHAB [79], is 10.14% (9.2%) which shows a factor of four improvement in the error.

As shown in table 6.10 improvement is also achieved in the P_γ values for, ^{166}Ho 80 keV, ^{170}Tm 84 keV and ^{187}W 134 keV gamma lines.

Table 6.9. calculated values of I_0 from the solution values of $I_0/g\sigma_0$, and reported values of I_0

Target nuclide	I_0 from this work (± error)	I_0 values from MUGHABGHAB (± error)	I_0 values from F.DE.CORTE et at (± error)
^{71}Ga	31.58 ± 0.63	31.2 ± 1.9	30.6 ± 1.6
^{76}As	68 ± 2	61 ± 4	52.5 (-)
^{82}Br	51.2 ± 1.1	50 ± 5	49.8 ± 1.6
^{87}Sr	3.33 ± 0.08	4.79 ± 0.24	3.17 ± .06
^{116m}In	2650 ± 53	2650 ± 101	2638 ± 105
^{122}Sb	213 ± 6	200 ± 20	209 ± 9
^{134}Cs	33.6 ± 1.2	———	32.3 ± 1.4
^{153}Sm	2954 ± 88	2970 ± 101	3168 ± 101
^{159}Gd	72.4 ± 6.7	73 ± 7	96 (-)
^{160}Tb	497 ± 16	418 ± 20	426 ± 17
^{166}Ho	642 ± 17	650 ± 22	636 ± 32
^{170}Tm	1774 ± 170	1720 ± 29	1532 (-)
^{176}Lu	563 ± 20	550 ± 30	581 ± 28
^{180}Hf	6.27 ± 0.12	6.9 ± 0.6	6.4 ± 0.3
^{182}Ta	613 ± 12	660 ± 23	679 (-)
^{187}W	484 ± 12	485 ± 15	530 ± 28
^{198}Au	1531 ± 12	1550 ± 28	
^{239}U	297 ± 33	277 ± 3	284 ± 7

Table 6.10. Calculated gamma-ray intensities.

Product nuclie	Gamma-ray energy (keV)	% p_γ (% error) from this work	% p_γ (% error) by G. ERDTMANN
^{116m}In	417	27.4 (1.6)	29.2 (4.9)
^{159}Gd	363	10.14 (9.2)	8 (38)
^{166}Ho	80	6.68 (2.4)	6.2 (6.5)
^{170}Tm	84	3.61 (2.5)	3.26 (4.9)
^{187}W	134	9.54 (2)	9.5 (4.2)

CHAPTER SEVEN

SUMMARY AND CONCLUSION

The model used in this work to describe the activity induced in a detector, in terms of nuclear data and flux parameters, is based on the model described by AHMAD [15]. In this model, the saturated gamma-ray emission rate per unit mass of target element is related to the flux parameters and nuclear data (for well diluted samples i.e ignoring self shielding) as follows:

$$N_s = N_{AV}\eta\left[\phi_{th} + \phi_e\left[\frac{W'}{g} + f_1(\alpha) + \bar{E}_r^{-\alpha}\left[\frac{I_0}{g\sigma_0} - f_2(0)\right] + f_2(\alpha)\right]\right] \quad 7.1$$

If the detector is irradiated under cadmium cover, the equivalent model is:

$$N_{Cd} = N_{AV}\eta\phi_e\left[\bar{E}_r^{-\alpha}\left[\frac{I_0}{g\sigma_0} - f_2(0)\right] + f_2(\alpha)\right] \quad - 7.2$$

In order to obtain an unbiased set of flux parameters and nuclear data when solving equation 7.1 or 7.2, it is desirable to measure more isotopes than the minimum required to determine these flux parameters and nuclear data. This produces an over determined set of solutions which can be treated in a least-square sense to find the best values.

The object of this work is to apply the described procedure which, from measured experimental activation data and their uncertainties, provides a simultaneous determination

of the flux parameters and the nuclear data without any priori information. it also provides a test of the flux model used in this work.

Using the procedure outlined in chapter two, it is possible to determine gamma-ray emission rates with a precision of about 1%, even at very small source-to-detector distances.

Making use of the assumption that a germanium detector behaves as a point detector the photopeak efficiency for any energy at any source-to-dector distance can be represented by a formula of twelve parameters, without any information or assumptions about the detector crystal geometry and configuration as shown in chapter three. With the minimum of experimental measurements an empirical efficiency function can be developed so that the photopeak efficiency can be calculated instead of measured.

When the least-square technique was applied to the measured reaction rates the chi-square value obtained is 34 for 27 degrees of freedom which passes the test at the 90% probability level. This result proves the relevance of the flux model used in this work. The solution provided an unbiased set of $I_0/g\sigma_0$ and η values for the isotopes used, flux parameters for the irradiation positions used and their variance-covariance matrix in a single analysis. This method is useful when studying isotopes with little or non reliable information.

In order to get direct information on I_0, using the technique described in this work, the variable $I_0/g\sigma_0$ was decoupled and the errors were correctly propagated taking all covariances into account as shown in chapter six.

Also, by decoupling the variable η information about P_γ was obtained and in some cases with a better precision than the published values. In the case of the P_γ value for the 363 keV transition in ^{159}Gd the precision is four times better than ERDTMANN [80]. Similar improvement in the P_γ value has been achieved for ^{116m}In(417keV), ^{166}Ho(80keV), ^{170}Tm(84keV) and ^{187}W(134keV).

The precision on the measured parameters can be improved further by increasing the number of measurements compared to the number of parameters to be estimated (increasing the number of degrees of freedom).

REFERENCES

1) C.H. WESTCOTT, J. Nucl. Energy 2 (1955) 59.

2) R.W. STOUGHTON and J. HALPERIN, Nucl. Sci. Eng 6 (1959) 100.

3) O.T. HOGDHAHL, Radiochemical Methods of Analysis, I.A.E.A. Vienna, 1 (1965) 33.

4) M.M.R. WILLIAMS, The Slowing Down and Thermalization of Neutrons. North Holland (1966).

5) K.W. GEIGER and L. VAN DER ZWAN, Metrologia 2 (1966) 1.

6) T.B. RYVES and E.B PAUL, J. Nucl. Energy 22 (1968) 759.

7) T.B RYVES, Metrologia 5 (1969) 119.

8) T. BEREZNAI and T.D. MACMAHON, J. Radioanal. Chem. 45 (1978) 423.

9) F. DE CORTE, L. MOENS, A. SIMONITS, A. DE WISPELAERE and J. HOSTE, J. Radioanal. Chem. 52 (1979) 295.

10) S.M. JEFFERIES, Ph.D Thesis, University of London (1983).

11) A. AHMAD, Ph.D Thesis, University of London (1982).

12) E.M. GRYNTAKIS and J.I. KIM, NEA DATA BANK ND1540 (1980).

13) S.M. GHURBAL, Ph.D Thesis, University of London (1987).

14) J.V. SANDBERG, P.D. LUND, J. Radioanal. Chem. 76, No.1 (1983) 151.

15) A. AHMAD, Ann. Nucl. Energy. Vol. 10, pp. 41 to 50, 1983.

16) K. DEBERTIN and U. SCHOTZIG, Nucl. Instr. & Meth. 140 (1977) 337.

17) W. MICHAELIS, Nucl. Instr. & Meth. 70 (1969) 253.

18) P. QUITTNER, Nucl. Instr. & Meth. 76 (1969) 115.

19) J.T. ROUTTI and S.G. PRUSSIN, Nucl. Instr. & Meth. 72 (1969) 125.

20) R. GUNNINK and J.B. NIDAY, University of California Radiation Laboratory report, UCRL-51061, VOL. 1-4 (1972).

21) L.A. MCNELLES and J.L. CAMPELL, Nucl.Instr. & Meth. 127 (1975) 73.

22) J.L. CAMPELL and H.H. JORCH, Nucl. Instr & Meth. 159 (1979) 163.

23) D.C. ROBINSON, Nucl. Instr & Meth. 78 (1970) 120.

24) R.G. HELMER and M.A. LEE, Nucl. Instr & Meth. 178 (1980) 199.

25) J. KERN, Nucl. Instr Meth. 79 (1970) 233.

26) G.W. PHILLIPS and K.W. MARLOW, Nucl Instr & Meth. 137 (1976) 525.

27) J. LIBERT, Nucl. Instr. & Meth. 109 (1973) 609.

28) H.H. JORCH and J.L. CAMPELL, Nucl. Instr. Meth. 143 (1977) 551.

29) W. TEOH, Nucl. Instr. & Meth. 109 (1973) 509.

30) M. DOJO, Nucl. Instr. & Meth. 115 (1974) 425.

31) N. SASAMOTO, K. KOYAMA and S. TANAKA, Nucl. Instr. & Meth. 125 (1975) 507.

32) F. JAMES and M. ROOS, Computer physics communications 10 (1975) 343.

33) H.G. BALIAN and N.W. EDDY, Nucl. Instr. & Meth. 145 (1977) 389.

34) L. WIELOPOLSKI and R.P. GARDNER, Nucl. Instr. Meth. 133 (1976) 303.

35) M. WIERNIK, Nucl. Instr. & Meth. 96 (1971) 325.

36) K. HUYSMANS, R.GIJBELS and J.HOSTE, J. Radional. Chem. 20 (1974) 51.

37) E. JUNOD, J. Radional. Chem. 20 (1974) 113

38) O.U. ANDERS, Nucl. Instr. & Meth. 68 (1969) 205.

39) H.H. BOLOTIN, M.G. STRAUSS and D.A. MCCLURE, Nucl. Instr. & Meth. 83 (1970) 1.

40) E.J. COHEN, Nucl. Instr. & Meth. 121 (1974) 25.

41) M. IRFAN and S.A. HUSSAIN, Nucl. Instr. & Meth. 143 (1977) 177.

42) L. MORTENSEN and J. OLSEN, Nucl. Instr. & Meth. 113 (1973) 151.

43) G. AZUELOS, S.E. CRAWFORD and J.E. KITCHING, Nucl. Instr & Meth. 117 (1974) 233.

44) M. WIERNIK and S. AMIEL, L. Radional. Chem. 3 (1969) 245.

45) G.J. MCCALLUM and G.E. COOTE, Nucl. Instr. & Meth. 130 (1975) 189.

46) R.J. GEHRKE, R.G. HELMER and R.C. GREENWOOD, Nucl. Instr & Meth. 147 (1977) 405.

47) K. DEBERTIN and U. SCHOTZIG, Nucl. Instr & Meth. 158 (1979) 471.

48) A. LUUKKO and P. HOLMBERG, Nucl. Instr & Meth. 65 (1968) 121.

49) P.W. GRAY and A. AHMAD, Nucl. Instr. & Meth. A237 (1985) 577.

50) Y. YOSHIZAWA, Y. IWATA, T. KAKU, T. KATOH, J. RUAN, T. KOJIMA and Y. KAWADA, Nucl. Instr & Meth. 174 (1980) 109.

51) L. MOENS, J. DE DONDER, LIN Xi-Lei, F. DE CORTE, A. DE WISPELAERE, A. SIMONITS and J. HOSTE, Nucl. Instr. & Meth. 187 (1981) 451

52) R.G. HELMER, Int.J.Appl.Radiat.Isot. 34:8 pp.1105-1108

53) J. LIPPERT, Int.J.Appl.Radiat.Isot. 34:8 PP.1097-1103

54) L. MOENS and J. HOSTE Int.J.Appl.Radiat.Isot. 34:8 pp 1085-1093

55) A. NOTEA, Nucl. Instr. & Meth. 91 (1971) 513.

56) D.F. CRISLER, J.J. JARMER and H.B. ELDRIDGE, Nucl. Instr. & Meth. 94 (1971) 285.

57) K. KAWADE, M. EZUKA, H. YAMAMOTO, K. SUGIOKA and T. KATOH, Nucl. Instr. & Meth. 190 (1981) 10.

58) H. GOLDSTEIN, J.A. HARVEY, J.S. STORY and C.H. WESTCOTT, Recommended Definitions for Resonance Integral Cross-sections, EANDC-12 (1961).

59) A. SIMONITS, F. DE CORTE and J. HOSTE, J. Radioanal. Chem. 24 (1975) 31.

60) T.B. RYVES and K.J. ZIEBA, J. Phys. A: Math. 7 (1974) 2318.

61) L. MOENS, F. DE CORTE, A. SIMONTS, A. DE WISPELAERE and J. HOSTE, J. Radioanal. Chem. 52 (1979) 379.

62) F. DE CORTE et al. INW/KFKI Interim report june (1986).

63) I.A.E.A, Neutron Fluence Measurements, Rept. No 107, Vienna, 1970.

64) D.J. HUGHES, Pile Neutron Research, Addison-Wesley, Reading, Massachusetts, 1953.

65) F. DE CORTE, L. MOENS, K. SORDO-EL-HAMMAMI, A. SIMONITS and J. HOSTE, J. Radioanal. Chem. 52 (1979) 305.

66) B.R. MARTIN, Statistics for Physicists, Acadamic Press, 1971.

67) W.H. BERGER, Handbook of Tables for Probability and Statistics, Second Edition Published by The Chemical Rubber Co.

68) A.M. MOOD, F.A. GRAYBILL AND D.C. BOES, Introduction to the Theory of Statistics, Third Edition, McGraw-Hill, London, 1974.

69) W.N. SELANDER, Rep. AECL-1077 (1960).

70) N.P. BAUMANN, Rep. DP-817 (1963).

71) S.M. JEFFERIES, T.D. MACMAHON, J.G. WILLIAMS AND A. AHMAD. Proc. Int. Conf. on "Nuclear Data for Science & Technology". 6-10 Sept. 1982, Belgium.

72) G.M. ROE, Rep. KAPL-1241 (1954).

73) T. ELNIMR, F. DE CORTE, L. MOENS, A. SIMONITS and J. HOSTE, J. Radioanal. Chem. 67 (1981) 421.

74) C.H. WESTCOTT, "EFFECTIVE CROSS SECTIONVALUES FOR WELL-MODERATED THERMAL REACTOR SPECTRA" 3rd edition. AECL-1101.

75) A. SIMONITS et al. J. Radioanal. and Nucl. Chem. 82, No.1 (1984) 169.

76) A. SIMONITS et al. J. Radioanal. and Nucl. Chem. 82, No.1 (1984) 397.

77) S. JOVANOVIC et al. J. Radioanal and Nucl. Chem. 92, No.2 (1985) 399.

78) T. ELNIMR and F.H. ELA-ASSALY, J. Radioanal. and Nucl. Chem. 109, No.1 (1987) 3.

79) S.F. MUGHABGHAB et al. "NEUTRON CROSS SECTION" Vol.1, Part A & B (1981).

80) G. ERDTMANN and W. SOYKA. Gamma Rays of the Radionuclides Verlag Chemie Weinheim/N.Y (1979).

81) C.M. LEDERER and V.S. SHIRLEY, Table of Isotopes 7th Edition. JOHN WILEY & Sons (1978).

APPENDIX A

1.A Finite Source Size Correction

Let N be the [illegible] count rate due to dv at (x_1,x_2,x_3). Expanding in a Taylor series gives to 2nd order the approximation:

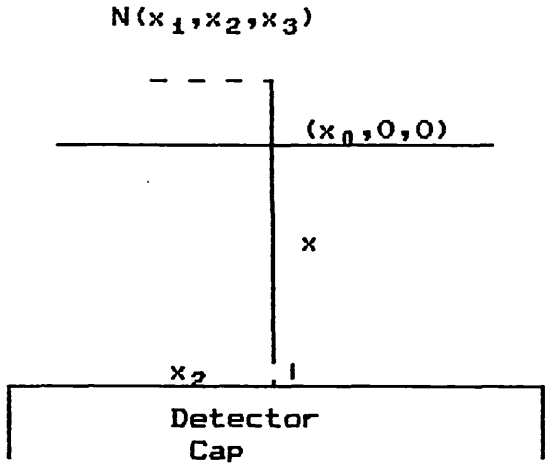

$$N(x_1,x_2,x_3) = N_0 + \sum_{i=1}^{3} \alpha_i (x_i - x_{i0}) + \sum_{i=1}^{3}\sum_{j=1}^{3} \beta_{ij} (x_i - x_{i0})(x_j - x_{j0})$$

-A1

where $\alpha_i = \dfrac{\partial N(x_{10},x_{20},x_{30})}{\partial x_i}$, $\beta_{ij} = \dfrac{1}{2}\dfrac{\partial^2 N(x_{10},x_{20},x_{30})}{\partial x_i \partial x_j}$ and

$$N_0 = N(x_{10},0,0)$$

If it can be assumed that the detector is cylindrical and coaxial with the end cap, then $N = N(x_1,t)$

where $t = x_2^2 + x_3^2$.

And if the expansion takes place about $x_2=0$, $x_3=0$ since only

the variation in the x_i is considered and by transfering to t space (see section 3.A below), equation A1 becomes

$$N(x_i,t) = N_0 + \frac{\partial N}{\partial x_i}(x_i - x_{i0}) + \frac{\partial N}{\partial t} x_2^2 + \frac{\partial N}{\partial t} x_3^2 + \frac{1}{2}\frac{\partial^2 N}{\partial x_i^2}(x_i - x_{i0})^2$$

$$N(x_i,t) = N_0 + \frac{\partial N}{\partial x_i}(x_i - x_{i0}) + \frac{1}{2}\frac{\partial^2 N}{\partial x_i^2}(x_i - x_{i0})^2 + \frac{\partial N}{\partial t} t \,. \qquad A2$$

In order to determine the bias in the count rate N due to the source being of finite size, first assume that the radioactive liquid drop can be approximated by a cylinder of radius R, height H and volume $V = \pi R^2 H$ as shown in fig.A1. Given a uniform distribution in the source, then the total count rate arising in the source is given by:

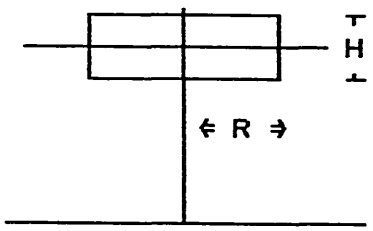

Fig.A1.

$$N = \int_V \frac{N(x_i,t)}{V}\, dV$$

where $dV = \pi dt dx_i$, so that

$$N = \frac{1}{\pi R^2 H}\int_V N(x_i,t)\,\pi dt dx_i = \frac{1}{R^2 H}\int_{x_{i0}-\frac{H}{2}}^{x_{i0}+\frac{H}{2}}\int_0^{R^2} N(x_i,t)\,dt dx_i$$

substituting for $N(x_i,t)$ from equation A2, then the count rate is given by:

$$N = N_0 + \int_{x_{i0}-\frac{H}{2}}^{x_{i0}+\frac{H}{2}} \int_{0}^{R^2} \left[\frac{\partial N}{dx_i} (x_i - x_{i0}) + \frac{1}{2} \frac{\partial^2 N}{\partial x_i^2} (x_i - x_{i0}) + \frac{\partial N}{\partial t} t \right] \frac{dx_i dt}{R^2 H}$$

To perform the integration, let $\lambda = x_i - x_{i0}$; $d\lambda = dx_i$ and substitute in the above equation we get

$$N = N_0 + \int_{-\frac{H}{2}}^{\frac{H}{2}} \int_{0}^{R^2} \left[\frac{\partial N}{\partial x_i} \lambda + \frac{1}{2} \frac{\partial^2 N}{\partial x_i^2} \lambda^2 + \frac{\partial N}{\partial t} t \right] \frac{d\lambda dt}{R^2 H}$$

$$= N_0 + \frac{1}{R^2 H} \int_{-\frac{H}{2}}^{\frac{H}{2}} \left[\frac{\partial N}{\partial x_i} \lambda R^2 + \frac{1}{2} \frac{\partial^2 N}{\partial x_i^2} \lambda^2 R^2 + \frac{\partial N}{\partial t} \frac{1}{2} R^2 \right] d\lambda$$

$$= N_0 + \frac{1}{R^2 H} \left[\frac{R^2}{24} \frac{\partial^2 N}{\partial x_i^2} H^3 + \frac{R^4}{2} H \frac{\partial N}{\partial t} \right]$$

$$N = N_0 + \left(\frac{H^2}{24} \frac{\partial^2 N}{\partial x_i^2} + \frac{R^2}{2} \frac{\partial N}{\partial t} \right) \qquad A3$$

where the second term on the right hand is the bias due to deviation from a point source.

Linearize about R_0 and H_0; and let R and H be

0 0

independent random variables, so that R and H are functions of

$$R_0,\ \sigma_R^2 \quad \text{and} \quad H_0,\ \sigma_H^2 \ \text{respectively.}$$

This variation corresponds to changing source size, without changing source strength. And the variance in the bias of equation A3 is given by:

$$\sigma_B^2 = \left(\frac{\partial N}{\partial t}\right)^2 R_0^2 \sigma_R^2 + \left(\frac{\partial^2 N}{\partial x_i^2}\right)^2 \frac{H_0^2}{144}\ \sigma_H^2 .$$

Using a point detector model of the form $N = A/r^2$ where

$$r = ((x_i+d)^2 + t)^{1/2}$$

and d is the distance below the detector cap. Then transfering to r coordinates (see below section 4.A), equation A3 is then given by:

$$N = N_0 + \frac{R_0^2}{4r}(-)\frac{2A}{r^3} + \frac{H_0^2}{24}\frac{6A}{r^4}$$

$$N_0 = N\left[1 + \frac{R_0^2}{2r^2} - \frac{H_0^2}{4r^2}\right] = N(1+B)$$

hence the correction factor to multiply the count rate is

(1+B), where

$$B = \left[\frac{1}{2r^2}\left(R_0^2 - \frac{H_0^2}{2}\right)\right]$$

and its fractional variance is given by:

$$\frac{\sigma_B^2}{N^2} = \frac{1}{r^4}\left[R_0^2\ \sigma_R^2 + \frac{H_0}{4}\ \sigma_H^2 \right] \qquad A4$$

The values of d are found by fitting $\epsilon_p^{-\frac{1}{2}}$ of the peak efficiency against distance (see chapter three) without the finite size correction. R, σ_R, H and σ_H are estimated from the standard sources assembly and the estimated values are:

$$R_0 = 0.15cm,\ \sigma_R = 0.05cm,\ H_0 = 0.015cm \text{ and } \sigma_H = 0.005cm$$

2.A Source Location Sensitivity

Consider equation A1, and let x_i (i=1,3) be independent random variables with means x_{i0} and standard deviations σ_i. Then given a little algebra and bearing in mind that the expectation value $E(x_i^4) = 3\sigma_i^4$ and the expectation of odd numbers of the x_i are zero. Then

$$E(N) = N_0 + \sum_{i=1}^{3} \beta_{ii}\sigma_i^2 \qquad \text{and}$$

$$\sigma_{sl}^2 = \sum_{i=1}^{3} (\alpha_i^2\ \sigma_i^2 + 3\beta_{ii}^2\ \sigma_i^4) + \sum_{\substack{i,j=1 \\ i<j}}^{3} 2(\beta_{ii}\beta_{jj} + 2\beta_{ij}^2)\sigma_i^2\ \sigma_j^2$$

If $\sigma_{x_2} = \sigma_{x_3}$ then:

$$E(N) = N_0 + 2\frac{\partial N}{\partial t}\sigma_{x_2}^2 + \frac{1}{2}\frac{\partial^2 N}{\partial x_i^2}\sigma_{x_i}^2 \qquad \text{and}$$

$$\sigma_{sl}^2 = \left(\frac{\partial N}{\partial x_i}\right)^2\sigma_{x_i}^2 + 2\frac{\partial N}{\partial t}\frac{\partial^2 N}{\partial x_i^2}\sigma_{x_i}^2\sigma_{x_2}^2 + \frac{3}{4}\left(\frac{\partial^2 N}{\partial x_i^2}\right)^2\sigma_{x_i}^4 + 8\left(\frac{\partial N}{\partial t}\right)^2\sigma_{x_2}^4$$

Using a point detector model of the form $N = A/r^2$, then transfering to r coordinates, it can easily be shown that:

$$\frac{\sigma^2_{sl}}{N^2} = 4\frac{\sigma^2_{x_1}}{r^2} + \frac{1}{r^4}\left[8\sigma^4_{x_2} + 27\sigma^4_{x_1} - 12\sigma^2_{x_1}\sigma^2_{x_2} \right]$$

where σ_{x1} and σ_{x2} are estimated from the variation in the position of the radioactive liquid drop on the source assembly. The estimated values are:

$$\sigma_{x_1} = 0.01\text{cm and } \sigma_{x_2} = 0.15\text{cm}$$

Similar expressions can be obtained for uncertainties, in source mount on the source holder (σ_{sh}) with

$$\sigma_{x_1} = 0.01\text{cm and } \sigma_{x_2} = 0.015\text{cm},$$

and for the source holder positioning on the shelf rig (σ_{sm}) with

$$\sigma_{x_1} = 0.005\text{cm and } \sigma_{x_2} = 0.01\text{cm}.$$

3.A Transformation to (t,x) System

Let $N = N(t,x_1)$, $t = x_2^2 + x_3^2$ and bearing in mind that the expansion is about $x_2 = 0$ and $x_3 = 0$ then

$$\alpha_1 = \left.\frac{\partial N}{\partial x_1}\right|_0$$

$$\alpha_2 = \left.\frac{\partial N}{\partial x_2}\right|_0 = \left.\frac{\partial N}{\partial t}.\frac{\partial t}{\partial x_2}\right|_0 = 2x_2\left.\frac{\partial N}{\partial t}\right|_0 = 0$$

$$\alpha_3 = \left.\frac{\partial N}{\partial x_3}\right|_0 = \left.\frac{\partial N}{\partial t}.\frac{\partial t}{\partial x_3}\right|_0 = 2x_3\left.\frac{\partial N}{\partial t}\right|_0 = 0$$

$$\beta_{ii} = \frac{1}{2}\frac{\partial^2 N}{\partial x_i^2}\Big|_0$$

$$\beta_{22} = \frac{1}{2}\frac{\partial^2 N}{\partial x_2^2}\Big|_0 = \frac{\partial N}{\partial t} + x_2\frac{\partial^2 N}{\partial x_2 \partial t}\Big|_0 = \frac{\partial N}{\partial t}\Big|_0$$

$$\beta_{33} = \frac{1}{2}\frac{\partial^2 N}{\partial x_3^2}\Big|_0 = \frac{\partial N}{\partial t} + x_3\frac{\partial^2 N}{\partial x_3 \partial t}\Big|_0 = \frac{\partial N}{\partial t}\Big|_0$$

$$\beta_{12} = \beta_{21} = \frac{1}{2}\frac{\partial^2 N}{\partial x_1 \partial x_2}\Big|_0 = x_2\frac{\partial^2 N}{\partial x_1 \partial t}\Big|_0 = 0$$

$$\beta_{13} = \beta_{31} = \frac{1}{2}\frac{\partial^2 N}{\partial x_1 \partial x_3}\Big|_0 = x_3\frac{\partial^2 N}{\partial x_3 \partial t}\Big|_0 = 0$$

$$\beta_{23} = \beta_{32} = \frac{1}{2}\frac{\partial^2 N}{\partial x_2 \partial x_3}\Big|_0 = x_2\frac{\partial^2 N}{\partial x_3 \partial t}\Big|_0 = 0$$

4.A Transformation to r System

Let $N = N(r)$, where $r = (t + (x_i+d)^2)^{1/2}$ then

$$\frac{\partial N}{\partial t} = \frac{\partial N}{\partial r}\frac{\partial r}{\partial t} = \frac{1}{2r}\frac{\partial N}{\partial r} \quad , \text{ where } \frac{\partial r}{\partial t} = \frac{1}{2r}$$

$$\frac{\partial N}{\partial x_i} = \frac{\partial N}{\partial r}\frac{\partial r}{\partial x_i} = \left(\frac{x_i+d}{r}\right)\frac{\partial N}{\partial r} \quad , \text{ where } \frac{\partial r}{\partial x_i} = \frac{1}{2r}\,2(x_i+d) = \frac{x_i+d}{r}$$

$$\frac{\partial^2 N}{\partial x_i^2} = \left(\frac{x_i+d}{r}\right)\frac{\partial^2 N}{\partial r^2}\frac{\partial r}{\partial x_i} + \frac{\partial N}{\partial r}\left[\frac{1}{r} + -\left(\frac{x_i+d}{r^2}\right)\left(\frac{x_i+d}{r}\right)\right]$$

$$= \frac{(x_1+d)^2}{r^2} \frac{\partial^2 N}{\partial r^2} + \frac{\partial N}{\partial r}\left[\frac{1}{r} - \frac{(x_1+d)^2}{r^3}\right]$$

and at $x_2 = x_3 = 0$ then

$$\left.\frac{\partial N}{\partial t}\right|_0 = \frac{1}{2r_0}\left.\frac{\partial N}{\partial r}\right|_0 ; \left.\frac{\partial N}{\partial x_1}\right|_0 = \left.\frac{\partial N}{\partial r}\right|_0 \text{ and } \left.\frac{\partial^2 N}{\partial x_1^2}\right|_0 = \left.\frac{\partial^2 N}{\partial r^2}\right|_0$$